JIMMA UNIVERSITY
JIMMA INSTITUTE OF TECHNOLOGY
FACULTY OF MECHANICAL ENGINEERING

GRADUATE PROGRAM IN
SUSTAINABLE ENERGY ENGINEERING

Exergy Analysis of Solar-Geothermal based Power Plant Integrated with Boiling and Reverse Osmosis Water Purification

by

WUBEREST BITEW

A thesis submitted to the faculty of graduate studies of Jimma University in partial fulfillment of the requirement for the Degree of Masters of Science in Sustainable Energy Engineering

February 16, 2021

Jimma, Ethiopia

JIMMA UNIVERSITY
JIMMA INSTITUTE OF TECHNOLOGY
FACULTY OF MECHANICAL ENGINEERING
GRADUATE PROGRAM IN
SUSTAINABLE ENERGY ENGINEERING

Exergy Analysis of Solar-Geothermal based Power Plant Integrated with Boiling and Reverse Osmosis Water Purification

A thesis submitted to the faculty of graduate studies of Jimma University in partial fulfillment of the requirement for the Degree of Masters of Science in Sustainable Energy Engineering

Advisor: Prof. A. Venkata Ramaya (Ph.D)
Co-Advisor: Mr. Balewgize Amare (Ass. Professor)

February 16, 2021
Jimma, Ethiopia

Declaration

I declare that this thesis is my original work, and as far as I am aware, it has not been presented with a title of **Exergy analysis of solar-geothermal based power plant integrated with boiling and Reverse Osmosis water purification** for the degree award in other universities.

This thesis has been submitted with our approval as advisors, examiner, and supervisor for the degree of masters in sustainable energy engineering.

Candidate: Wuberest Bitew
Signature: _____ **Date:** _____

External Examiner: _____
Signature: _____ **Date:** _____

Internal Examiner: _____
Signature: _____ **Date:** _____

Advisor: Prof. Dr. A. Venkata Ramaya
Signature: _____ **Date:** _____

Co-advisor: Balewgize Amare Z. (Assistant professor)
Signature: _____ **Date:** _____

Chairperson: Tarekegn Limore (MSc)
Signature: _____ **Date:** _____

Abstract

The emphasis on renewable energy sources is increasing due to the exhaustiveness of fossil fuels and their effect on the environment. Non- conventional energies are naturally available but exclusively cannot provide consistent power output. Organic Reheat Rankine cycle is applicable to combine it with diverse energy source types for multi-purpose and better efficiency that works at a low temperature with specifically selected suitable working fluid. In this work, solar and geothermal renewable energies have been integrated with the Organic Reheat Rankine cycle having a medium of the thermocline energy storage. The objectives of the designed plant are power generation, boiling, and advanced water treatment through different stages of filtration. Aspen plus V11 software has been used for the design of the system configuration. Parameters that have more impact on the system has been optimized like the dead state temperature, geothermal high pressure turbine outlet and inlet pressure, ambient temperature, geothermal injection well fluid flow rate, production well pressure, production well temperature, and geothermal low pressure turbine outlet pressure. Exergy analysis of each component has been carried out on EES and the components of higher exergy destruction associated with energy conversion have been identified. For the Organic Reheat Rankine cycle, an appropriate working fluid biphenyl/diphenyl oxide has been selected and characterized based on the criteria of stability, environment, temperature, and toxicity has been considered. The RO water treatment process has been analyzed on GPS-X hydromantis software. The RO system is efficient and effective method of water treatment, by considering permeate pump and energy recovery unit in the design, the energy consumption has reduced. The running cost of the filtration and RO water treatment system is 6149.11 $/yr and $3.35 KW/m^3$ *power is required to run the booster pump that pressurize the untreated water through semipermeable membrane. The geothermal well operating condition parameters have been estimated from the existing well source data and the newly under construction Aluto Langano power plant. In the end, the power output which can serve the case study area households and industry, at high exergetic efficiency of 51.64 % for the night time system and 49.25% for the daytime operating system with the 100 m3/day of treated water as a supplement to the municipal filtered water. As a conclusion the designed system can perfectly achieves the objectives and the thermal disinfection process consumes*

13.36% of the total exergy that sterilize the water from contaminants by boiling water exposing to waste heat beyond the boiling point temperature which is estimated 135^0C*. To increase the life span of RO system, the water has filtered in the clarifiers that removes large size industry and household wastes thrown in the lake.*

Keywords: Exergy analysis, solar thermal energy, Organic Rankine cycle, geothermal energy.

Acknowledgment

First and foremost, I would like to give thanks to Almighty God for giving me the strength and ability of opportunity seeking to undertake every achievement in my life. I need to express my deepest and heartfelt thanks as well as my most sincere appreciation to the main research advisor professor Venkata Ramaya for his consistent guidance, critical review, and for commenting on the work throughout the analysis up to the document preparation phases. Mr. Balewgize Amare deserves special thanks for having his time, sharing knowledge unlimitedly as co-advisor.

I have a great pleasure for my mother Firenesh W/meskel and father Bitew Shumiye since they are a backbone in my journeys from childhood so far. My younger brothers' love and respect is the power to effort with full potential to be a role model to them. The elder sister consultancy was also significant in my life.

The last special acknowledgment is going to my fiancé Mr. Addisu Kidanemariam, who is always beside me in every step.

Contents

Declaration i

Abstract ii

Acknowledgment iv

List of Figures ix

List of Tables xii

List of Abbreviations xiii

1 Introduction 1

1.1 Background 1

1.2 A synopsis of Geothermal and solar-thermal energies 3

1.2.1 Geothermal Energy Technology 3

1.2.2 Concentrated solar power Technologies 6

1.2.3 Energy storages 8

1.2.4 Organic Rankine cycle (ORC) 9

1.3 Organic reheat Rankine Cycle 10

1.4 Water treatment / Reverse Osmosis 10

1.5 Problem statement 11

1.6 Research Objective 12

1.6.1 Main objective 12

1.6.2 Specific objective 12

1.7 Significance of the study 12

1.8 Scope 13

1.9 Thesis Organization 13

2 Literature review **15**

2.1 Research gap 18

3 Materials and Methods **19**

3.1 Study area 19

3.2 Data collection process and types of data 20

3.2.1 Primary data collection 20

3.2.2 Secondary data collection 20

3.2.3 Data processing and analysis 21

3.3 System Descriptions and Models 22

3.3.1 Geothermal energy system description 23

3.3.2 Solar thermal system description 24

3.3.3 Boiling (Sterilization) and RO 25

4 Estimation of solar radiation **26**

4.1 Extraterrestrial solar radiation 26

4.2 The Solar Radiation On an Inclined and horizontal Surface 27

4.3 Solar time 28

4.4 Angle of Declination 29

4.5 Hour angle 30

4.6 Latitude angle and longitude angle 30

4.7 Solar altitude angle 31

4.8 Zenith angle 31

4.9 Surface azimuth angle 31

4.10 Inclination or tilt angle 32

4.11 Incidence angle 32

4.12 Incidence angle modifier 32
4.13 Single-axis tracking 33
4.14 Solar radiation 34

5 Thermal Analysis of the concentrating solar parabolic trough 35

5.1 Exergy Analysis of parabolic trough collector 39

6 Exergy analysis of Double flash Geothermal power plant 42

6.1 Exergy Balance of the double flash geothermal system 43
6.2 Exergy balance of the SPTC system 45

7 Result and discussion 47

7.1 HTF and Trough characterization 48
7.2 The effect of mass flow rate 50
7.3 The intensity of solar radiation effect evaluation 54
7.4 The effect of the variability of Temperature 56
7.5 Effect of the length of the SPTC 61
7.6 The effect of dead state entropy on the overall system 63
7.7 The effect of first turbine outlet pressure 65
7.8 Variation of the Production well pressure 67
7.9 The effect of Inlet pressure to the first turbine 69
7.10 The effect of second turbine outlet Pressure 72
7.11 Water treatment results 75
7.11.1 Turbidity 76
7.11.2 PO_4 76
7.11.3 PH 77
7.11.4 TDS 77

7.11.5 Water treatment Operating Cost Summary 80

7.12 Validation of receiver outlet HTF temperature 84

8 Conclusion and Recommendations 85

8.1 Conclusion 85

8.2 Recommendations 86

Reference I

Appendix A IV

Appendix B XV

Appendix C XVII

Appendix D XXV

List of Figures

1.1 Interdisciplinary triangle that exergy analysis cover, [4]. 2
1.2 Some key requirements of sustainable development, [4] 3
1.3 Reliability of renewable energies,[8] 4
1.4 Geothermal energy conversion technologies growth[10] 5
1.5 Geothermal installed capacity of continents,[13] 6
1.6 Solar concentrators (A) PTC (B) SPDs (C) Fresnel lens and (D) solar tower, [13]. 7
1.7 ORC system and T-S diagram, [15]. 9
1.8 Organic Rankine reheat cycle system and T-S diagram, [16]. 10
1.9 Energy consumption increment forecast by 2025 and 2030 considering transmission loss, [22]. 11

3.1 Google map image of the Ziway and Aluto Langano power plant 20
3.2 System process diagram 21
3.3 The system configuration and T-S diagram of the hybrid power plant consisting of essential components of SPTC, geothermal including boiling water treatment. 23
3.4 The water treatment system configuration consisting of essential stages of purification 25

4.1 Extraterrestrial radiation through out the year 28
4.2 Equation of time over the year 28
4.3 Declination angle through out the year 30
4.4 Solar elevation angles throughout the year 31
4.5 Incidence angle modifier 33
4.6 solar radiation over the day time 34

5.1 Specific heat of HTF variation with temperature 41

7.1 The instability of receiver outlet HTF temperature of the SPTC with the mass flow rate 49
7.2 The outlet receiver HTF temperature at different segment of SPTC length 49
7.3 The fluctuation of Exergy and Thermal efficiency of the SPTC with the mass flow rate 50

7.4 The variability of useful heat of the SPTC with the mass flow rate . . . 51
7.5 The Exergy Destruction in geothermal components with different mass flowrate . . . 52
7.6 The variation of exergy efficiency and work net throughout the integrated system with different mass flowrate . . . 53
7.7 The receiver outlet temperature and exergy efficiency of the SPTC concerning different beam radiation . . . 54
7.8 The thermal efficiency and receiver outlet temperature of the SPTC organic reheat Rankine cycle with respect to different beam radiation . 55
7.9 The exergy destruction of the SPTC with respect to dead state temperature 56
7.10 The exergy destruction of the SPTC with respect to dead state temperature 57
7.11 The exergy destruction of the geothermal components with varied production well temperature . . . 58
7.12 The exergy efficiency and work net variation with production well temperature . . . 59
7.13 The receiver outlet temperature and thermal efficiency variation with an ambient temperature . . . 60
7.14 The receiver outlet temperature and useful heat gain variation with the length of the collector . . . 61
7.15 The thermal and exergy efficiency at different length of the collector . . 62
7.16 The formation of exergy destruction of the SPTC organic reheat Rankine cycle to dead state entropy . . . 63
7.17 The change of exergy work net of the SPTC organic reheat Rankine cycle to dead state entropy . . . 64
7.18 The formation of exergy destruction of the geothermal components due to the variation of first turbine outlet pressure. . . . 65
7.19 The exergy efficiency and work net of the double flash geothermal and solar system due to the variation of first turbine outlet pressure. . . . 66
7.20 The work net of the double flash geothermal and solar system due to the variation of production well pressure. . . . 67
7.21 The exergy destruction rate of componenets of the combined double flash geothermal system due to the variation of production well pressure 68
7.22 The exergy efficiency of the combined double flash geothermal and solar system due to the variation of production well pressure. . . . 69

7.23 The exergy efficiency and work net of the double flash geothermal system due to the variation of first turbine inlet pressure. 70
7.24 The exergy destruction rate of the double flash geothermal system due to the variation of first turbine inlet pressure. 71
7.25 The exergy destruction rate of the combined double flash geothermal and solar system due to the variation ofsecond turbine outlet pressure. 72
7.26 The work net of the combined double flash geothermal and solar system due to the variation of second turbine outlet pressure. 73
7.27 The work net of the combined double flash geothermal and solar system due to the variation of second turbine outlet pressure. 74
7.28 TDS level of the water during the purification process. 78
7.29 PH, Color, PO_4 variation with osmosis pressure 78
7.30 The variation total alkalinity of the water with time 79
7.31 Total operating cost of the water treatment process 80
7.32 power consumption rate of the water purification units 82

List of Tables

1.1 CST fundamental information's 8

4.1 Number of days in a month of the year 29

5.1 SPTC system-relevant parameters 35

6.1 The integrated power and water purification plant EES results 43

7.1 The integrated power and water purification plant EES results 47
7.2 Input parameters (Ziway lake characterization) 75
7.3 Exepermental results of the tap water quality in Ziway city 76
7.4 Water treatment Operating Cost Summary 80
7.5 Water treatment system energy consumption Summary 81
7.6 Occurrence of water born pathogens in ziway tap water, [37]. 82
7.7 validation of the temperature of the HTF at the recievier outlet 84

List of Abbreviations

$\overline{H}$	Solar radiation on Horizontal surface
$\overline{n}_s$	Sunshine hours
$\overline{N}_s$	Maximum possible sunshine hours
A_{ci}	Inside the area of the glass cover
A_{co}	The outside area of the glass cover
A_{ri}	Inside the area of the receiver tube
A_{ro}	The outside area of the receiver tube
a_x	Correlation regression constant
a_y	Correlation regression constant
CH_4	Methane
CO_2	Carbon dioxide
$COND$	Condenser
Cp_{HTF}	Specific heat of the heat transfer fluid
CST	Concentrated solar thermal
D_{ci}	Inside diameter of the glass cover
D_{co}	The outside diameter of the glass cover
D_{ri}	Inside diameter of the receiver tube
D_{ro}	The outside diameter of the receiver tube
EEP	Ethiopian Electric and Power
$EEPCo$	Ethiopian Electric Power Corporation
EES	Engineering equation solver
e_g	Glass cover emittance
E_{ot}	Equation of time
$EVAP$	Evaporator
e_r	Receiver emittance
F'	Collector efficiency factor
F”	Collector flow factor
FCH_1	First flash chamber
FCH_2	Second flash chamber
F_R	Heat removal factor
G_b	Beam radiation
G_{bhor}	Horizontal surface beam radiation
G_{bi}	Inclined surface beam radiation

GDP	Growth domestic product
G_o, G_{ext}	Extraterrestrial radiation
G_{sc}	Solar constant
H_2S	Hydrogen sulfide
h_{cca}	forced convective heat transfer coefficient
H_{crf}	Convective heat transfer, recievr-HTF
H_o	Extraterrestrial solar radiation on a horizontal surface
Hp	Horse Power
HPT_1	The high-pressure turbine of the geothermal system
HPT_2	The high-pressure turbine of the solar system
h_{rca}	Radiation heat transfer coefficient
h_{rrc}	Convection heat transfer coefficient
HTF	Heat transfer fluid
IAM	Incidence angle modifier
inf	Influent
Inf_2	Influent 2
$Infc$	Influent water from the clarifier to the equalization tank
$Infth$	Influent water comes from a thickener unit
$JICA$	Japan International Cooperation Agency
K_{HTF}	Thermal conductivity of the HTF
KNO_3	Potassium Nitrate
LL	longitude of the location [degrees]
LPT_1	The low-pressure turbine of the geothermal system
LPT_2	The low-pressure turbine of the solar system
LST	Local solar time
MW_e	Megawatt of electricity
$MLSS$	Mixed liquid with suspended solids
$MLSSc$	Mixed liquid with suspended solids in the clarifier
N	Number of day of the month
$NaNO_3$	Sodium nitrate oxide
$NaOH$	Sodium Hydro oxide
NH_3	Ammonia
$Nu\#$	Nusselt number
$OFWH$	Open feedwater heater
ORC	Organic Rankine cycle

$ORRC$	Organic Reheat Rankine Cycle
PEM	Proton Exchange Membrane
P_{rHTF}	Prandtl number of the HTF
PTC	Parabolic trough collector
PV	Photovoltaic
Q_u	useful heat gain
R	Thermal resistance
R_b	Correction factor
R_e	Reynolds number
RO	Reverse Osmosis
SDS	Sustainable development scenario
SEP_1	First separator
SEP_2	Second separator
$Sludgec$	Sludge removed from clarifier
$Sludgeth$	Sludge thickener
$SMLTZ$	Standard meridian local time zone
$SPDS$	Solar parabolic dishes
TS	Solar Time
t	Transmittance
T_{amb}	Mean temperature
T_{avg}	Average temperature
T_c	The temperature of the glass cover
T_e	The outlet temperature of the HTF
T_{fi}	Inlet heat transfer fluid temperature
T_r	The surface temperature of the absorber tube (receiver)
T_{sun}	Temperature of the sky
T_{std}	Local standard time
TW	Treated water
UL	the overall heat loss coefficient
USA	United States of America
USD	United States Dollar
V	The velocity of the HTF
WHO	World Health Organization
U_o	Overall heat transfer coefficient
h_{fi}	Convective heat transfer coefficient

S_o, T_o, P_o, H_o	Dead state entropy, temperature, pressure and enthalpy
E_{xn}	Exergy destruction of n component
A_a	Aperture area of the collector
Q_s	Solar heat absorbed by the collector
K_θ	Incidence angle modifier
α	Solar altitude angle
β	Tilt angle
Γ	Solar azimuth angle
δ	Soar declination angle
η_{th}	The thermal efficiency of a solar collector
θ	Solar incidence angle
θ_z	Solar Zenith angle
μ_{HTF}	The viscosity of the heat transfer fluid
ρ	the reflectance of the mirror
ρ_{HTF}	The density of the heat transfer fluid
τ	the transmittance of a glass cover
ω	Hour angle
ω_s	Sunrise hour angle

Chapter 1

Introduction

1.1 Background

In Ethiopia's energy generation history renewable energies share comes first, hydroelectric power is the heart of the energy load distributed in the country. The amount of energy generated is mostly serving industry and in urban areas.

The case study area for the project is based on the existing geothermal energy source of Aluto Langano which is implemented in 1998 with a capacity of 8.5MWs (11,400hp). The amount of net power produced by the plant is about 7 MWs (9800hp). The modification has been carried to raise the potential of the geothermal plant to 70MW in 2015. The operator of the project was Ethiopian Electric Power (EEP), in the country for the past long years the energy generated in the private sector was locked business or the produced energy should be expected to be fed to the grid. Currently, the government encourages investors to make business in power production. Geothermal production walls have an electrical energy capacity of 5.6 to 10 MWe Aluto Langano power plant has 10 production wells, two of the wells are drilled directionally in 2015 and the rest of all eight (8) wells are vertically drilled on the first phase installation time in 1980.[1]

Global energy consumption is reliant on fossil fuel which consequence creates a drastic change to the climate system due to the greenhouse gas released from non-renewable energy sources. The access to electricity between 1990-2010 has been augmented and delivered for 1.7 billion peoples. After 2011 the alternative power share crossed 20% from the total energy converted globally and planned to pass 32% in 2030, [1].
Sustainable unceasing natural renewable energy sources jumped 28% by 2020 with 60% of modern renewables like hydro, solar, wind, biomass, and biofuel the remaining 40% is the usage of traditional biomass for heating and cooking that is consumed in developing country residents, [2].

The intermittency in power production from renewable energies can be resolved with the consolidation of diverse energy sources termed hybrid as an approach to convert and afford a consistent quantity of energy for the obtainable demand. According to anticipations, the carbon dioxide emission is forecasted to decrease by 75% from the level in 1985 with augmentation of energy efficiency, conservation, and alternative energy implementation technologies, [3].

Ethiopia has a considerable resource of geothermal energy in rift valley regions. A geothermal energy source is formed due to the volcanic reaction inside the earth and different projects have also been planned for power generation. Combining solar with geothermal benefits to produce peak load of electrical engineering. In updated researches, the organic Rankine cycle is one of the main operational ideas to recover waste heat from industries due to the ease and accessibility of its components and also merged with geothermal solar for improved energy performance and various outputs. The purposes of the systems are focused on the cooling interior, indoor heating, electricity, hydrogen production, for drying, and hot water applications. Thermodynamically computing systems lead to efficiency enhancement of the system, to make cost-effective on the investment side and running costs, and even to explore the consequence on the environment. The exergy analysis is interdisciplinary that can address efficiency, environment, sustainability, and as well the economic aspect as shown in figure 1.1.

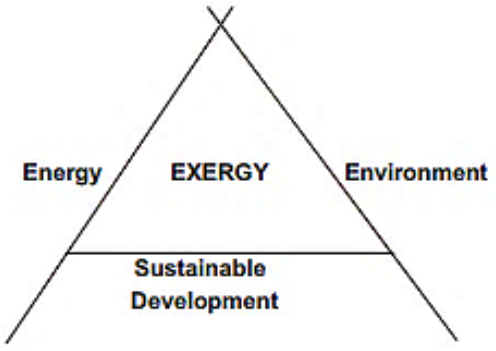

Figure 1.1: Interdisciplinary triangle that exergy analysis cover, [4].

The exergy destruction is different for the same energy sources. It depends on the specific application of the generated energy by the system. Just to explain a solar thermal system the input energy is concentrated from the sun then that energy will assist to produce work then after there is a rejected heat. To increase the efficiency up to the maximum efficiency diminishing the amount of energy rejected is a perfect solution, and Carnot's efficiency using a high and low temperature of the system can

be calculated as a maximum efficiency that is possible to achieve. Whatever things are improved at a high level accomplishing the efficiency above the optimum level of Carnot cycle efficiency of the system is impossible. Building any serviceable things currently have to be efficient in different features to come up with identified problems under the sustainable development for the future, so sustainable development linkage is wide as shown in figure 1.2.

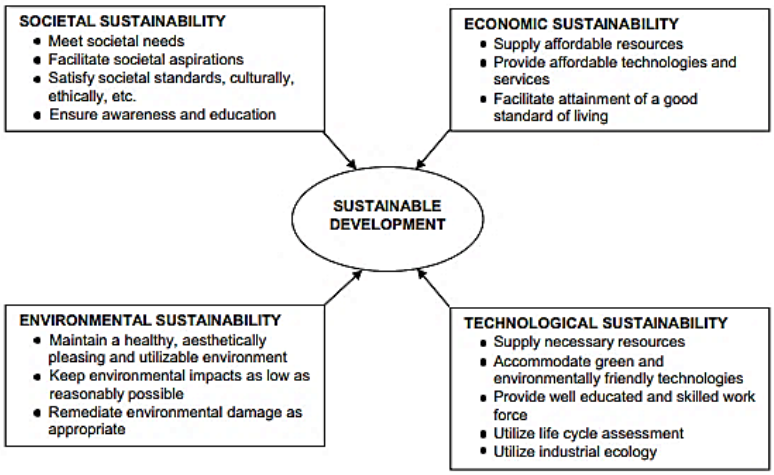

Figure 1.2: Some key requirements of sustainable development, [4]

" For affordable, reliable, sustainable, modern energy for all and climate change mitigation and the reduction of environmental and health impacts that happens to be part of the goal of sustainable development ", [5].
To degrade the quality of a useful part of the energy, exergy efficiency determination which is created due to irreversibility in the system is required. Entropy generation increases with exergy formation in the system mean the movement from order to disorder in the system rises due to exergy of thermodynamic irreversibility.

1.2 A synopsis of Geothermal and solar-thermal energies

1.2.1 Geothermal Energy Technology

The core of the earth is full of energy with renewable and non-renewables coal, crude oil, petroleum, natural gas, and environmentally friendly Geothermal energy. The earth's heat is captured to maintain comfortable indoor air in industries and domestic use or steam for energy generation. According to the SDS, the growth of geothermal technology over the last five years has not exceeded 3% per year, even though in 2030 this sector intended as a goal to increase the potential 10% in each year within 500MW power generation, [6].

Among the alternating energy sources, geothermal energy is highly reliable and less maintenance necessity with long purposeful years, as well efficient with substantial environmental impact prevention by reducing 80% of fossil fuel practice.

The inner core of the earth has a significant amount of heat which is estimated greater than 5000^0C, temperature increases between $20 - 30^0$C per kilometer to the ground. To generate electricity using geothermal energy drilling the earth 2-3km is required typically. The pressure of the underground rises 14 psi or 1 atm per 10 meters depth to the ground, [7]. The reliability of renewable energies as shown in the

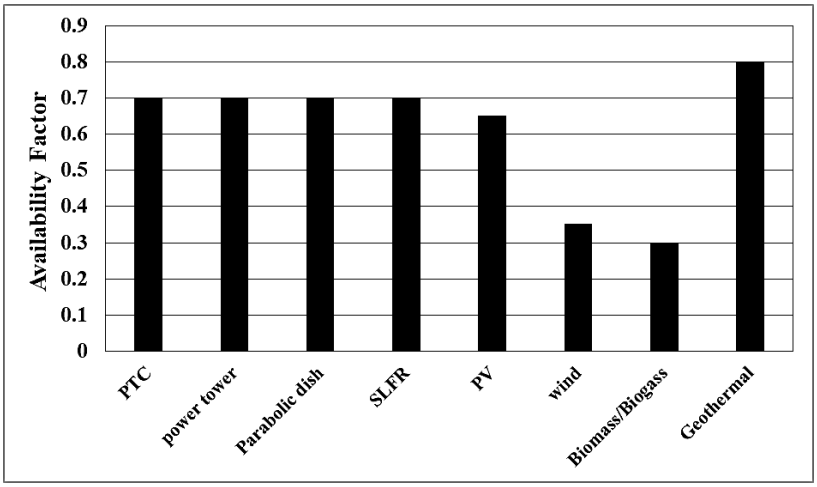

Figure 1.3: Reliability of renewable energies,[8]

above histogram graph that explained in the availability factor starting with 0.1 as a low-reliability indicator while the 0.8 reveals that the highly reliable energy source. The availability factor is the ratio of the amount of time that the power plant can generate electrical energy over a certain period and the total amount of time of the period. As we can see in figure 1.3, geothermal energy is more reliable while solar concentrators are the second reliable energy source.

The flash steam, binary cycle, and dry steam geothermal technologies are used for power generation, heating, and cooling applications worldwide. Flash steam is leading by installed capacity which operates at a higher temperature beyond 182^0C, through the extraction of high-pressure hot water passing into useful components of flashing unit and separator to distinct the steam that runs steam turbines coupled with a generator for electrical energy conversion. The binary cycle differs from the flash type the hot water is pumped to the heat exchanger to boil the heat transfer fluid due to functionality under low-temperature range. In dry steam type geothermal directly

steam is mined to rotate the steam turbine directly piped from the underground wells. Italy was the first country to install dry steam type geothermal power in 1904, [9].

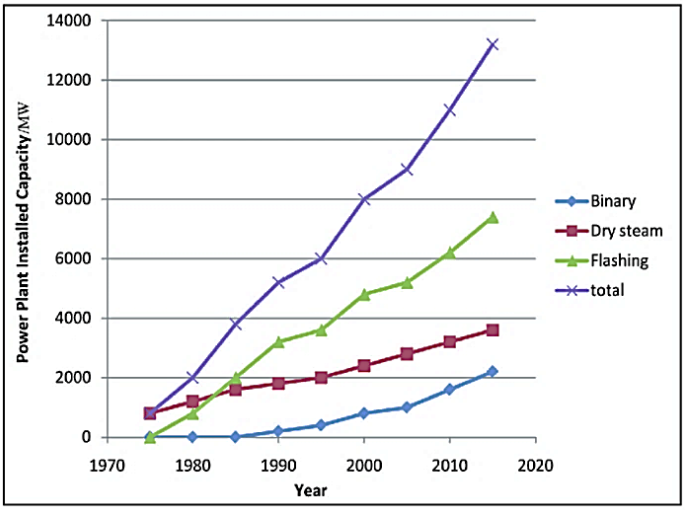

Figure 1.4: Geothermal energy conversion technologies growth[10]

Figure 1.4 provides the information of the globally installed capacity of the different kinds of Geothermal energy technologies results flashing is widely usable than the others.

The geothermal energy technology installation capacity expected as augmented within few years, as observed from the figure 1.4, the total power plants available in the world have a wide difference in the range of 8000 MW from 1980 to 2015. This potential meets the goal beyond the forecasted and the resource utilization considerably to satisfy the energy demand is growing continuously in source full countries.

Conforming to the 2030 strategy of Ethiopia to balance the reliance on the hydropower in order with other renewable energy sources to answer the electricity need in the country, hence in the next ten years to exploit 1000 MW power the feasibility analysis has conducted to corbetti, tulu moye, aluto Langano, Abaya and tendaho as a visionary site for the bright future of the population.[12]

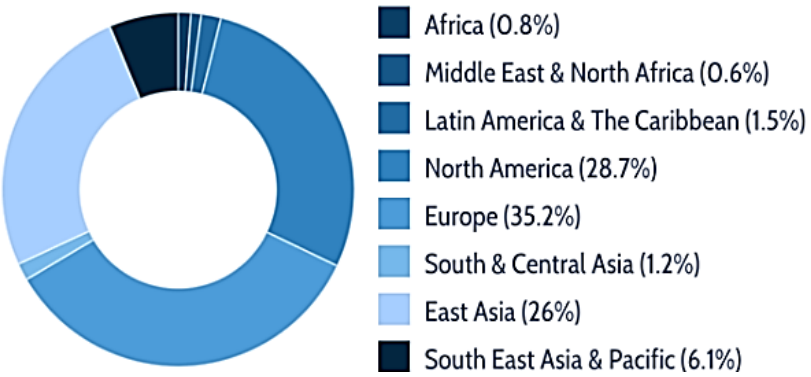

Figure 1.5: Geothermal installed capacity of continents,[13]

According to the world, energy council report figure 1.5 represents the share of geothermal power plant in all continents China, the USA, Turkey, Sweden, Iceland, Philippines, Indonesia, Japan, New Zealand, and Italy are the top ten countries by the potential of geothermal installed capability.

1.2.2 Concentrated solar power Technologies

Now a day's solar energy is a promising renewable energy source that can capture heat from the sun using different concentrating collectors. The concentrating collectors focus the sun's heat to make steam and electricity. The natural heat from the sun reflected against the mirror focus all of that heat in one area, connecting it with a power systems turbine and generator to produce renewable-based energy. The concentrating solar technologies are more expensive and need significant maintenance work.

The concentration ratio of concentrating collectors greater than one from the ratio of aperture area and focus area. The concentration space is smaller and has a larger aperture area that rises the concentration ratio. Clean and consistent energy-generating technique by transforming solar energy into heat for valuable work. The solar energy is concentrated by using mirrors and lenses as a concentrator then directed to the receiver. There are four types of CST. They are:

1. Solar parabolic trough collector (SPTC)
2. Solar power tower
3. Linear Fresnel and
4. Solar parabolic dish

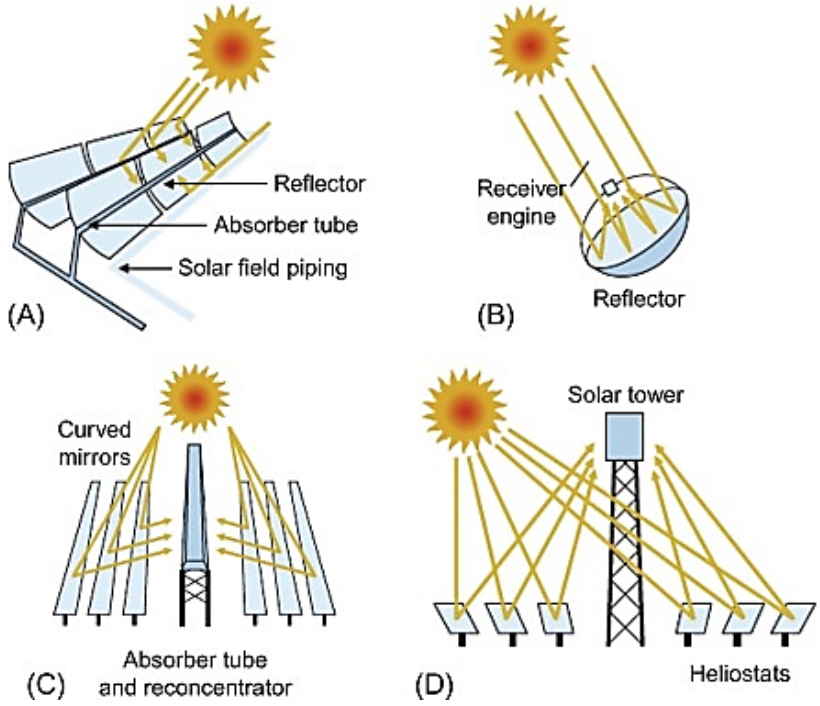

Figure 1.6: Solar concentrators (A) PTC (B) SPDs (C) Fresnel lens and (D) solar tower, [13].

Parabolic trough collector: one axis of rotation type solar collector known as single-axis tracking that collects the sun radiation falls parallel to its axis. The collector rotates horizontally, vertically, or tilted, the most commonly used type is the horizontal single-axis tracking mechanism. The parabolic collector reflects the solar incident and passes onto the focal line toward a receiver tube. The heat transfer fluid temperature increased by absorbed heat by the receiver. The operating temperature of the parabolic trough collectors is in a range of 500-700K with approximately 200 of geometric concentration ratio.

Solar power tower: various heliostats concentrate the sunlight on to the central receiver adjusted on the top of the tower. The land requirement for installation is more.

Linear Fresnel: the sunray tracked by the several slightly curved downward-facing mirrors that move in a single axis independently to reflect into the stationary receiver pipe. The concentration of light that comes from a different angle onto the single point is improved by multiple refracting planes.

Parabolic Dish:is a bulky and high-cost device operating over 1800 K temperature of the system. The solar tracking system is a two-axis tracking system. The sunlight is concentred by a parabolic dish collector toward the receiver located on the focal point of the dish collector.

Table 1.1: CST fundamental information's

CST	**Solar tracking axis**	**Focusing**	**Concentration ratio**	**Temperature range**	**Efficiency**
PTC	Line	One-axis	30-100	60-700	60-80%
Linear Fresnel	Line	One-axis	10-40	60-250	34-82%
Solar tower	Point	Two-axis	300-1500	150-2000	29-68%
Parabolic dish	Point	Two-axis	600-2000	100-1500	15-35%

1.2.3 Energy storages

To convert energy from one form to another consistently energy storing devices and materials are installed with renewable energies. The pumped storage of the hydropower plant is the major in use type to fix the seasonal flow fluctuations. Wind energy and solar energy power plants also necessitate storages, in wind power plants energy is generated continuously, whereas the demand is at the baseload to prevent the waste energy the produced excess energy stored to be used in peak demand hours. Solar is an extremely intermittent renewable sustainable source of energy due to that to use the system in the sunset times heat energy is stored in the form of latent and sensible heat using different materials.

Sensible thermal energy storages function with increasing and decreasing of the material used as a storage. The material temperature is higher at the energy absorbed charging process and discharging happens with energy drop of the material reducing to loss its temperature. The energy stored cannot be released at a constant temperature as a drawback of using sensible heat storage.

PCM as a thermal energy storage that stores latent heat for the consistent power output throughout the day.Molten salt storage is a solid at atmospheric pressure and zero degree Celsius that used as a heat transfer fluid, as the temperature increases the salt changes the phase or stage from solid to hot liquid. Molten salt storage is well insulated and heat loss does not exceed 1-5%, once stored energy can long last for 2 months without utilization. Molten salt storage coupled with solar thermal

systems can provide energy continuously 24 hours. $NaNO_3$, KNO_3, and $NaOH$ are the most commonly used kinds of salts in the molten salt storage market, their working temperature range is 300,500 and 320^{o}C respectively.

Molten salt thermal energy storage boiling point, volumetric heat capacity, and power density are higher, while the viscosity and vapor pressure are lower. [14]

1.2.4 Organic Rankine cycle (ORC)

ORC is a mechanical cycle that converts the pressurized and high-temperature steam into Work using a turbine. The name organic implies the organic compound used as a working fluid for a low temperature of the boiling point than a water application.ORC system components are pump, evaporator, expander (turbine), and condenser. The low and medium-grade heat from different industry wastes and other energy sources like solar thermal used to generate useful power. Modifications on ORC are required compared to the conventional cycle the efficiency is lower due to the conversion of low-grade heat into work. An organic working fluid is evaporated through the evaporator, instead of boiling water to create steam in the boiler that turns a turbine to generate electrical power. The cycle operates at much lower temperatures than a steam Rankine cycle works. To recover the exhaust waste heat using the ambient air as a heat sink ORC is a tangible alternative.

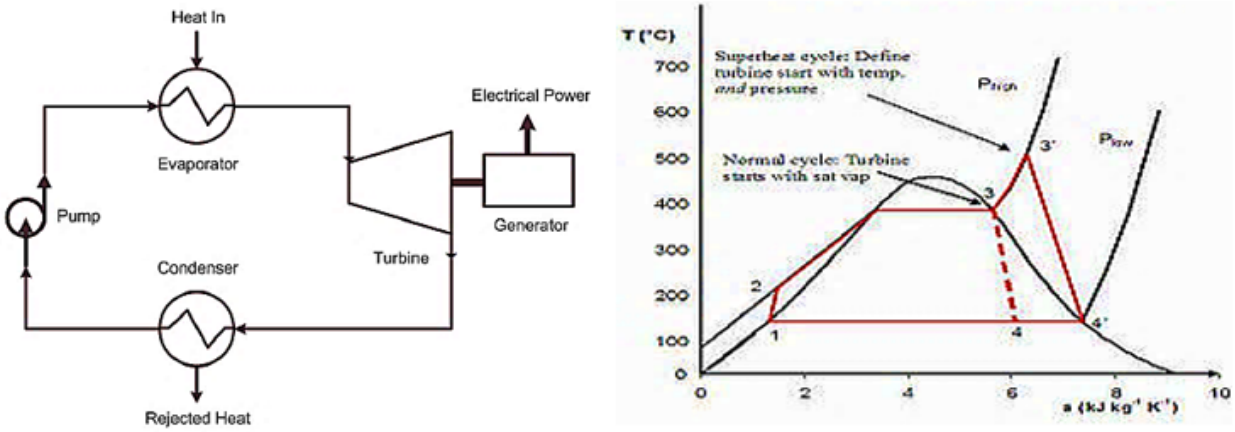

Figure 1.7: ORC system and T-S diagram, [15].

The four processes of an ideal ORC are, as shown in the figure isentropic compression in a pump, Constant pressure heat addition in an evaporator, and isentropic expansion in a turbine and condensation.

1.3 Organic reheat Rankine Cycle

The reheat ORC vaporizes the working fluid through the evaporator then arrives at the turbine to perform work after the organic compound vapor passes through the turbine, withdraws into the evaporator, and heat up. The reheated working fluid vapor moves to the second low-pressure turbine for better performance.

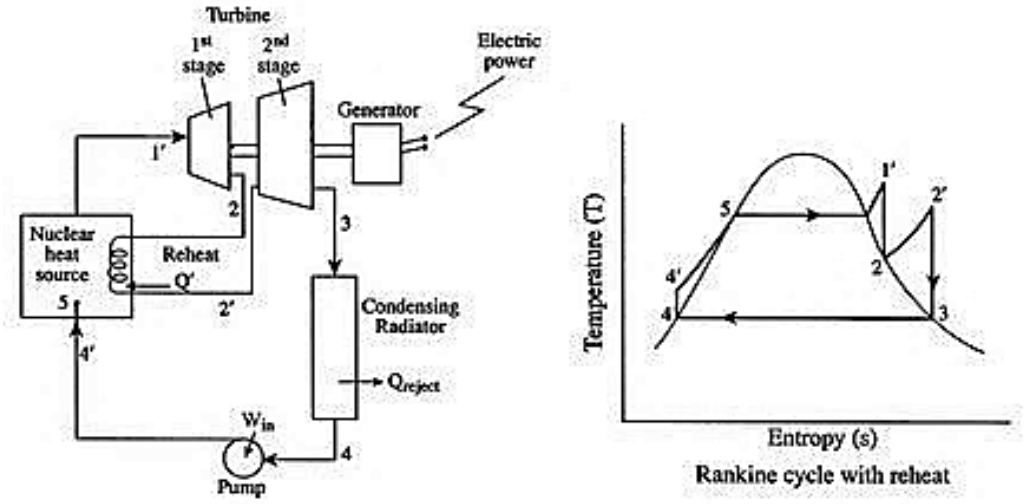

Figure 1.8: Organic Rankine reheat cycle system and T-S diagram, [16].

1.4 Water treatment / Reverse Osmosis

Naturally, water is pure since made from the only mixture of hydrogen and oxygen. The reason to be polluted and impurity of water is the place that kept by it. At present, the key to contaminate water is disposals which are man-made impurities such as plastics, organic wastes, solid wastes, and chemicals released to the water sources. According to the data from the water organization, in Ethiopia, the clean water supplied to the population is estimated at 42% while only 11% of the supplied water has sanitized using adequate purification methods.[17]

Water is treated in a standard way through coagulation/flocculation, sedimentation, filtration, disinfection, sludge drying, fluoridation, and PH correction for drinking purposes.

In the Reverse osmosis water purification process, influent water impurities are removed by pushing it at high pressure through the filtering membrane. The adsorption system is also one part of the RO advanced water treatment technology, the

contaminant particles stick on the adsorbent so it is a surface phenomenon. Adsorption cannot kill harmful living organisms available in the water, boiling is a technique that removes bacteria, worms, and other micro living organisms. For this purpose, the water has to boil at its boiling point which is considered as a sterilization thermal disinfectant. The water treatment using thermal disinfection method benefits to produce highly pure portable water based on the exposure to high temperature.

1.5 Problem statement

Global warming is a concerning issue since fossil fuel is a basis of environmental pollution and earth temperature raise. From the energy use pattern data of Ethiopia, the foremost quota of energy consumption is for the industrial sector and 91% of the population demand for energy relies on the traditional biomass energy, [18] due to the limited access to modern, clean and green energy sources. The energy source of the country is more focused on sustainable, renewable energies though the power is unaffordable for every population. The energy supplied by Ethiopian Electric Power Corporation /EEPCo/is incomparable to the need for energy in the country. However, the position in contrast to the realities on the ground, about 70 percent of the population in Ethiopia is living in dark without electricity. The access to electrical energy of primary schools and health centers have estimated 24% and 30%, [19].

The difference between abundant assets and unmet desires for energy indicates the need for a radical new approach.

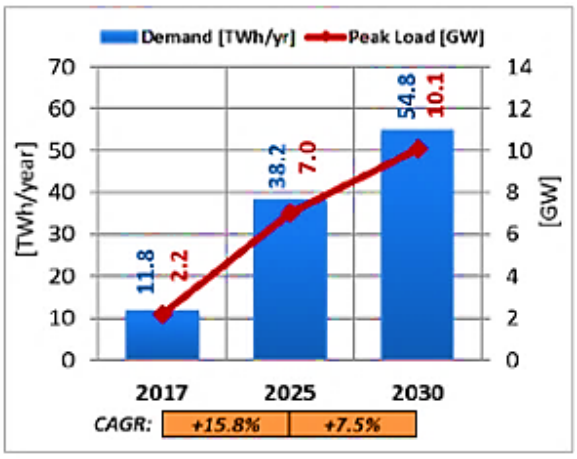

Figure 1.9: Energy consumption increment forecast by 2025 and 2030 considering transmission loss, [22].

The assessed 20-25% transmission loss through transferring the produced electrical power in different corners to the insufficient substations and the consumers,[22].

Concerning the water treatment requirement, protected water is inaccessible to 62 million of the population in Ethiopia whereas 97 million are in lack of improved disinfected water, [23]. The exposure to impure water consumption causing health risks are increasing.

In addition to the above-mentioned problems unemployment is a concerning issue, as a developing country due to the inadequate distribution of electrical energy, the industry sector production inconsistency, agricultural productivity reduction has a direct effect on the GDP growth.

1.6 Research Objective

1.6.1 Main objective

The general objective of this research is an Exergy analysis of SPTC- double-flash geothermal integrated power plant with sterilization and RO water treatment that is used to produce power and potable water from environmentally friendly energy sources.

1.6.2 Specific objective

- To estimate the solar radiation of the case study area.
- To investigate the performance of different parabolic troughs, and the thermal performance of SPTC.
- To examine the integrated hybrid system exegetically and look into irreversibility formation in components
- To determine the dominant parameters in the energy conversion system
- To check the performance of the water purification system
- Validation of the results.

1.7 Significance of the study

Ideas for Researches and projects started from the resource and/or demand availability, which is known as resource-based and demand-based. This research worth to be implemented since the legion need for energy and natural resource is at hand. The designed stand-alone combination of a solar thermal and geothermal system can overcome an extensive power shortage problem in the country. Cholera, diarrhea, typhoid, dysentery (intestinal infection), worms, and trachoma (eye infection), are the common health problems in Ethiopia, diseases caused due to consumption of raw

water. The advanced level of water treatment mechanisms can eliminate health risks. Solar thermal energy is the conversion of the solar energy that is obtainable only in the date period, this intermittency has covered with integration to another renewable energy source geothermal and thermal energy storage. The economic development of the community, reduction of deforestation, GDP growth, and employment opportunity comes with the provided green energy.

As research, this investigation used to identify the real performance of the plant relies on the second law of thermodynamics considering losses and useful available energy. It has analyzed in detail using actual data and reasonable assumptions so that worth to be a reference to the next researchers in worldwide publishing it in international journals.

1.8 Scope

The activity starts from designing the thermodynamic model on Aspen plus V11 software, which has multiple purposes including power generation using solar and geothermal renewable energy sources, boiling, and RO water treatment. The working fluid for the organic Rankine reheat cycle has been selected following the specified standard. Several parabolic troughs have been compared in performance to be selected to combine with the geothermal system. The exergy analysis of the system has conducted using EES software. The parameters that will affect the function have been identified (such as, ambient temperature, pressure, turbine outlet pressure, production well flow rate, and inlet temperature. The RO water treatment has been modeled and analyzed on GPS-X hydromantis software. Finally, the results have been validated with related recent research outputs.

1.9 Thesis Organization

The research document contains 7 chapters, a bibliography of the cited references, and important pieces of information as appendices. Chapter one is the general introduction about renewable energies specifically, overviewing solar and geothermal technologies. The objectives of the research, the boundary of the investigation as a scope, and its significance are also mentioned in this section. The second chapter is the review of the existing related articles and books as a literature review, more of the hybrid plants' thermodynamical investigation, water purification technologies, and the property of heat transfer fluids are reviewed to understand the research gap associated over the recent works. Chapter Three contains the methodology and materials used

for the achievement of the research, such as EES and GPS-X hydromantis software. The analysis part starts in the fourth and fifth chapters with the thermal analysis of the SPTC and exergy analysis of the overall integrated system. Chapter six deals with the outputs of the software as a result of graphical representation and their discussion based on scientific logic. The seventh chapter is the conclusion and recommendation part considering the important points in the overall work as a summary and to acclaim what more researches are needed for better performance.

Chapter 2

Literature review

The advancement of all forms of renewable energy over recent years has surpassed entire expectations as a result of global installed capacity and production potential. Alternative energies are an extensive tool to develop energy security, mitigation, and adoption to climate change with a recognized enhancement of economic advantage directly or indirectly by reduction of dependency on imported fossil fuels. Currently, renewable energy technologies have cost-competitive with non-renewable energy technologies.

The evaluation of the irreversibility formation impact on the incidence rate for the PTC driven ORC system results as a solar thermal unit is highly exergy destruction facing energy source with 74.9% collector exergy destruction and 18.2% irreversibility is in the condenser. The performance improvement with an increment of turbine inlet temperature rises the exergy efficiency, power output, and expansion ratio.[24].

Adsorption, absorption, sterilization, pasteurization, and disinfectant chemicals are the water treatment technologies used as a water improver. Specifically, the exergy analysis has been conducted for the solar-based distillation of saline water than freshwater to improve efficiency. The analyzed absorption material types are black ink and black dye in saline water as well as for water surface the black toner kindest. The energy and exergy efficiencies for all absorption material kinds are 41.3%, 43.42%, 45.79%, and 5.91%, 6.34% 7.1% respectively. The exergy destruction is visible on basin line benchmarking with glazing and saline water.[25]

The performance investigation of the organic Rankine cycle operating at a pressure and temperature above the critical point combined with the solar thermal and geothermal off-grid power plant results in 27-34% exergetic efficiency under the supercritical working condition. According to the validation supercritical exhibits better performance while compared to 23-32% exergy efficiency of the subcritical.[26]

The conventional coal power plant integrated with the solar tower to moderate the exhaust gaseous unconfined pollutants to the atmosphere to keep sustainability. In this investigation, exergy and economic analysis have been conducted and validated

with the coal-fired plant. As a result, the combined conventional and renewable energy reduces the released toxic gases to the environment by 4.6%, while the exergy efficiency of the system is 35.8%. According to the economic analysis, the capital investment of the hybrid is about 8050.32$/KW where the coal-fired is 5979.69$/KW this is due to the equipment's cost that makes costly the hybrid system. The customers have expected to pay the electricity bill of 0.19$/KW for solar towers coupled with coal plant power and 0.12$/KW for the coal-fired plant.[27]

The analysis to eliminate the energy fluctuation, hybrid systems are promising technologies with integrated solar and geothermal renewable energy sources connected to TES. Possibility of generating multiple outputs within a particular combined system such as heating, cooling, electrical energy, hot water, and drying application at 69.6% energy efficiency and 42.8%exergy efficiency.[28] Multiple technologies combination proposal of PV fixed with solar concentrated and geothermal using PEM fuel cell as an energy storage unit. The performance of the storage and the thermal efficiency has been evaluated including the parametric investigation. The outputs are power, cooling, and hydrogen production using the electrolysis method which is input to PEM fuel cell. The overall thermal efficiency and storage unit efficiency enhanced from 15.72% to 17.78% and 18.21% to 21.95% separately.[29]

In the development of a hybrid energy source that can generate multiple outputs including cooling through absorption, electrical energy, heating, and drying processes supplied by a combination of the solar parabolic trough with the geothermal system. This plant has also integrated with two thermal storages and two organic Rankine cycle and examined exegetically. From the computation, 51% of energy efficiency and 62% of exergy efficiency are recorded while the single generation exhibits 22% of energy efficiency and 54% of exergy efficiency.[30]

The economic feasibility and the irreversibility occurrence determination on geothermal power plants with R245fa considering as an HTF which is a nonflammable and dry type organic compound. The temperature sessional variation over the year the exergy efficiency fluctuated with 2% and 18.2% of energy efficiency with 21.3% of exergy efficiency is computed. From the economic analysis, the payback period of this power plant is 15 years since the drilling work costs 4.2M USD and for construction 521.5 M USD is used. The specific electrical power generation by the power plant is 31.43KJ/Kg and 172.97 KW/K net rate of entropy change has been evaluated [31].

The combined solar thermal and fossil fuel has been analyzed exegetically on

a specific date and time. The parameters are also varied such as different working temperatures, pressure, steam flow rate, collector output temperature, and others. The major exergy loss occurs in the parabolic trough collector and boiler which is estimated at around 68.32%. The minimum and maximum exergy losses are 32.7 and 23%with 26% of exergy efficiency at 95 bar pressure.[32]

A reheating and regeneration unit's addition to the organic Rankine cycle enhanced the overall exergy and energy output performance. Each component of the reheating and regeneration Rankine cycle plant is analyzed to identify the cause of the losses. From the study, 42% of thermal efficiency and 70% of the steam generation efficiency of the unit are calculated. An economizer absorbed 39% of maximum heat while coal consumption has an estimated 40TPH. This system improves the plant thermal efficiency of about 6-8% due to reusing the waste heat with additional turbines and regenerating unit.[33]

The usage of phase change material as a heat energy storage in the form of latent heat to the erratic solar thermal energy generator drier and heating purposes is an auspicious entity to improve the useful energy efficiency. Organic, inorganic, and eutectic PCM latent heat storage freezes and vapourises approximately at constant temperature and performs compared to sensible storage by 5-14 times. Phase change materials store energy through the change of liquid and solid to the gaseous state, solid-phase change to gas, solid to solid due to the conversion of crystalline to another form that results smaller in volume and latent heat value. Solar concentrator integrated into the organic Rankine cycle with PCM exhibits enhanced exergy efficiency by 10 % improvement through exploiting power after the sun goes down moderately than the concentrating collector without energy storage ,[34].

Mathematical exergetic performance evaluation of the geothermal power generation plant potential with injection and by guiding the exhaust waste heat into the evaporation pond component has inspected exergetically, even though the power plant with the vapourization pool develops the major loss that affects the overall exergy efficiency by 4%. According to the study, the usual injection and evaporation pond connected system results in 51.5% and 47.5% exergy efficiency respectively, [35].

According to the WHO assessment, the consumption of untreated potable water is a cause of 485,000 people's death per year. Thermal disinfection of water to remove active microorganisms such as pathogens, bacteria, and viruses. Wastewater released from industries, toilets, hospitals, and other wastewater discharging systems can be

purified and reused, while these wastes are not in the recommended distance to the safe water consequences danger health risks to death. Heat recovery assembly to the pasteurization method treatment operating at 140^0C, 10 minutes of exposure time with pressure above a partial pressure of operating temperature results energy-efficient purification mechanism relatively to other technologies,[36].

2.1 Research gap

Plentiful researches has been done, which relates to the proposed work however there are gaps to be filled as yet. Solar and geothermal renewable energies has been combined to complement each other perfectly to enhance reliability, to lower electricity cost, to flatten the customers' peak load, to reduce carbon emissions, and to apply energy-saving options.

The solar geothermal hybrid systems investigated so far are reviewed in this paper show that using numerous components especially heat exchangers are the reasons for lower overall exergy efficiency and exergy destruction formation.

The exergy analysis of the solar parabolic trough with a geothermal hybrid power plant for the application of power generation and water purification using sterilization and RO water treatment has not been investigated.

The proposed work differs from the existing works by its applications that are customized based on the need available in the country. So far Ethiopian researchers has studied the Aluto Langano production wells potential, chemicals formation under the ground, and the general performance evaluation of the plant but the existing plant Aluto Langano exergy analysis is not researched as yet.

- From the abundant investigates on hybrid systems has been designed with multiple applications such as cooling, heating, electrical energy, hot water, drying process, etc. Based on the problem in our country in this work the hybrid system modeled to solve one of the major concerns, shortage of pure water for drinking including power generation.
- The other main gap is the water treatment studies focus on a single treatment mechanism which is impossible to provide 100% pure water, while this work combines two different water purification techniques to provide high-quality potable water.

Chapter 3

Materials and Methods

The flow of the research starts with getting data from existing related recent studies as of the literature review. After the technical and deep review, all the information has been gathered to identify the research gap that has to be solved. A newly designed model has been evaluated with different software.

3.1 Study area

Choosing the area which is available for a power plant installation is an important criterion. Since the production of electrical energy from renewable sources depends on the geographical location of natural phenomena (temperature, beam radiation, ground heat source). The sites suitable for this thesis is Ziway and around ZIway areas, the power plant can be also applicable in the rift valley areas of Ethiopia. The specific site area is at Aluto langano power generation site which is existing and under the new assessed in feasibility analysis system excavation work. In Zway there are beyond 43,660 peoples.
The study area selection in this research has been made through the direct visiting of the existing and new Under the excavation Aluto Langano power plant.

Ziway is one of the towns located 150 km away from Addis Ababa in the south of central Ethiopia in Oromia Reginal State in East Shewa Zone bounded. The town has geographical coordinates of $7^0 56N 38^0 43E$ latitude and longitude with 1643 meters of an altitude above sea level.

Figure 3.1: Google map image of the Ziway and Aluto Langano power plant

Aluto Langano exploration, feasibility analysis, and the final work took 18 years from 1981 to 1999 for the 7.3 MWe electrical power generation. To expand the power plant based on the available resource at the location of the aluto volcano rift valley area to 70 MWe EEP deals with different companies in 2019 and the excavation work has started by JICA.(japan international cooperation Agency)

3.2 Data collection process and types of data

The primary and secondary data source methods have used in this study through field visiting and relevant data collections especially input data for the analysis from the articles correspondingly.

3.2.1 Primary data collection

The data gathering process has been done by the researcher, professionals, and engineers to be able to collect reliable data. The data collectors' has moved to the Aluto Langano power station and directly asked the respective responsible authority to share input parameters of operating condition about the new under excavation power plant.

3.2.2 Secondary data collection

Secondary data is existing summarized and collated data that used to increase the inclusive efficacy of research. Articles, books, Metrological data from the agency, television news, and newspapers were used as a reference that has recent evidence for the current work.

3.2.3 Data processing and analysis

This research is a quantitative method using type, Mathematical data analysis has been used to design and investigate the integrated solar parabolic trough and geothermal energy system combined to an advanced level of water treating process.

The computer programing tools and software's used for quantitative analysis and model designing are:

- Phyton program
- EES program
- LaTex
- Aspen Plus software
- GPS-X hydromantis

solar angles, exergy calculations of the integrated system in the daytime and night time fraction including collector exergy study, water treatment system performance analysis, designing the model and the document write up has carried out using the above-mentioned programming languages and software.

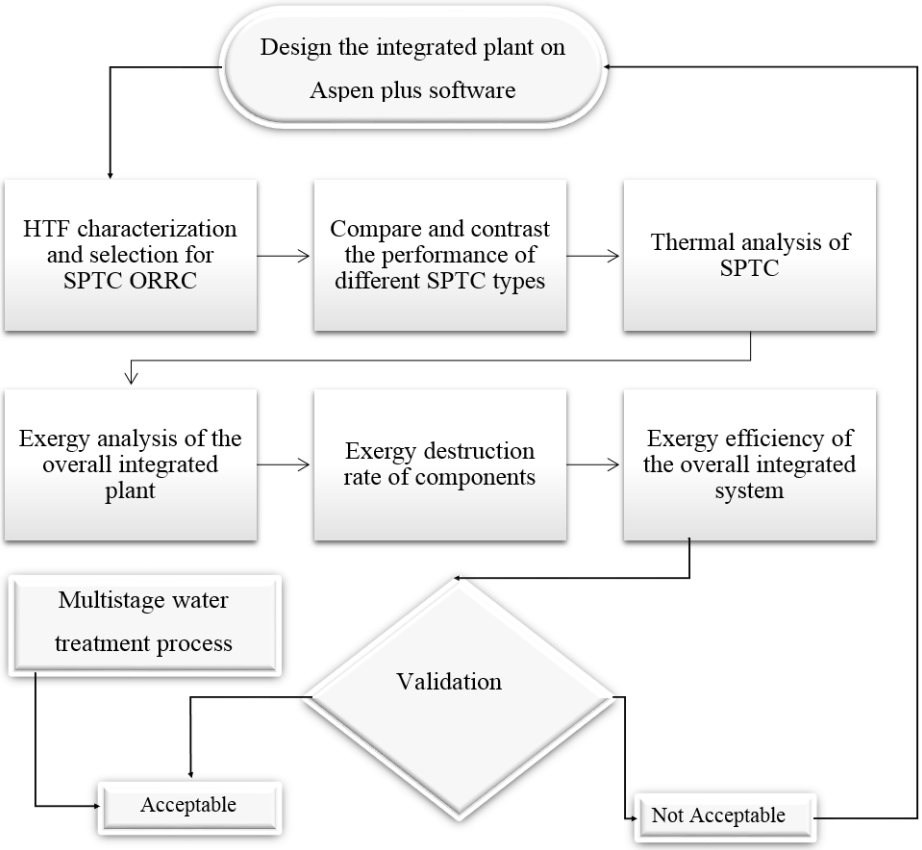

Figure 3.2: System process diagram

3.3 System Descriptions and Models

According to the specified main objective of the work, an integrated energy conversion system with water treatment application considering Aluto Langano (Ziway) as a study site has been designed and evaluated using accurate tools.

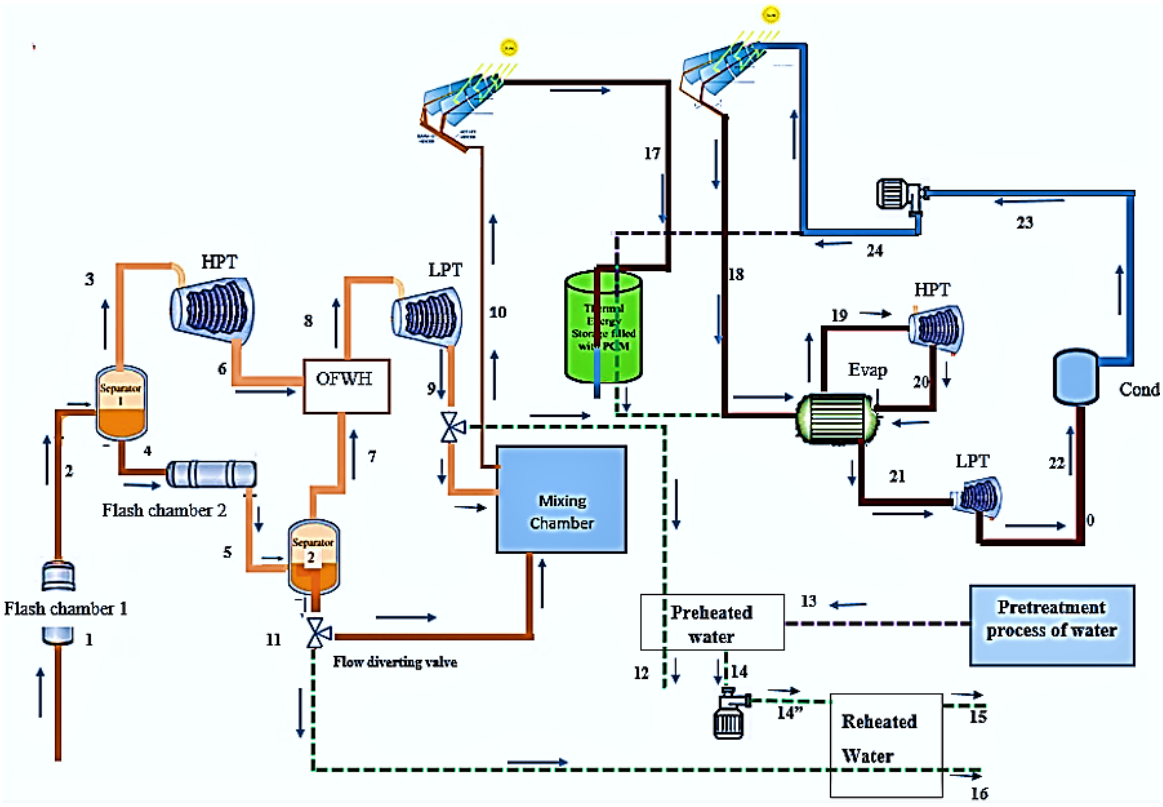

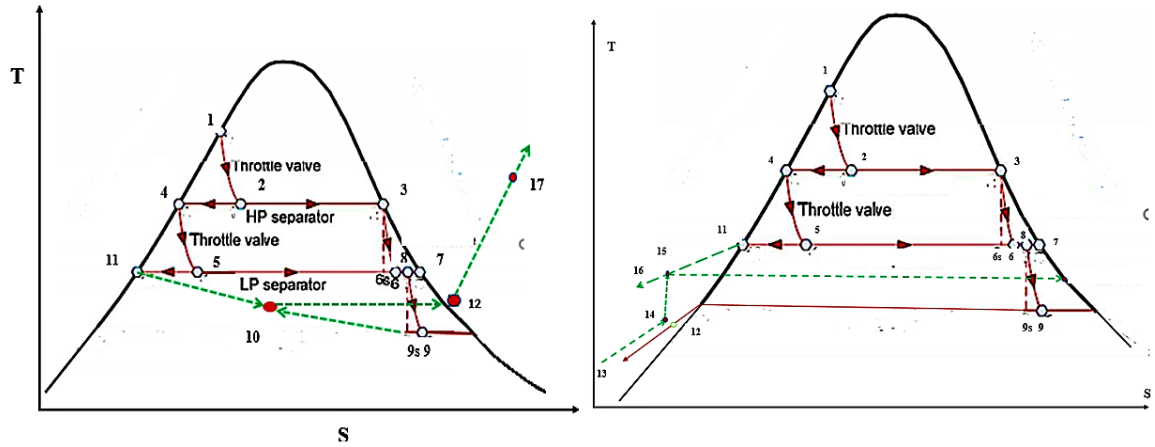

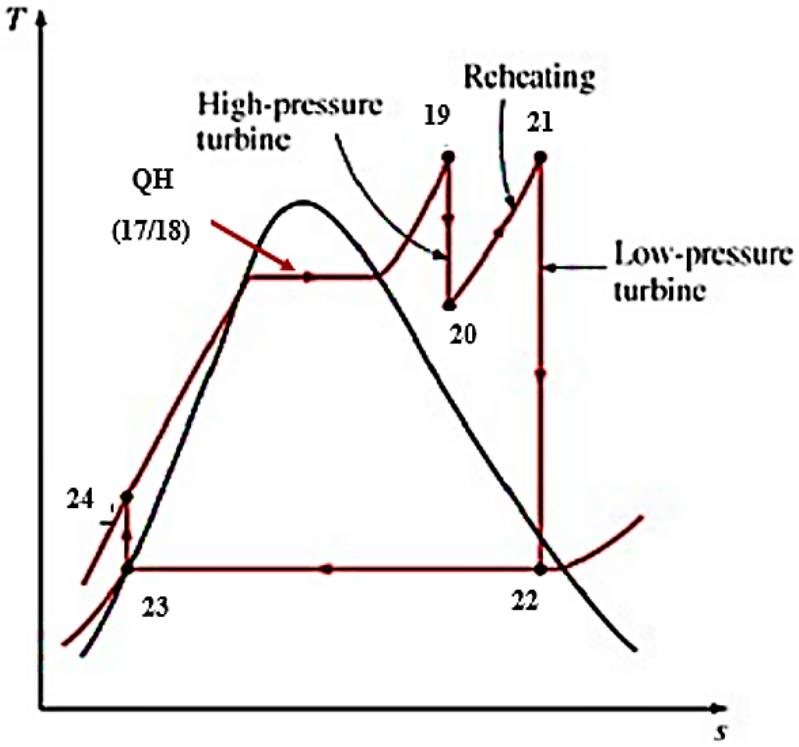

Figure 3.3: The system configuration and T-S diagram of the hybrid power plant consisting of essential components of SPTC, geothermal including boiling water treatment.

Figure 3.3 shows the system configuration of the hybrid power plant consisting of essential components of SPTC, geothermal, and RO water treatment arrangements.

The proposed plant consists:

- Organic reheat Rankine cycle
- Solar thermal energy - Parabolic trough collector
- Geothermal energy – Double flash Cycle
- Water treatment through the boiling sterilization method
- RO water purification

3.3.1 Geothermal energy system description

The hot water from the core of the earth is extracted at the point of (1) production wall to the first flash chamber. The flash chamber depressurizes the hot water and supply to the separator (2) detached the steam from the hot water, then the clean and dry steam has been directed to the high-pressure turbine (3). After the first stage turbine, the steam enters the open feedwater heater (6), the first separator releases the hot water to the second flash chamber (4) the depressurized working fluid enters to the second separator (5), then applied to open feedwater heater (7), the steam in the open

feedwater heater supplied to the low-pressure turbine (8) at equivalent temperature and lower pressure. The steam released from the low-pressure turbine (9) is directed to the the sterilization water treatment process tank 1 to preheat the pretreated water entering the container (13) using the waste heat from a geothermal low-pressure turbine. Indirect heating of the water represented in state 9 to 12, then the preheated water (14) pumped (14") to the other tank to indirectly reheat the preheated water beyond its boiling point to remove all kinds of contaminant microorganisms using the reinjected heat from the second separator (11) and passes through the tank and removed (16). The thermal-disinfection water treatment process has been carried out during night time. In the day time, the waste heats from LPT (9) and second separator (11) combined in mixing chamber, and the mixed heat at (10) directed to the independent SPTC heat exchanger since the waste heat is not enough to be used for the energy storage by melting the PCM. The solar heat exchanger increases the fluid temperature to the required level (17) and passes through the PCM unit to conduct the phase change process. PCM charging time varies with mass flow rate, supplied temperature, and its amount.

3.3.2 Solar thermal system description

The solar thermal system converts photon energy into thermal energy through parabolic trough collectors, which is highly efficient. The charged molten salt thermal energy storage tank (17) used for night time heat supplement to vaporize the HTF based on the manufacturer specification commercially available molten salt can be stand by for 7.5 hours. The SPTC concentrates and collects the solar energy heats the heat transfer fluid and then directed it to the heat exchanger (Evaporator) (18), an evaporator changes the state of working fluid from liquid to gaseous state by increasing pressure and temperature. Vaporize working fluid turns the high-pressure turbine (19) and re-enters to the evaporator to be reheated again (20). The reheated working fluid is directed to the low-pressure turbine (the pressure of the second stage turbine is about one-fourth of the first stage turbine and the temperature is almost equivalent in both turbines (21). Finally, in the solar system, the heat transfer fluid is rejected by the LPT and applied to the condenser (22), condensed, and pressurized through the pump (23) and the process will restart (24). The broken line state 22 is for the night time after the sunset working cycle continuous using the stored energy in the PCM.

3.3.3 Boiling (Sterilization) and RO

The sterilization water disinfection process heat source is an exhaust heat of geothermal system specifically low-pressure and second separator outlet waste heats. state (13) is pre-treated water supplied to the water tank to be disinfected by heat (9) and (11) for more purification of protozoa, bacteria, and virus.

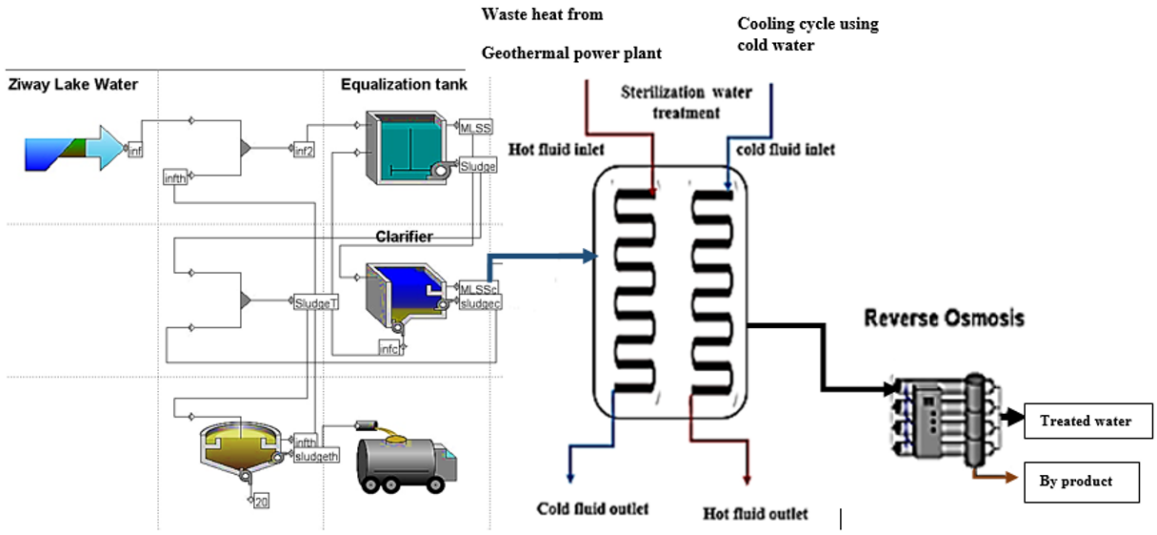

Figure 3.4: The water treatment system configuration consisting of essential stages of purification

Figure 3.4 system configuration shows the water treatment in different stages of preliminary secondary and advanced RO treatment. The preliminary treatment purpose is to settle the influent water that comes from the lake specifically Ziway lake, this lake composition is the same as wastewater due to the released water from households and industries flow to it. The equalization tank services to maintain a constant velocity of fluid based on the requirement of the next purification stages and as a removal of weighty pollutants like plastic, stones and others, additionally, the large particle pollutants discharged to the sludge thickener. A single clarifier has been used that removes midiate particles from the water and is pumped to the advanced water purification process stage. The reverse osmosis system works under a specific amount of pressure to treat influent water. The thickener unit removes the water content that comes with the sludge and the sludge is disposed to the fields considering the sludge composition.

Chapter 4

Estimation of solar radiation

The solar radiation estimation of the case study area to implement the designed system has been carried out based on the meteorological data gathered from the agency website. Ambient temperature, sunshine hours, latitude, and longitude of the location was the major inputs for the analysis.

4.1 Extraterrestrial solar radiation

The heat energy emitted by the sun that reaches and shoots the top of the earth's atmosphere is extraterrestrial solar radiation, in the opposite if the ray release is from the earth to the atmosphere it is terrestrial radiation.

The extraterrestrial radiation equation is given by:

$$G_0 = G_{sc}(1 + 0.033\cos(\frac{360n}{365})) \tag{4.1}$$

The extraterrestrial radiation result varies in a different number of the day in the month over the year from the maximum to the minimum.

Where the solar constant $G_{sc} = 1366W/m^2$ The incidence of solar radiation to the horizontal line plane uses the zenith angle as additional solar angle parameters on the extraterrestrial equation.

$$G_0 = G_{sc}(1 + 0.033\cos(\frac{360n}{365})\cos\theta_z \tag{4.2}$$

The general expiration of the extraterrestrial radiation on a horizontal surface of the earth can be calculated using:

$$G_{ext} = \frac{24 * 3600 * G_0}{\pi}\left[(1 + 0.033\cos(\frac{360n}{365})\right]\left[\frac{\pi\omega}{180}\sin\phi\sin\delta + \cos\phi\cos\delta\cos\omega\right] \tag{4.3}$$

4.2 The Solar Radiation On an Inclined and horizontal Surface

The prediction of monthly and yearly mean global solar radiation on a horizontal and inclined the surface is estimated based on the correlation using the sunshine hours.

$$\frac{\overline{H}}{\overline{G}_{ext}} = a_x + a_y \frac{\overline{n}_s}{\overline{N}_s} \tag{4.4}$$

Regression equation obtained as follows:

$$a_x = -0.11 + 0.235\cos\phi + 0.323(\frac{\overline{n}_s}{\overline{N}_s}) \tag{4.5}$$

$$a_y = 1.449 - 0.533\cos\phi + 0.694(\frac{\overline{n}_s}{\overline{N}_s}) \tag{4.6}$$

The maximum length of sunshine hours in the day and sunrise hour angle can be computed by equation 4.7.

$$\overline{N}_s = \frac{2}{15}\omega_s \tag{4.7}$$

where

$$\omega_s = \cos^{-1}(-\tan\phi\tan\delta) \tag{4.8}$$

Parabolic trough collector concentrates the direct beam radiation and converts it into useful work.

Incidence of beam radiation that reaches an inclined surface G_bi can be computed by equation 4.9:

$$G_{bi} = G_{sc}\cos\theta \tag{4.9}$$

The incidence of Beam radiation incident on horizontal surface G_{bhor} is given by equation 4.10

$$G_{bhor} = G_{sc}\cos\theta_z \tag{4.10}$$

The conversion factors to the beam radiation are given by equation 4.11

$$R_b = \frac{Gbi}{G_{bhor}} = \frac{G_{bi}\cos\theta}{G_{bi}\cos\theta_z} = \frac{\cos\theta}{\cos\theta_z} \tag{4.11}$$

Total Solar beam Radiation on an Inclined Surface used by SPTC is

$$G_T b = G_b R_b \tag{4.12}$$

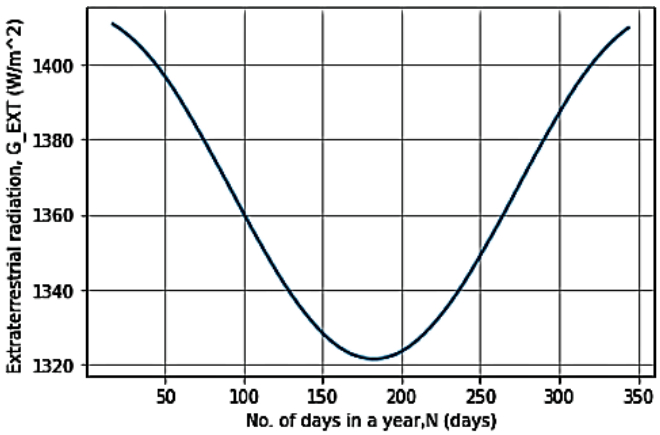

Figure 4.1: Extraterrestrial radiation through out the year

4.3 Solar time

The sun position relative to the SPTC changes over the day as the Earth rotates concerning the sun. The amount of intensity of solar radiation that hits the collector in the sunny hours affects the potential of the energy conversion system.

$$TS = T_{std} + 4(SML * TZ - LL) + EoT \tag{4.13}$$

The expression of the equation of time is:

$$EoT = 9.87\sin(2B) - 7.53\cos(B) - 1.5\sin(B) \tag{4.14}$$

Where:

$$B = \frac{360}{365}(n-1) \tag{4.15}$$

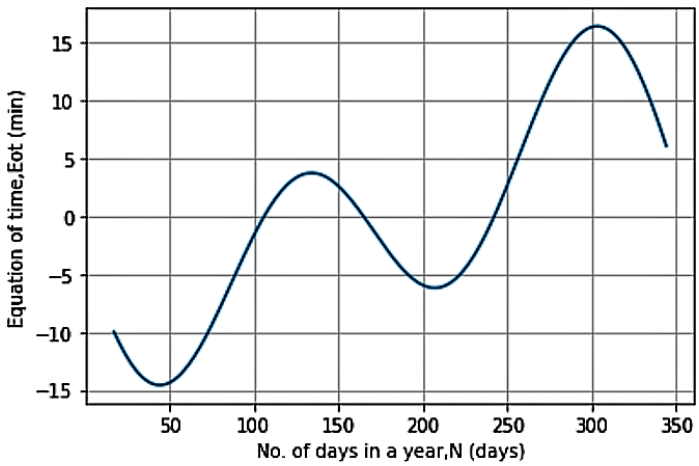

Figure 4.2: Equation of time over the year

4.4 Angle of Declination

The angle of declination is different throughout the year due to the rotation of the earth on its axis every day and every year 365 days around the sun that creates a day and a month respectively.
The angle of declination δ at the "n" days can be calculated by using equation 4.16 ,where n represents different days every 12 months

$$\delta = 23.45 \sin\left[\frac{360(284+n)}{365}\right] \tag{4.16}$$

Table 4.1: Number of days in a month of the year

Month	**The day number of the month, N**
January	i
February	31 + i
March	59 + i
April	90 + i
May	120 + i
June	151 + i
July	181 + i
August	212 + i
September	243 + i
October	273 + i
November	304 + i
December	334 + i

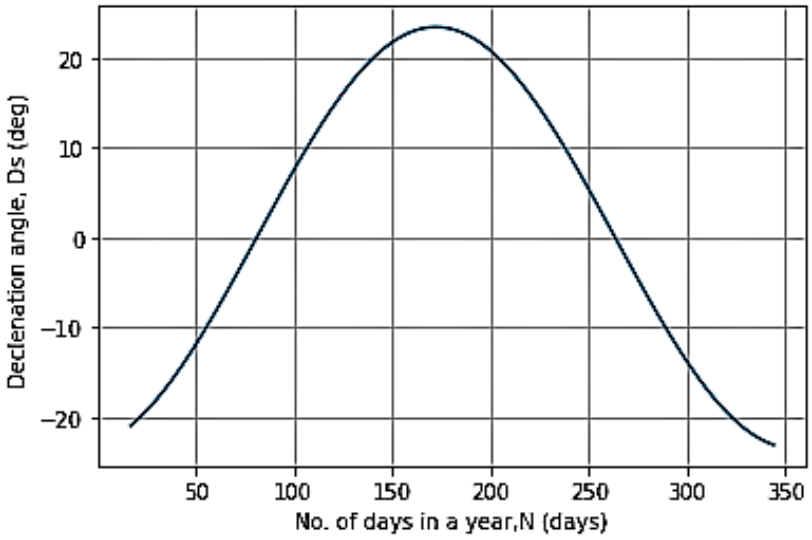

Figure 4.3: Declination angle through out the year

4.5 Hour angle

The hour angle differs from the sunrise from east to sunset west direction in the whole day time which is for 24 hours, 15 degrees in each hour measured angularly. In Ziway the maximum temperature occurs averagely from 9 a.m. to 5 p.m. The hour angle mathematical expression based on the local time hours' relation is:

$$\omega = 15(12 - LST) \tag{4.17}$$

$$LST = L_{std} + \frac{EoT}{60} + \frac{4}{60}(Ls - LL) \tag{4.18}$$

4.6 Latitude angle and longitude angle

The geographic coordinates of the earth's surface of the study area latitude angle from north to south vary in between $\leq -90^0 and \leq 90^0$ at the equator the angle is 0^0. For the Oromia region, the latitude angle is 7.93333^0 N. To specify the precise coordinate of the location longitude angle is the basic requirement for some solar angle parameter determination that ranges between 0^0 and 90^0. The case study area Ziway longitude angle is $38^0 43' E$.

4.7 Solar altitude angle

The angular difference from the sun radiation to the horizontal plane is an altitude angle which varies with the time of the day as an hour angle, the latitude of the location, and declination angle. The solar altitude angle can be calculated from equation 4.19:

$$\sin\alpha = \cos\omega\cos\delta\cos\phi + \sin\delta\sin\phi \tag{4.19}$$

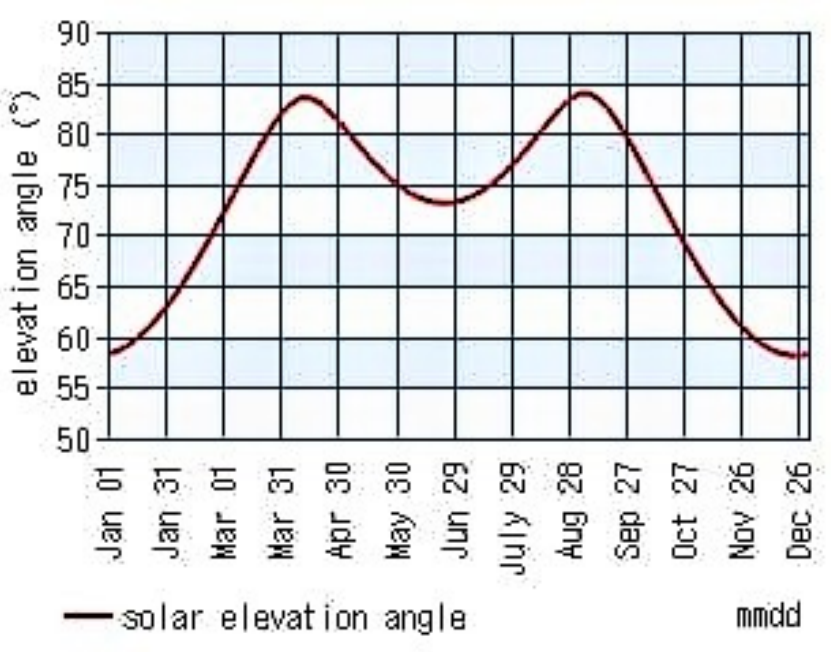

Figure 4.4: Solar elevation angles throughout the year

4.8 Zenith angle

The angular difference from the sun radiation to the Vertical plane is a zenith angle which varies with the time of the day as an hour angle, the latitude of the location, and declination angle.

$$\cos\theta_z = \cos\omega\cos\delta\cos\phi + \sin\delta\sin\phi \tag{4.20}$$

4.9 Surface azimuth angle

The horizontal facing projection of the collector relative to the equator is an azimuth angle that ranges between negative 180^0 and positive 180^0. The maximum

the solar radiation has achieved means the azimuth angle approaches zero to the south direction.

4.10 Inclination or tilt angle

The collector installation at a specified tilt angle, the angle between the horizontal axis plane and the concentrator to collect maximum available solar incidence ray to operate efficiently.
To harness the maximum beam radiation at a high exergetically efficient, the tilt angle should be equal to the latitude angle accordingly latitude angle of Ziway, $\beta = \phi = 7.93333^0 N$.

4.11 Incidence angle

The angle of incidence measured between the beam radiation of the sun is perpendicular line to the strike earth surface. The angle of incidence is a set of tilt, declination, latitude, hour, and azimuth solar angles. The angle is different with changes of a set of parametric solar angles over the day and year.

The equational expression of the angle of incidence angle is:

$$\begin{aligned}\cos\theta = {} & \sin\delta\sin\varphi\cos\beta - \sin\delta\cos\varphi\sin\beta\cos\gamma + \cos\delta\cos\varphi\cos\beta\cos\omega \\ & + \cos\delta\sin\varphi\sin\beta\cos\gamma\cos\omega + \cos\delta\sin\beta\sin\gamma\sin\omega\end{aligned} \tag{4.21}$$

4.12 Incidence angle modifier

Incidence angle modifier is the measurement of the SPTC fluctuation in performance as the angle of incidence increases due to the change of the sun position with earth rotation in the morning, mid-day, and afternoon.

The angle of incidence modifier mathematical expression considering the angle of incidence is given by:

$$K_\theta = 1 - 5.25097 * 10^{-4}\frac{\theta}{\cos\theta} - 2.859621 * 10^{-5}\frac{\theta^2}{\cos\theta} \tag{4.22}$$

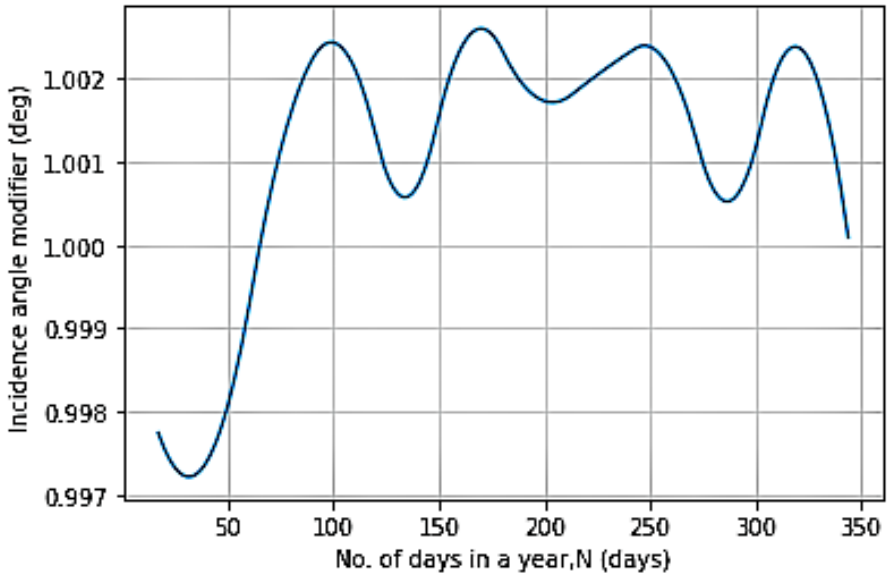

Figure 4.5: Incidence angle modifier

4.13 Single-axis tracking

The horizontal tracking concentrator angle of incidence given by:

$$\tan_t = \frac{\sin(\gamma - \alpha_s)}{\tan \alpha} \tag{4.23}$$

$$\cos \theta_{hor} = \sqrt{1 - \cos^2 \alpha \cos^2(\gamma - \alpha_s)} \tag{4.24}$$

East-west tracking orientation at $\gamma = 90^0$ the previous equation reduced to:

$$\tan_t = \frac{\cos \alpha_s}{tan_\alpha} \tag{4.25}$$

$$\cos \theta_{E-W} = \sqrt{1 - \cos^2 \alpha \cos^2(\gamma - \alpha_s)} \tag{4.26}$$

North-south tracking orientation at $\gamma = 0^0$ the previous equation is reduced to:

$$\tan_t = -\frac{\sin \alpha_s}{tan\alpha} \tag{4.27}$$

$$\cos \theta_{N-S} = \sqrt{(1 - \cos^2 \alpha \sin^2 \alpha_s} \tag{4.28}$$

4.14 Solar radiation

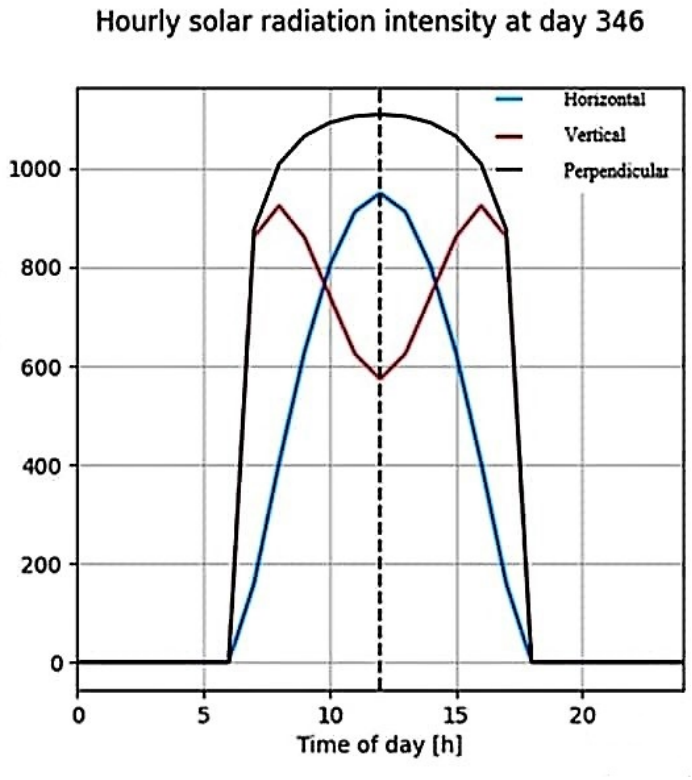

Figure 4.6: solar radiation over the day time

The solar radiation of the case study area using its latitude, longitude, and tilt angle the horizontal, vertical and perpendicular variation is graphed in the above figure 4.6 the higher sun radiation has recorded at noontime.

Chapter 5

Thermal Analysis of the concentrating solar parabolic trough

The incidence of solar radiation shoots the parabolic trough receiver tube allows HTF through it under the pyrex glass cover, the HTF temperature increase due to the heat transfer occurrence over the collector.

Table 5.1: SPTC system-relevant parameters

Location	**Zeway**
Voltage line access	132 kV
Solar parabolic trough information	
Parabolic trough type	ET-150
SPTC Heat transfer fluid	Diphenyl/biphenyl oxide ($C_{12}H_{10}O$)
PTC inlet temperature	285
PTC outlet temperature	415
Isentropic efficiency of pump and steam turbines	90% & 85%
Storage capacity	7.5 hours from the manufacturer
TES type	Molten salt
TES type	PCM (latent heat)
TES content	60% $NANO_3 + 40\% KNO_3$

The thermal analysis of the collector was examined to determine the parameters like useful energy gain, thermal efficiency, and losses which are directly required for the exergy analysis of the collector. The heat transfer fluid inside the concentrated solar parabolic trough tube temperature will raise due to the exposure of the focal line that towards a receiver to the incident solar radiation reflected by the collector. The heat transfer process through convection, conduction, and radiation takes place with increasing in the receiver temperature.

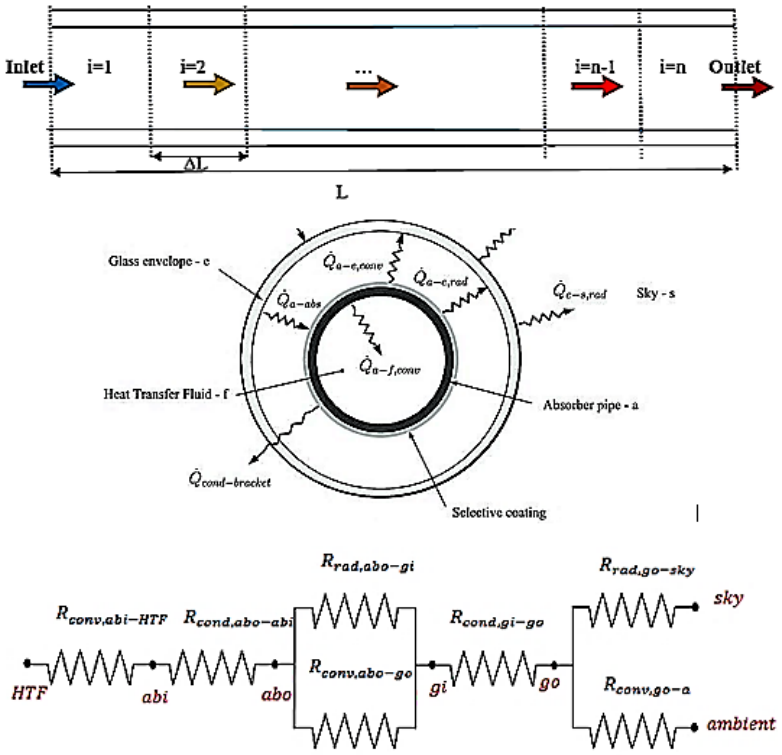

1. q1-2 – convection heat transfers between the inner surface of the absorber and the heat transfer fluid.
2. q2-3 – conduction heat transfers between the outer and inner surface of the absorber
3. q3-4 – radiation heat transfers between the outer surface of the absorber and the inner surface of Pyrex glass
4. q3-4 - convection heat transfer between the outer surface of the absorber and the inner surface of Pyrex glass
5. q4-5 – conduction heat transfers between the inner and outer surface of Pyrex glass.
6. q5-6 – radiation heat transfers from the outer surface of Pyrex glass to the sky
7. q5-7 – convection heat transfers from the outer surface of Pyrex glass to the ambient environment
8. qsolabs, go - solar beam radiation to Pyrex glass outer surface
9. qsolabs, abo - solar beam radiation to absorber outer surface

The following assumptions are considered to simplify the thermal analysis of the parabolic trough collector.

- Incompressible organic heat transfer fluid
- The non-transparent glass is used for infrared radiation

- The steady-state working condition performance of the PTC is conceded based on hourly time intervals.
- The parabolic shape of the concentrator is symmetrical
- Solar energy fluxes, temperatures, and other thermodynamic properties are considered uniform around the receiver and glass envelope surface.
- The conduction thermal losses have not been taken into consideration

The equational expression of the convective heat transfer coefficient from the glass cover to the ambient is

$$HC_{ca} = \frac{Nu\#k}{D_{co}} \tag{5.1}$$

$$H_{crf} = D_{ri} HC_{ca}(T_c - T_{fi}) \tag{5.2}$$

The Nusselt number and heat transfer coefficient estimation based on the Reynolds number by using the Dittus-Boelter equation is:

$$\text{For the } Re > 2300,\ Nu\# = 0.023 Re^{0.8} Pr^{0.4}$$
$$\text{For the } Re < 2300,\ Nu\# = 4.364$$

The Reynolds number and Prandtl number is expressed as follows:

$$Re = \frac{\rho V D_{co}}{\mu} \tag{5.3}$$

$$PrHTF = \frac{CpHTF * \mu HTF}{KHTF} \tag{5.4}$$

The average fluid temperature (T_{avg}) expression is

$$T_{avg} = \frac{T_e + T_{fi}}{2} \tag{5.5}$$

Radiative heat transfers between the outer surface of Pyrex glass cover to the ambient numerical expression is:

$$Hrca = egt(Tc + Tamb) * (Tc^2 + Tamb^2) \tag{5.6}$$

Radiative heat transfers from the outer receiver tube to the glass cover numerical expression is

$$Hrrc = \frac{t(Tr^2 + Tc^2) * (Tr + Tc)}{(1/er) + (Aro/Aco) * ((1/eg) - 1))} \tag{5.7}$$

The total amount of absorbed solar energy is distributed into useful heat gain and thermal loss.

$$Heatabsorbed = usefulheatgain + Heatloss \tag{5.8}$$

The thermal losses of the solar collector can be calculated as

$$Ql = Aro\sigma(Tr^4 - Tc^4)1 - \varepsilon r + 1 - \varepsilon g(AroAci) \tag{5.9}$$

The useful heat gain can be written as:

$$Q_u = F_r((G_b * A_{co}) - (A_{ro} * U_o * (T_{fi} - T_{amb}))) \tag{5.10}$$

$$Q_u = mcp(T_e - T_{fi}) \tag{5.11}$$

$$Q_s = A_a * G_b \tag{5.12}$$

To start the exergetic analysis, the thermal analysis of the system has to be conducted first for the determination of the important parameter. The thermal efficiency of the collector calculated as follows:

$$\eta_{th} = \frac{Q_{useful}}{Q_{solar}} \tag{5.13}$$

$$\eta_{th} = \frac{m_r cp_{HTF} \Delta T}{Q_s} \tag{5.14}$$

The expression of useful heat gain of the concentrating solar power converter based on the Hottel Whillier equation:

$$Q_u = F_r A_a \left[S - \frac{A_{ro}}{A_a} UL(T_{fi} - T_{amb})\right] \tag{5.15}$$

The heat removal factor of the collector is identified from the ratio of actual heat transfer associated with the temperature gradient in the absorber tube to the maximum possible heat transfer available in the SPTC.
The expression for the heat removal factor (F_r) is

$$F_r = \frac{m_r c_p}{AroU_L}\left[1 - exp\left(\frac{-ULFA_{ro}}{m_r c_p}\right)\right] \tag{5.16}$$

$$F' = \frac{\frac{1}{U_o}}{\frac{1}{U_o} + \frac{D_{co}}{h_{fi} * D_{ci}} + \frac{D_{co}}{2K} * \ln\frac{D_{co}}{D_{ci}}} \tag{5.17}$$

Where:$F' = \frac{U_o}{U_l}$

$$U_L = h_{cca} + h_{rca} + h_{rrc}$$

Overall heat transfer coefficient can be calculated as follow:

$$U_o = \left[\frac{\frac{1}{U_L} + \frac{D_{co}}{h_{cca} D_{ci}} + D_{co} ln(\frac{D_{co}}{D_{ci}})}{2k} \right] \tag{5.18}$$

Heat loss coefficient is given by:

$$U_L = \frac{A_{ro}}{(h_{cca} + h_{rca}) A_{co}} + \frac{1}{H_{rrc}} \tag{5.19}$$

The glass cover temperature is specified by:

$$T_c = \frac{(A_{ro} H_{rrc} T_r) + (A_{co}(H_{rca} + H_{cca})) T_{amb}}{(A_{ro} H_{rrc}) + (A_{co}(H_{rca} + H_{cca})} \tag{5.20}$$

The parabolic trough collector flow factor is given as:

$$F'' = \frac{F_R}{F'} \tag{5.21}$$

The exit heat transfer fluid temperature at the outlet of the receiver can be calculated from:

$$Q_u = m_r c_p (T_e - T_{fi}) \tag{5.22}$$

Rearranging :

$$T_e = T_{fi} + \frac{Q_u}{m_r c_p} \tag{5.23}$$

5.1 Exergy Analysis of parabolic trough collector

The exergy analysis of the SPTC assists to design the collector with reduced exergy loss and exergy destruction.

The exergy balance under the steady-state working condition comprises internal exergy loss within and out exergy rates that are used to determine the exergy destruction and efficiency of the SPTC.

The general expression of the exergy balance of the SPTC is as follows:

$$\sum Ex_{inlet} = \sum Ex_{leaving} + \sum Ex_{change} + \sum Ex_{destroyed} \tag{5.24}$$

$$\dot{Ex}_{inlet} - \dot{Ex}_{outlet} - \dot{Ex}_{destructed} = 0 \tag{5.25}$$

The rate of the Inlet exergy can be calculated by:

$$\sum Ex_{inlet} = mc_p(T_{fi} - T_{amb} - T_{amb} \ln \frac{T_{fi}}{T_{amb}}) \tag{5.26}$$

The rate of the outlet exergy can be calculated by:

$$\sum Ex_{outlet} = m_r c_p(T_e - T_{amb} - T_{amb} \ln \frac{T_e}{T_{amb}}) \tag{5.27}$$

The potential exergy rate as useful exergy gain that is accumulated by HTF flow in the absorber tube determination is:

$$\sum Ex_{usefulpotential} = \sum Ex_{outlet} - \sum Ex_{inlet} \tag{5.28}$$

By dividing the potential exergy rate, the change of the outlet and inlet exergy rate to the inlet exergy rate give as exergy efficiency.

$$ExE_{ff} = \frac{Ex_{usefulpotential}}{Ex_{inlet}} \tag{5.29}$$

Ineffective use of accessible energy used to be consumed through the entropy generation that reduces the performance of the SPTC is known as an exergy loss. The Heat transfer from high to low temperature is the major reason for the exergy is destruction.

Exergy loss caused by different 4 terms are listed as follows:

1. The exergy loss rate due to heat leakage from the receiver tube to the ambient is:
$$Ex_{Loss1} = U_L A_{ro}((T_r - T_{amb})(1 - \frac{T_{amb}}{T_r})) \tag{5.30}$$
2. The exergy loss rate due to the temperature difference between the absorber tube and the sun is:
$$Ex_{Loss2} = Eff_o G_b A_{ro} T_a((\frac{1}{T_r}) - (\frac{1}{T_{sun}})) \tag{5.31}$$
$Eff_o = E_r E_g$
3. The exergy loss rate caused by solar radiation losses from the collector surface to the absorber tube is:
$$Ex_{Loss3} = G_b(A_{co} - (E_{ffo} A_{ro}))1 - \frac{T_a}{T_{sun}} \tag{5.32}$$
4. The exergy loss rate due to the temperature difference between the absorber

tube and fluid is:

$$Ex_{Loss4} = m_r c_p T_a (ln\frac{T_e}{T_{fi}} - (\frac{T_e - T_{fi}}{T_r}) \tag{5.33}$$

5. The other mathematical expression to determine the exergy efficiency of the SPTC is:

$$ExE_{ff} = \frac{m_{HTF} cp_{HTF}}{e_{ffo} G_b A_a} \left[T_e - T_{fi} - \frac{T_{amb} ln T_e}{T_{fi}} \right] \tag{5.34}$$

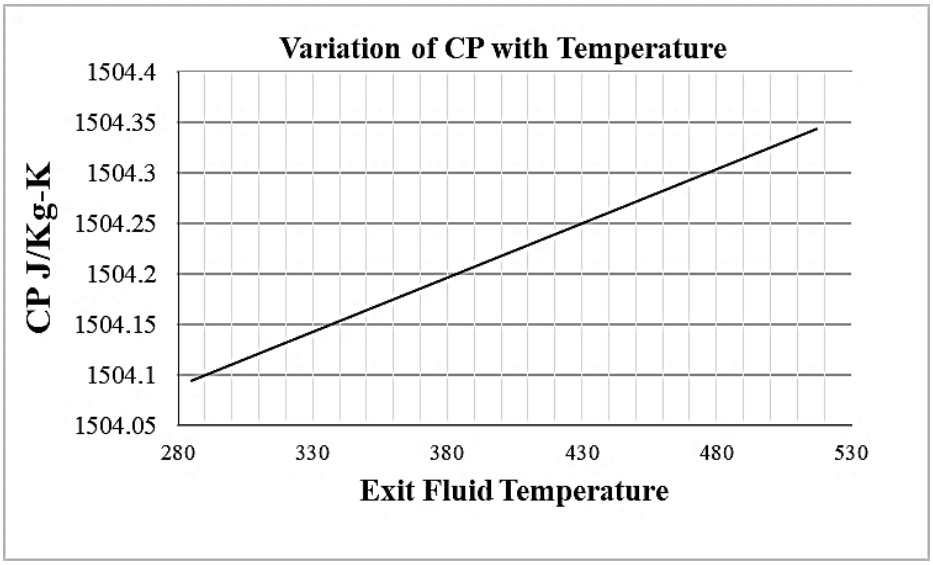

Figure 5.1: Specific heat of HTF variation with temperature

The specific heat of the heat transfer fluid is not constant at different phases, unless varies with its temperature minimally.

Chapter 6

Exergy analysis of Double flash Geothermal power plant

The share of flashing geothermal energy in MWe comes first relatively to other types, there are different stages of flashing single, double, and triple to maximize the electrical energy production efficiently by using several components. Using the parameters of Aluto Langano power plant operating condition double-flash geothermal power plant having two separators, flash chambers, and expanders has been analyzed in this study.

Exergy is unconserved, through the exergy analysis the quality of useful energy can be calculated. To determine the exergy destruction rate in each component including the performance of the power plant through the exergetic efficiency some assumptions has been made.

- Steady-state operating condition.
- Negligible pressure drops throughout the heat exchangers specifically in the evaporator and open feed water heater as well as in the pipelines due to its insignificance to the analysis.
- The turbines and pumps work at the isentropic thermodynamic process so that for the calculations recommended isentropic efficiencies of the pump and steam turbines are considered.
- Negligible kinetic and potential energy changes.
- The geothermal fluid property at the production well is in a saturated liquid condition in the reservoir (x = 0) and the steam separation to be directed to the steam turbines has carried out in the separators efficiently estimated about 99.9 %.
- Water thermodynamic properties has been used as a working fluid to transfer heat throughout the system from the inlet to the final re-injection.
- Negligible temperature and pressure losses of the geothermal fluid are in the separation processes.
- The flashing process is accomplished at constant enthalpy in both flash chambers. $\Delta H = 0$ which means $h_2 = h_1$ and $h_5 = h_4$

Table 6.1: The integrated power and water purification plant EES results

Input parameter type	**Parameter value**	**Unit**	**Component**
Temperature	335	^0C	Production well
Pressure	3.5	bar	Production well
Inlet pressure	0.5	bar	High-pressure turbine (geothermal)
Mass flow rate	28	kg/s	Production well

6.1 Exergy Balance of the double flash geothermal system

The exergy balance helps to determine the exergy rate in components and exergy efficiency of the energy conversion cycle. Considering the above assumption the exergy of a specific component and exergy rate using HTF mass flow rate are given by:

$$Ex_n = (H_n - H_0) - T_0(S_n - S_0) \tag{6.1}$$

$$Ex_{rate} = Ex_n m_r \tag{6.2}$$

The exergy balance of each geothermal units used in the cycle is calculated by the exergy balance of the High-pressure steam turbine operating at $0.5Mpa$ of pressure as collected data from the study site is calculated from equation 6.3

$$Ex_{desHPT} = (m_2 Ex_3) - W_{hpt} + (m_6 Ex_6) \tag{6.3}$$

The exergy balance of the low pressure operating at equivalent temperature with high-pressure turbine is given by equation 6.4

$$Ex_{desLPT} = (m_8 Ex_8) - W_{lpt} + (m_9 Ex_9) \tag{6.4}$$

$$Ex_{desLPT} = (m_8 Ex_8) - W_{lpt} + (m_{10} Ex_{10}) \tag{6.5}$$

The exergy balance of an open feedwater heater is computed by equation 6.6

$$Ex_{desOFWH} = (m_6 Ex_6 + m_7 Ex_7) - (m_6 Ex_8) \tag{6.6}$$

The exergy balance of the first flash chamber purposes to depressurize the geothermal fluid is calculated using equation 6.7

$$Ex_{desFCH1} = (m_1 Ex_1) - (m_2 Ex_2) \tag{6.7}$$

The exergy balance of the second flash chamber that provides the fluid to the second separator and re-injection well calculated from equation 6.8

$$Ex_{desFCH2} = (m_4 Ex_4) - (m_5 Ex_5 + m_{11} Ex_{11}) \tag{6.8}$$

The exergy balance of the first separator functions to separate the steam and directs to the high-pressure turbine determined using equation 6.9

$$Ex_{desSep1} = (m_2 Ex_2) - (m_3 Ex_3) \tag{6.9}$$

The exergy balance of the second steam separator unit connected with an open feedwater heater based on equation 6.10

$$Ex_{desSep2} = (m_5 Ex_5) - (m_7 Ex_7) \tag{6.10}$$

Exergy Destruction rate in preheating and reheating water tank is computes as follows based on equations 6.11 and 6.12

$$Ex_{desP.T} = (m_9 Ex_9) - (m_{12} Ex_{12}) \tag{6.11}$$

$$Ex_{desR.T} = (m_{11} Ex_{11}) - (m_{16} Ex_{16}) \tag{6.12}$$

Exergy Destruction Rate of the Mixing chamber is calculated by equation 6.13

$$Ex_{desMCH} = ((m_9 Ex_9) + (m_{11} Ex_{11})) - (m_{10} Ex_{10}) \tag{6.13}$$

The Exergy efficiency of double flash geothermal system is given by:

$$Ex_{effgeo} = \frac{\sum Ex_{worknet} GS}{\sum Ex_{in} GS} \tag{6.14}$$

6.2 Exergy balance of the SPTC system

The exergy destruction of each component used to convert the solar energy into electrical energy connecting with organic reheat Rankine cycle determined based on the thermodynamic exergy balance.

The exergy balance of the SPTC organic reheat Rankine cycle High-pressure steam turbine is calculated from equation 6.15

$$Ex_{desHPTss} = (m_{19}Ex_{19}) - W_{hptss} + (m_{20}Ex_{20}) \tag{6.15}$$

The exergy balance of the SPTC organic reheat Rankine cycle low pressure operating at equivalent temperature with high-pressure turbine working temperature is given by equation 6.16

$$Ex_{desLPTss} = (m_{21}Ex_{21}) - W_{lptss} + (m_{22}Ex_{22}) \tag{6.16}$$

The exergy balance of a pump is computed by equation 6.17:

$$Ex_{despump} = (m_{23}Ex_{23}) - (W_{pump} + (m_{24}Ex_{24})) \tag{6.17}$$

The exergy balance of the SPTC organic reheat Rankine cycle heat exchanger (Evaporator) is calculated using equation 6.18:

$$Ex_{desh-E} = ((m_{18}Ex_{18}) + (m_{20}Ex_{20})) - ((m_{19}Ex_{19}) + (m_{21}Ex_{21})) \tag{6.18}$$

The exergy balance of the SPTC organic reheat Rankine cycle heat exchanger (Condenser) is calculated using equation 6.19:

$$Ex_{deshx-C} = ((m_{22}Ex_{22}) + (m_{23}Ex_{23} + ExQ_{out}(1 - \frac{T_0}{T_{con}}) \tag{6.19}$$

The exergy balance of the thermal energy storage PCM determined using equation 6.20

$$Ex_{desPCM} = ((m_{PCM}Cp_{pcm})(T_{PCMi}T_{PCMe}))(1 - (T_eT_{PCM,melting})) \tag{6.20}$$

The exergy efficiency of the SPTC organic reheat Rankine cycle is given by equation 6.21

$$Ex_{effSPTC} = \frac{\sum Ex_{worknet}SS}{\sum Ex_{in}SS} \tag{6.21}$$

The exergy efficiency of the SPTC-geothermal integrated power plant with sterilization and RO water purifier calculated using equation

$$Ex_{effOS} = \frac{\sum Ex_{worknet}OS}{\sum Ex_{in}OS} \tag{6.22}$$

Chapter 7

Result and discussion

The SPTC performance has been assessed in different operating parameters, heat transfer fluids, and numerous commercially accessible trough models from a variety of manufacturing companies. The integrated system has been designed on Aspen Plus software even though the investigation of thermal analysis of the SPTC carried out using EES. In this analysis, the heat transfers through the glass cover to the receiver, glass cover to the atmosphere, and sky as radiation, convective and conductive heat transfer modes are computed, furthermore, the heat loss, heat removal factor, and useful heat output of the receiver were under analysis.

The metrological data like sunshine hours, ambient temperature, the longitude and latitude of Ziway, Ethiopia are taken to determine solar angles, daily and monthly beam radiation variation, incident angle of a modifier, and tilt angle of the collector for the better harness of energy throughout the sunny hours.

Table 7.1: The integrated power and water purification plant EES results

No.	**Temprature (K)**	**Pressure (MPa)**	$H(\frac{KJ}{Kg})$	$S(\frac{KJ}{Kg-K})$	**Exergy rate**(Kw)
1	608	3.5	3067	6.597	30939
2	608	0.5	3067	7.464	20059
3	574.3	0.5	2855	6.821	23705
4	574.3	0.5	1874	3.603	1647
5	475.7	0.2236	1874	3.821	1137
6	475.7	0.2236	2663	6.821	7984

7	475.7	0.2236	2712	5.834	984.8
8	475.7	0.2236	2749	5.776	11711
9	372.8	0.1	2531	5.776	5451
10	393.4	0.1913	2707	6.293	8479
11	475.7	0.2236	1651	3.374	2978
12	300	0.1	112.6	0.3928	1.224
13	293	0.1	83.3	0.294	0.317
14	346.5	0.1	413.8	0.9956	3809
14”	346.5	0.207	413.8	0.9956	3809
15	366	0.1	388.9	1.225	116.9
16	445	0.1	2448	7.433	3809
17	839	0.1	3357	7.203	13489
18	688	1.5	854	2.702	7408
19	688	1.5	1033	2.155	15818
20	559.3	0.194	774.4	2.155	9070
21	688	0.194	987.7	2.26	12536
22	293	0.01	810.7	2.26	5954
23	293	0.01	791	2.08	1960
24	293	1.5	158.8	2.08	425.8

7.1 HTF and Trough characterization

The organic reheat Rankine cycle system configuration combines hot and cold heat exchangers with two high pressure, low-pressure expanders, and a pump as a component. Different working fluids have been characterized by the solar thermal system.

In this work a synthetic HTF which is known as Diphenyl/ Biphenyl oxide in its composition made from a eutectic mixture of diphenyl oxide (diphenyl ether) and diphenyl (biphenyl) each with 73.5% and 26.5% respectively. The heat transfer fluid of the ORRC has good thermal stability, insignificant or no toxicity, chemically stable under normal conditions, low viscosity, and is stabilized at a liquid state for a large temperature range.

To compare and contrast the various collectors' performance by achieving higher exit fluid temperature at the outlet of the receiver examined with a small divided

length of the tube.

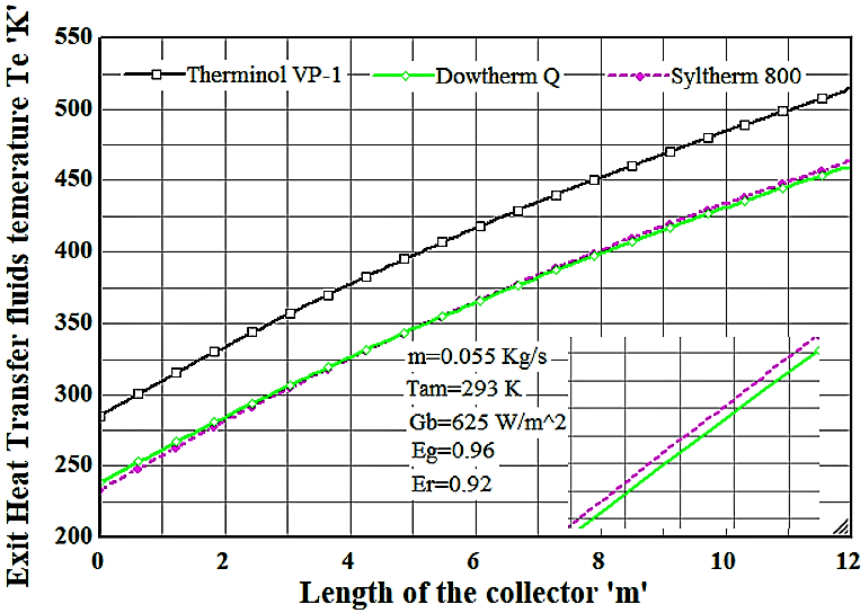

Figure 7.1: The instability of receiver outlet HTF temperature of the SPTC with the mass flow rate

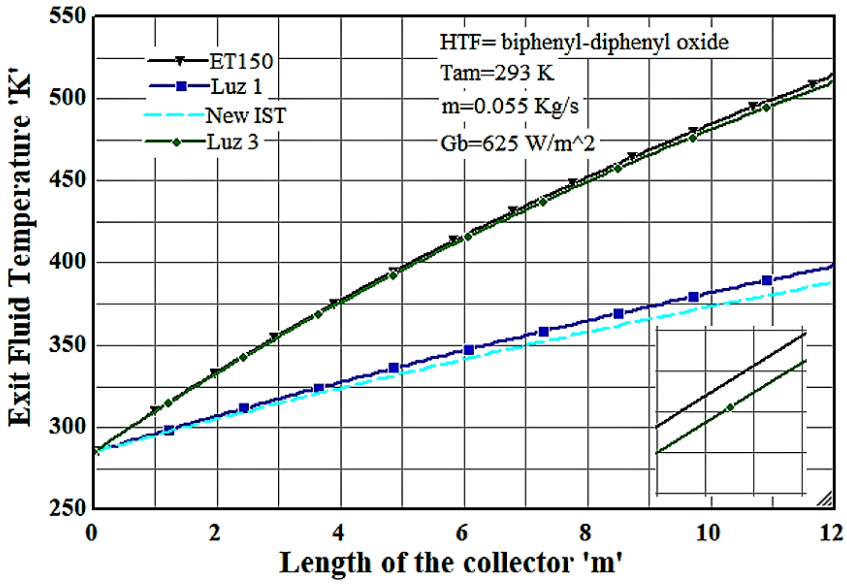

Figure 7.2: The outlet receiver HTF temperature at different segment of SPTC length

To compare and contrast the various collectors' performance by achieving higher exit fluid temperature at the outlet of the receiver examined with a small divided length of the tube.

The outputs of the SPTC vary with the increment and decrement of different parameters such as ambient temperature, mass flow rate, length of the collector, size

of the collector, beam radiation, and inlet fluid temperature. As observed in Figure 7.1, the heat transfer fluid biphenyl-diphenyl oxide(Therminol VP-1) has considered as functioning fluid at 12oC to 430 oC from the characterized fluids of sylthrem at -40 oC liquid phase to 400 oC vapor phase and dowtherm Q -35 liquid phase to 330 oC vapor phase due to the higher exit temperature at the outlet of the receiver and thermal efficiency of the collector. In Figure 7.2 ET150 European Trough is improved in performance relatively than Luz 1, Luz 3, and New IST through the investigation of the same operating conditions of 0.055 kg/s of mass flow rate, 298 k of ambient temperature at 625 W/m^2 beam radiation using biphenyl-diphenyl oxide(Therminol VP-1) except the mentioned size by the manufacturers. The ET150 SPTC design is considered to be manufactured as a high-performance achieving, long-lasting, consistent, and reduced cost collector.

7.2 The effect of mass flow rate

The varied mass flow rate effect in SPTC combined to Organic reheat Rankine cycle, geothermal and water purifier system, as well as the dominance in the overall integrated system, are computed.

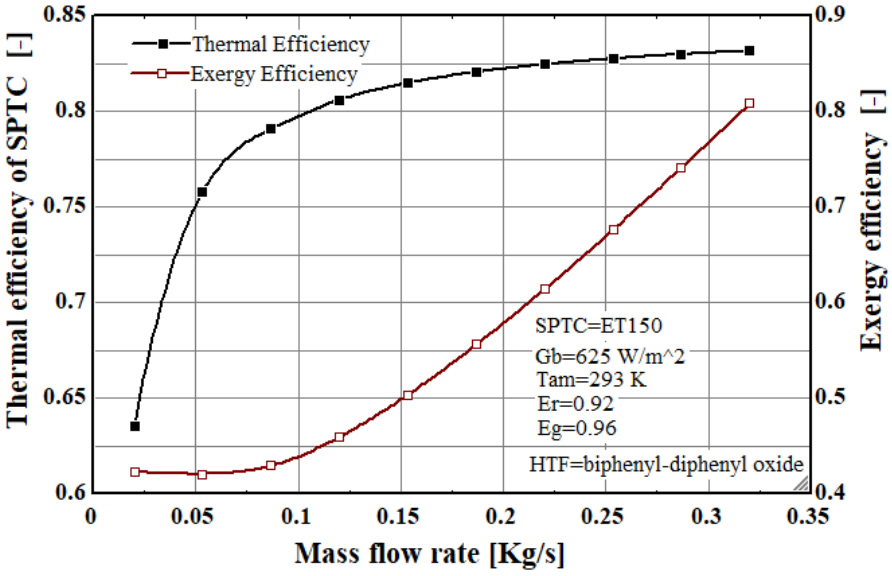

Figure 7.3: The fluctuation of Exergy and Thermal efficiency of the SPTC with the mass flow rate

As shown in the above Figure 7.3 the increasing of the mass flow rate throughout the SPTC organic reheat cycle benefits to enhance the thermal and exergy efficiency

computed relying on the first law of thermodynamics and the second law of thermodynamics under the constant parameters of 625 W/m^2 intensity of solar radiation, 293 K atmospheric temperature, 0.96 and 0.92 glass cover and receiver(absorber) tube emissivity, biphenyl-diphenyl oxide, and ET150 as HTF and SPTC respectively.

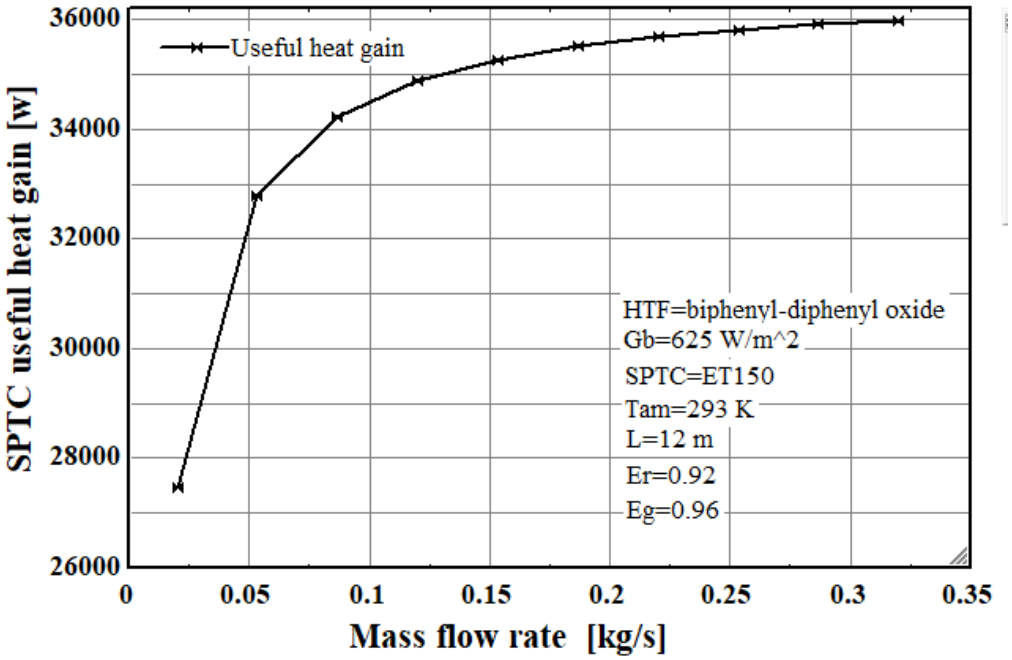

Figure 7.4: The variability of useful heat of the SPTC with the mass flow rate

Figure 7.4 represents the useful heat gain of the SPTC organic cycle increases with the rise of mass flow rate and subsequently while the mass flow rate exceeds 0.2 Kg/s the level of increment tends to constant. The heat transfer throughout the system continuously escalates with the rise of the HTF mass flow rate. Noticeably, the higher the mass flow rate leads to collect a greater amount of useful heat that makes the system efficient.

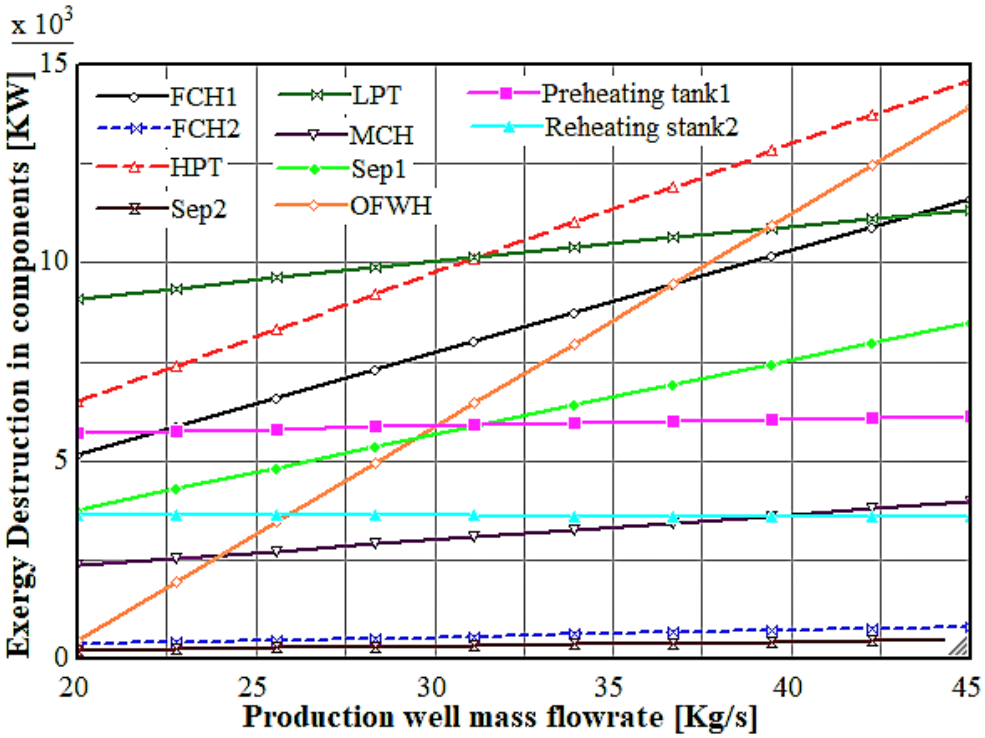

Figure 7.5: The Exergy Destruction in geothermal components with different mass flowrate

The usable and available energy in the designed system is destroyed in an irreversible process when the heat utilization is higher and work output is reduced. As shown in Figure 7.5 steam turbines, the first flash chamber, separator, and open feedwater heater are highly exergetically destructed relatively from other components. The variation of the geothermal fluid mass flow rate has a minimal effect on the second flash chamber, separator, water sterilizing tanks, and separators since its assumed negligible temperature and pressure loss.

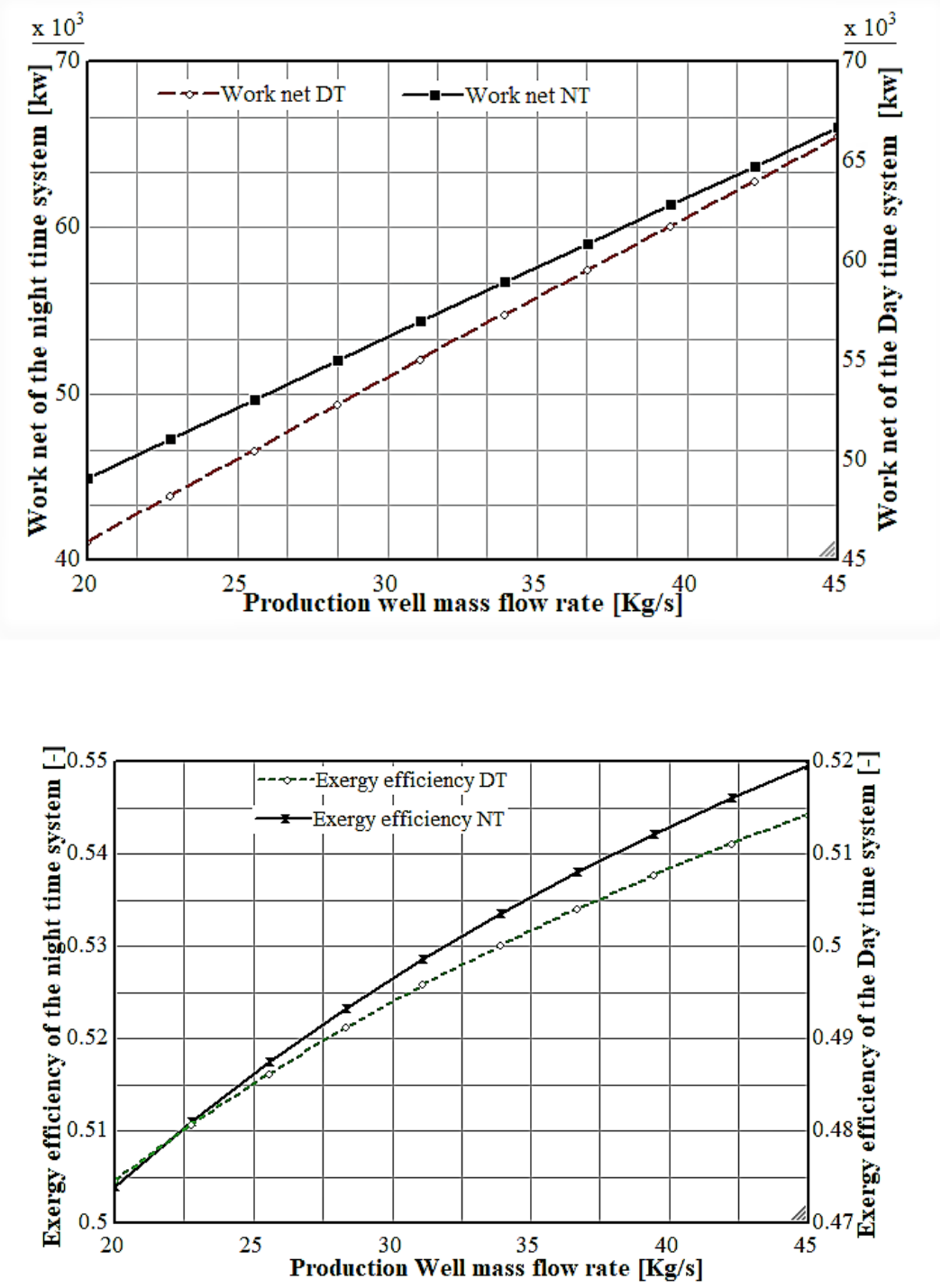

Figure 7.6: The variation of exergy efficiency and work net throughout the integrated system with different mass flowrate

To check out the actual potential of the assimilated SPTC, double flash geothermal and water purification plant with exergetic thermodynamic examination that used to clarify the energy quality that would be consumed at varied mass flowrate

results enhanced performance. Depending on specified parameters such as, beam radiation $800w/m^2$, exit fluid temperature determined on thermal analysis of SPTC 688K and 608K and 3.5 MPa of production well geothermal fluid temperature and pressure the consequence of the mass flowrate increasing on the integrated system exergy efficiency and exergy work net are represented graphically in Figure 7.6 shows that both parameters are continuously kept increasing concerning the mass flow rate.

7.3 The intensity of solar radiation effect evaluation

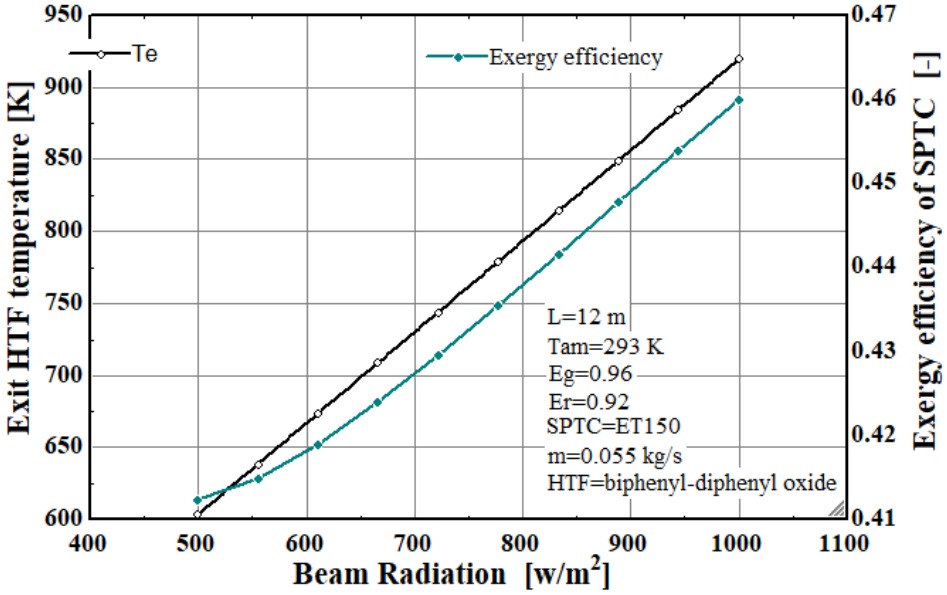

Figure 7.7: The receiver outlet temperature and exergy efficiency of the SPTC concerning different beam radiation

The intensity of solar radiation is classified into two as a beam and diffusive radiation, specifically beam radiation is the sunray that is not deflected by the atmosphere and things on earth and sky, while the scattered and reflected ray is the diffused type. The parabolic trough concentrators run as a result of gathering the radiation directly released from the sun which is not diffused. Different quantity of beam radiation has collected in the day and overall the year at a changed number of days every 12 months in a year, this fluctuation affects the capacity of the SPTC at the lower sunny hours of the day with reducing the expected receiver exit temperature and exergy efficiency of the collector. The higher the beam radiation is collected and directed to the receiver means the greater performance of the SPTC system accomplish through the exit HTF temperature rise and exergy efficiency improvement in consistently increasing line as observed in Figure 7.7.

To select the study site looking in detail the metrological data of the location is required to observe sunny hour's length of the day, warm months to check out the summer and winter month's length since solar energy fluctuates seasonally.

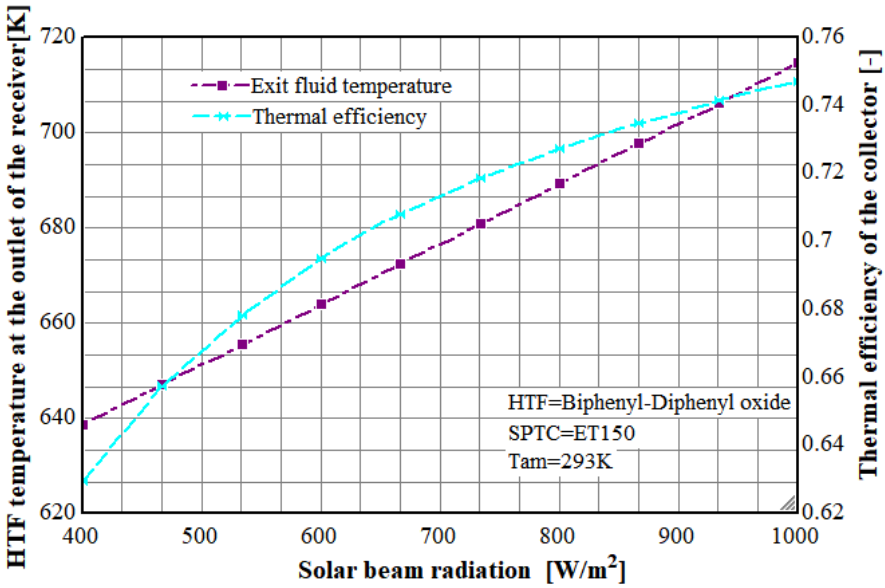

Figure 7.8: The thermal efficiency and receiver outlet temperature of the SPTC organic reheat Rankine cycle with respect to different beam radiation

The thermal efficiency of the collector is evaluated based on the first law of thermodynamics to investigate the general capacity of the SPTC but the unprecise potential compared to exergy efficiency. In Figure 7.8 under the specific mass flow rate, ambient temperature, Pyrex glass cover, and receiver emittance with the increasing rate of solar radiation per unit area the thermal efficiency of the SPTC has increased well. The solar beam radiation of the case study area is lower from June to the end of August, during this time the capacity of the parabolic trough collector is expected to decrease.

7.4 The effect of the variability of Temperature

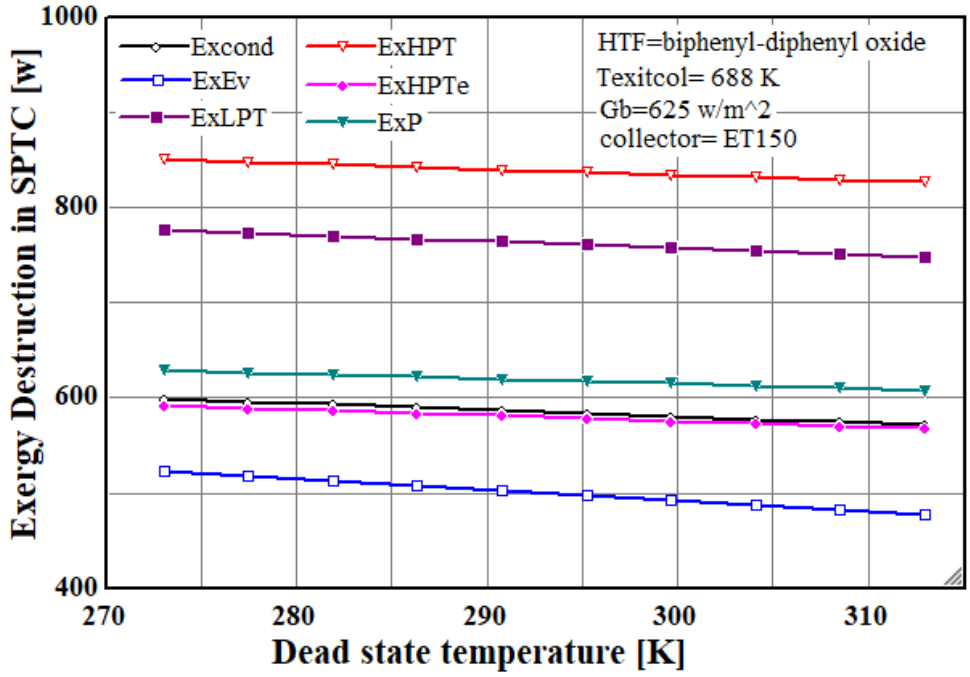

Figure 7.9: The exergy destruction of the SPTC with respect to dead state temperature

If the denominator temperature has increased the result approaches zero that means the entropy generation decreases, based on this definition when the dead state temperature keeps increasing the exergy destruction in all components high-pressure steam turbine, low-pressure steam turbine, pump, condenser, and evaporator decreases as seen in the above Figure 7.9. The reduction rate is higher in the evaporator and both turbines relative to other relevant components of the organic cycle. The exergy destruction rate decreasing means the components are operating efficiently and minimum loss is occurring.

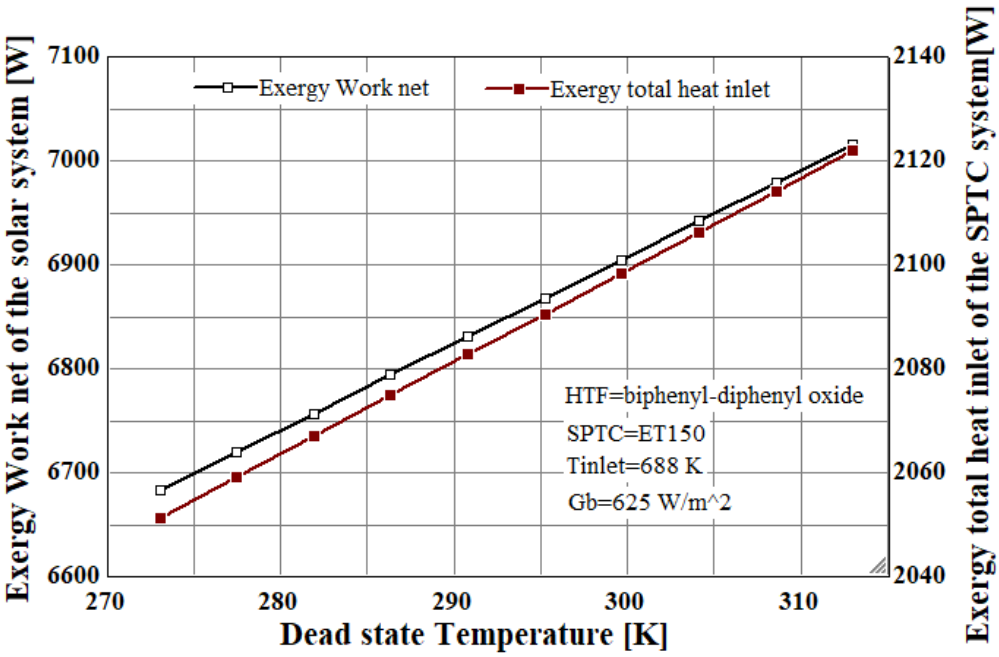

Figure 7.10: The exergy destruction of the SPTC with respect to dead state temperature

The dead state temperature implies the surrounding environment that can have an impact on the SPTC. As shown in Figure 7.10, if the surrounding temperature is in the increasing motion the amount of inlet heat exergy to the organic Rankine reheat cycle is higher and the greater exergy work output can be generated in the heat energy conversion to the mechanical work and finally to electrical energy production. In this estimation, the thermophysical property and dimensions of biphenyl-diphenyl heat transfer fluid and ET150 have been taken into consideration respectively.

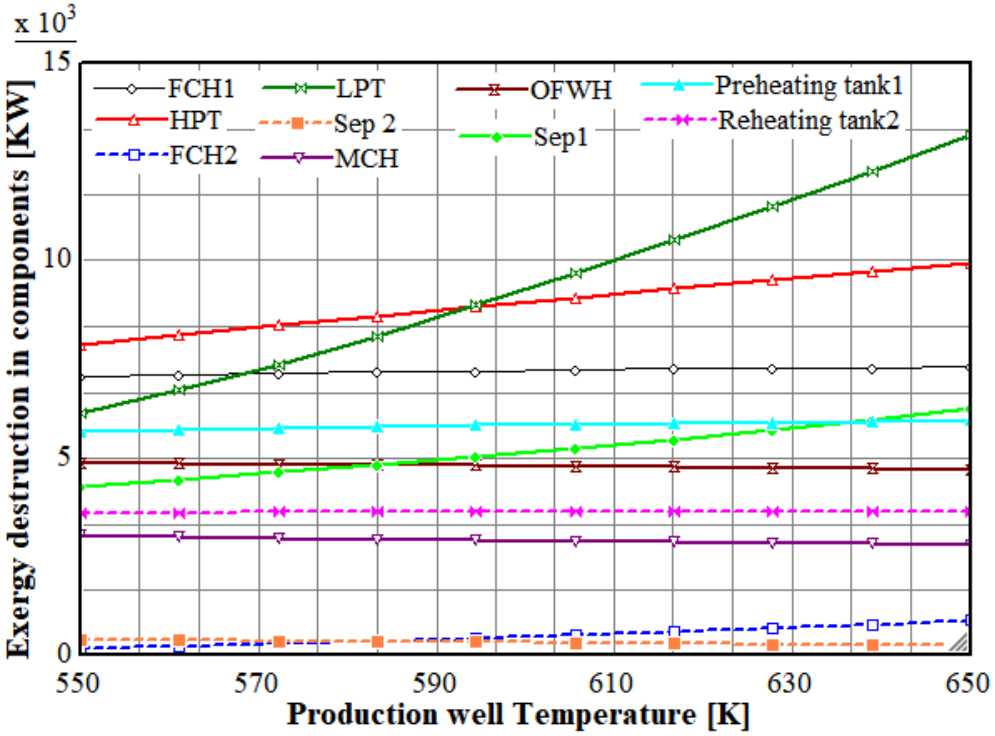

Figure 7.11: The exergy destruction of the geothermal components with varied production well temperature

As mentioned under the explanation of the above graph the higher the operating temperature means the lower the exergy destruction is occurring in each component. The mass flow rate and pressure at well conditions are fixed and the geothermal fluid temperature is differentiated to see it is the effect on the exergy destruction of all relevant functional components in Figure 7.11, the exergy destruction tanks, and second separator the exergy destruction rate is decreasing while the steam turbines, both flash chambers, and first separator components the exergy destruction rate has increased.

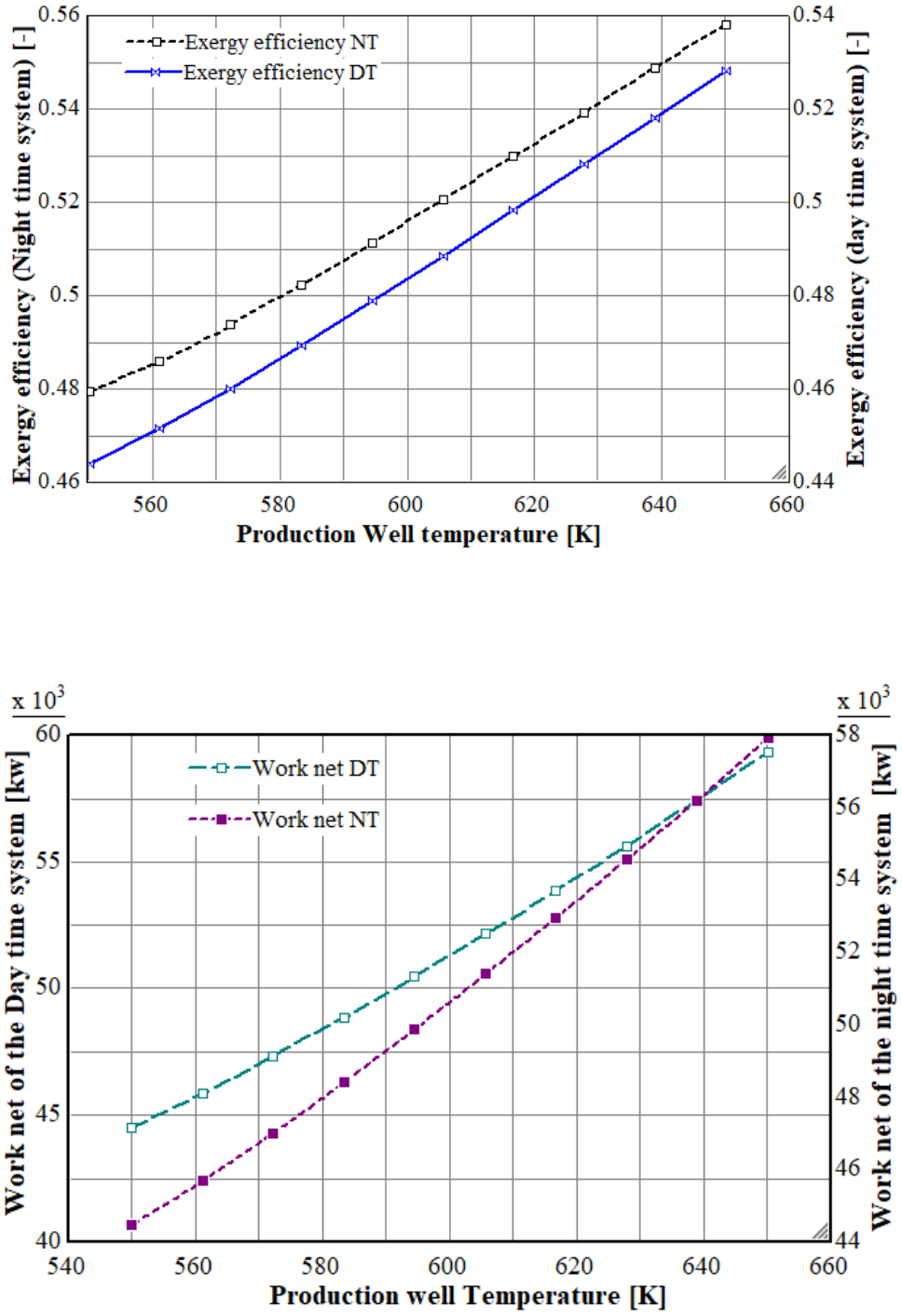

Figure 7.12: The exergy efficiency and work net variation with production well temperature

As the heat of the geothermal fluid, temperature increases the connected system's overall exergy efficiency is increasing which is seen in Figure 7.12 the fluid temperature depends on the natural source of the site. Aluto Langano site has a relatively higher

underground temperature even no need to use organic compound heat transfer fluids working at low temperature. Possible to convert the underground heat into other forms of energy specifically to electrical energy for the designed integrated power plant at a conversion performance with a higher temperature.

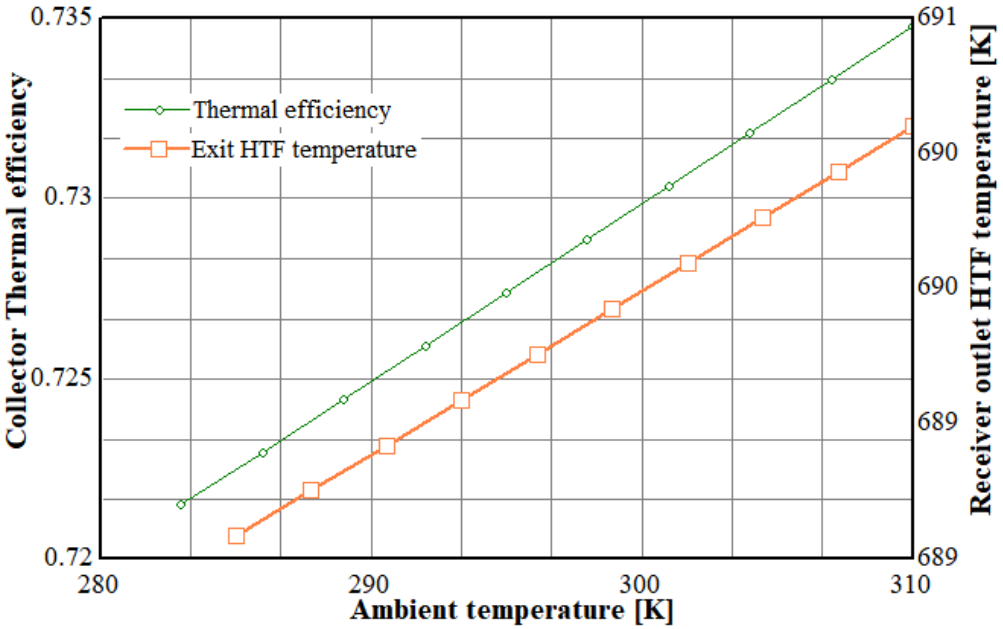

Figure 7.13: The receiver outlet temperature and thermal efficiency variation with an ambient temperature

The ambient temperature is directly related to solar radiation, as the sun ray strength increases the ambient temperature also increases. The higher beam radiation is available means in the area of the SPTC system has installed the amount of energy extracted maximized what improves the overall collector thermal efficiency. Thermal efficiency is the ratio of heat gained by the SPTC and the direct beam solar energy reached to the collector.

7.5 Effect of the length of the SPTC

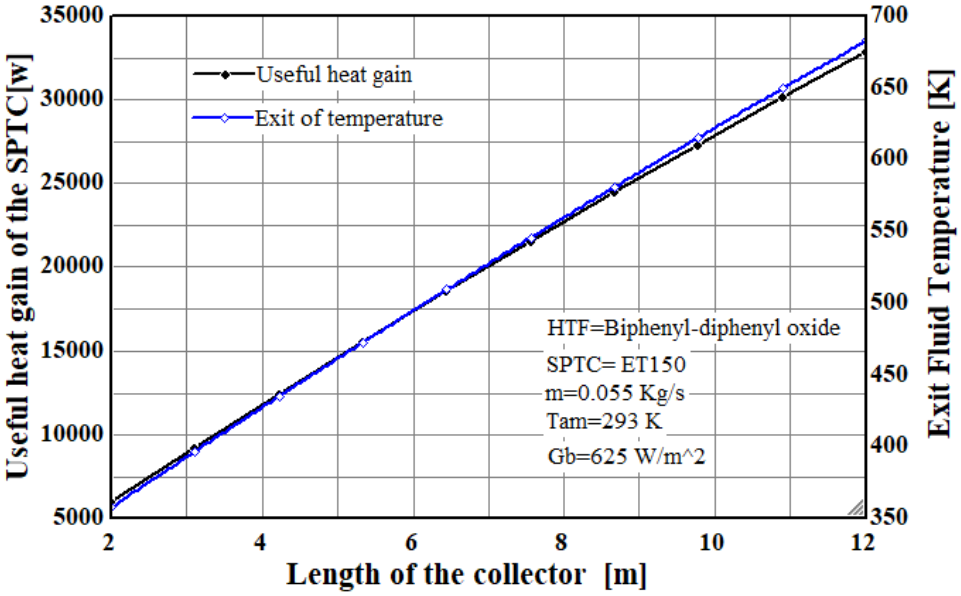

Figure 7.14: The receiver outlet temperature and useful heat gain variation with the length of the collector

By using biphenyl-diphenyl oxide as a working fluid Et150 European SPTC which is good in performance based on the characterization at a specified mass flow rate, ambient temperature, and beam radiation the useful heat gain and receiver outlet temperature fluctuation has investigated under small segments of the length of the collector in Figure 7.14, simply with adding the length or assembling different collectors, there is a possibility to increase the heat transfer fluid temperature at the outlet of the receiver that directly improves the capacity with higher amount of useful energy in watts. While assembling several collectors the exergy and energy loss is existing, for the simplicity of transporting the parts the manufacturers produce smaller length collectors.

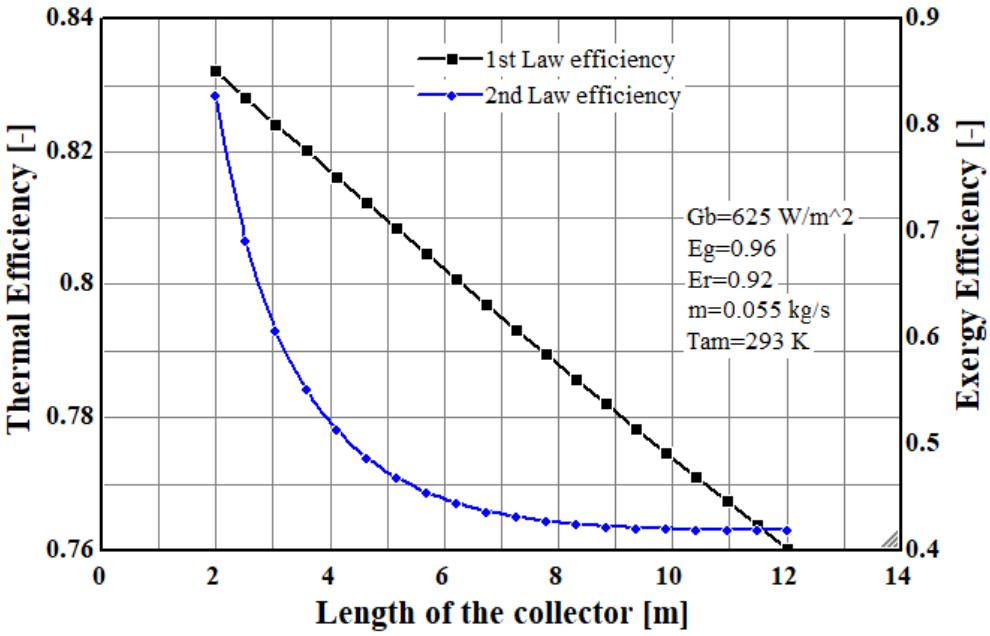

Figure 7.15: The thermal and exergy efficiency at different length of the collector

To determine the amount of exit heat transfer fluid temperature from the absorber tube the 12 m length of SPTC has discretized in 100 segments, as shown in the Figure when the collector becomes longer different forms of heat losses are occurs. So that Figure represents the linear decrement of thermal efficiency and slightly reduced exergetic efficiency which comes to its constant level after 8 m. The constant beam radiation, mass flow rate, ambient temperature, glass cover, and receiver emissivity has been considered with varying the length to see its effect on system exergy and energy efficiency.

7.6 The effect of dead state entropy on the overall system

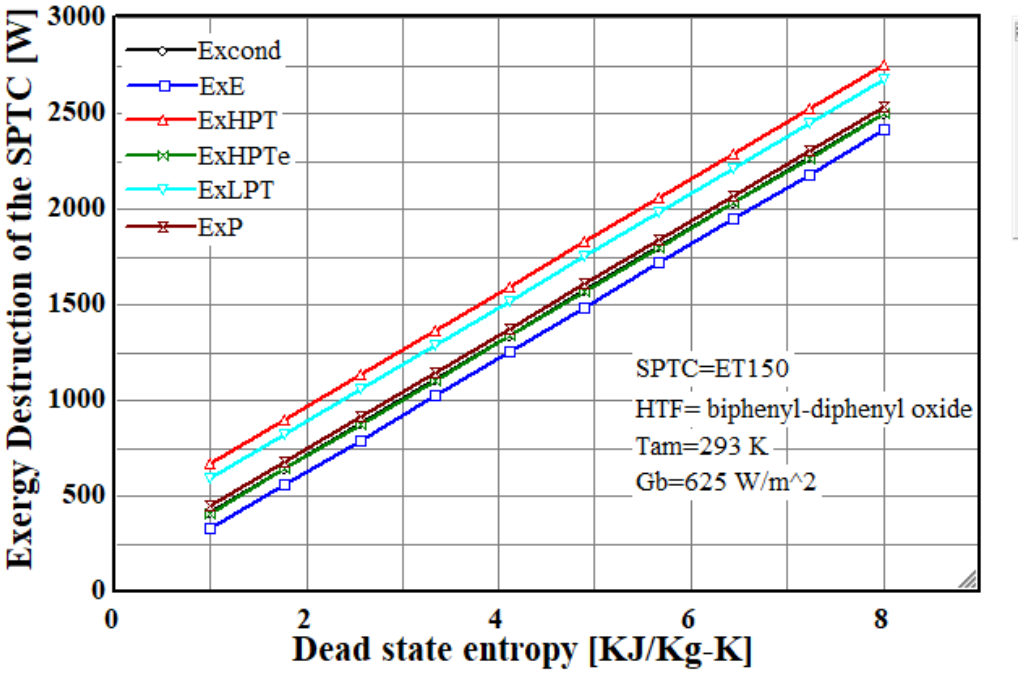

Figure 7.16: The formation of exergy destruction of the SPTC organic reheat Rankine cycle to dead state entropy

Thermo-physical property of the heat transfer fluid based on the dead state temperature and pressure has computed on EES, these properties are enthalpy and entropy at the dead state, shown in the above Figure 7.16, the entropy is higher if the given dead state condition when the system is at a complete equilibrium with the surrounding rises so that the exergy destruction in each component has increased in SPTC system. In this characterization ET150 Europian trough and biphenyl-diphenyl oxide heat transfer fluids are used, additionally under constant ambient temperature with average beam radiation collected by the SPTC in the case study area. The exergy destruction of the high-pressure turbine and low-pressure turbine is higher relative to other units. The reheating process and condensation exergy destruction are very close.

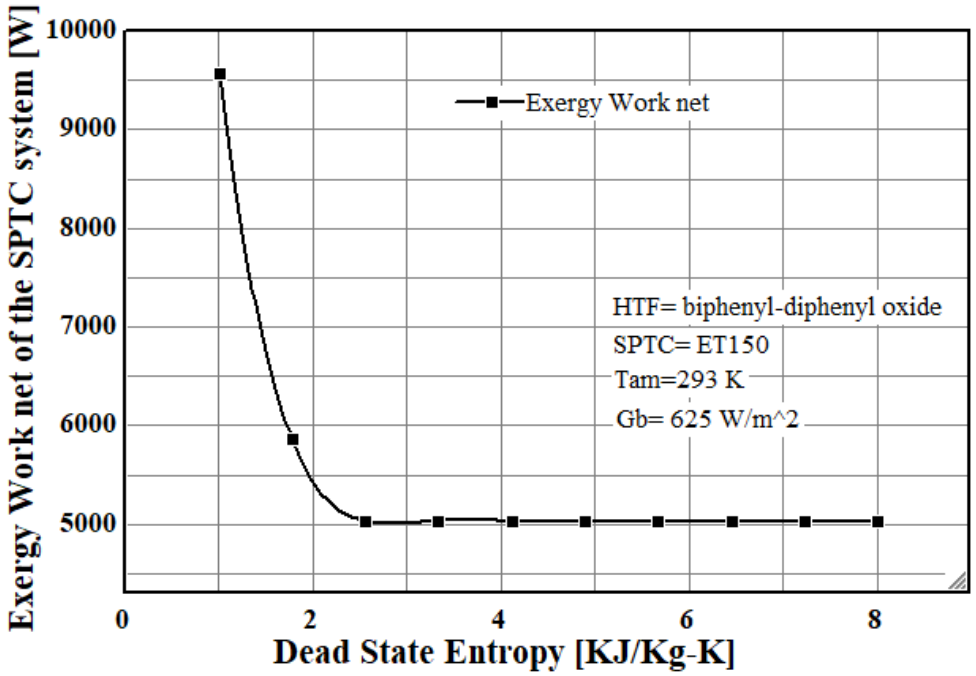

Figure 7.17: The change of exergy work net of the SPTC organic reheat Rankine cycle to dead state entropy

The surrounding parameters like temperature and pressure affect the exergy work net of solar with double-flash geothermal power plant integrated to sterilization water treatment. In the Figure 7.17, the conversion of heat energy to mechanical and electrical forms is considered as work out. The more exergy work net is accomplished by the overall system means the higher exergy efficiency is scored, even though the dead state entropy increment starts reducing significantly and when it reaches the optimum value is constant without any change.

7.7 The effect of first turbine outlet pressure

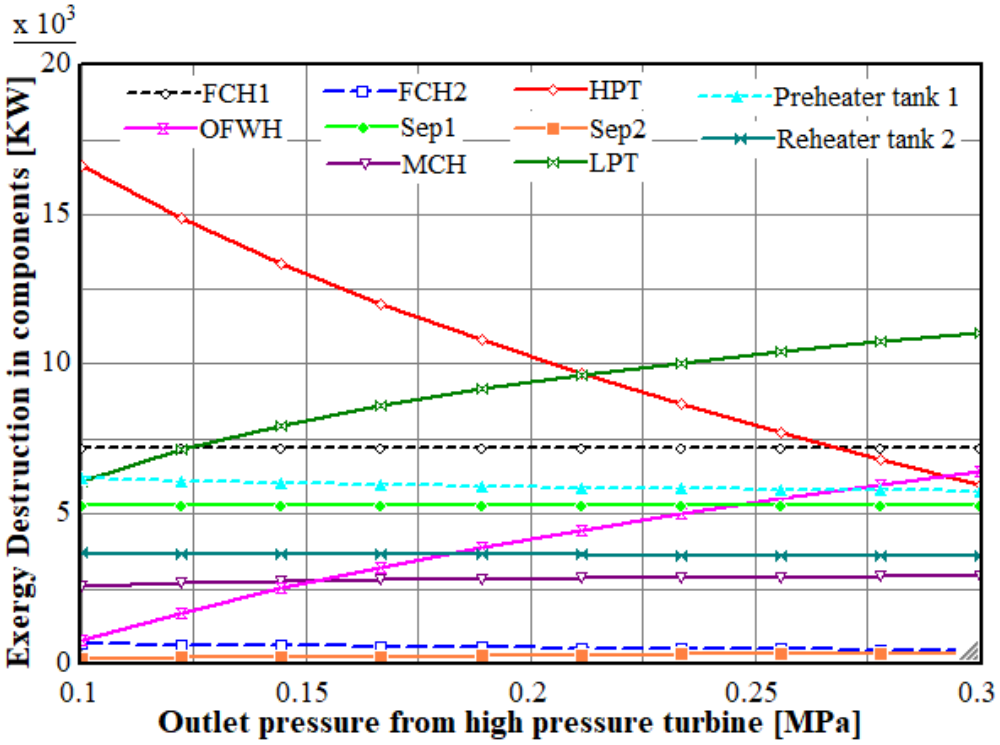

Figure 7.18: The formation of exergy destruction of the geothermal components due to the variation of first turbine outlet pressure.

Exergy destruction formation differs from component to component along with their function and direct connection to the varied parameter. The first geothermal turbine outlet pressure raise has an effect on the low-pressure turbine with an exponential increase of exergy destruction. In addition to the low-pressure turbine the exergy destruction rate increases at the mixing chamber, open feedwater heater, and second separator. There is no change in the first flash chamber and first separator. The irreversibility formation in the high-pressure turbine, the water preheating unit and the reheating system shows from high to low amount of exergy destruction rate decrement.

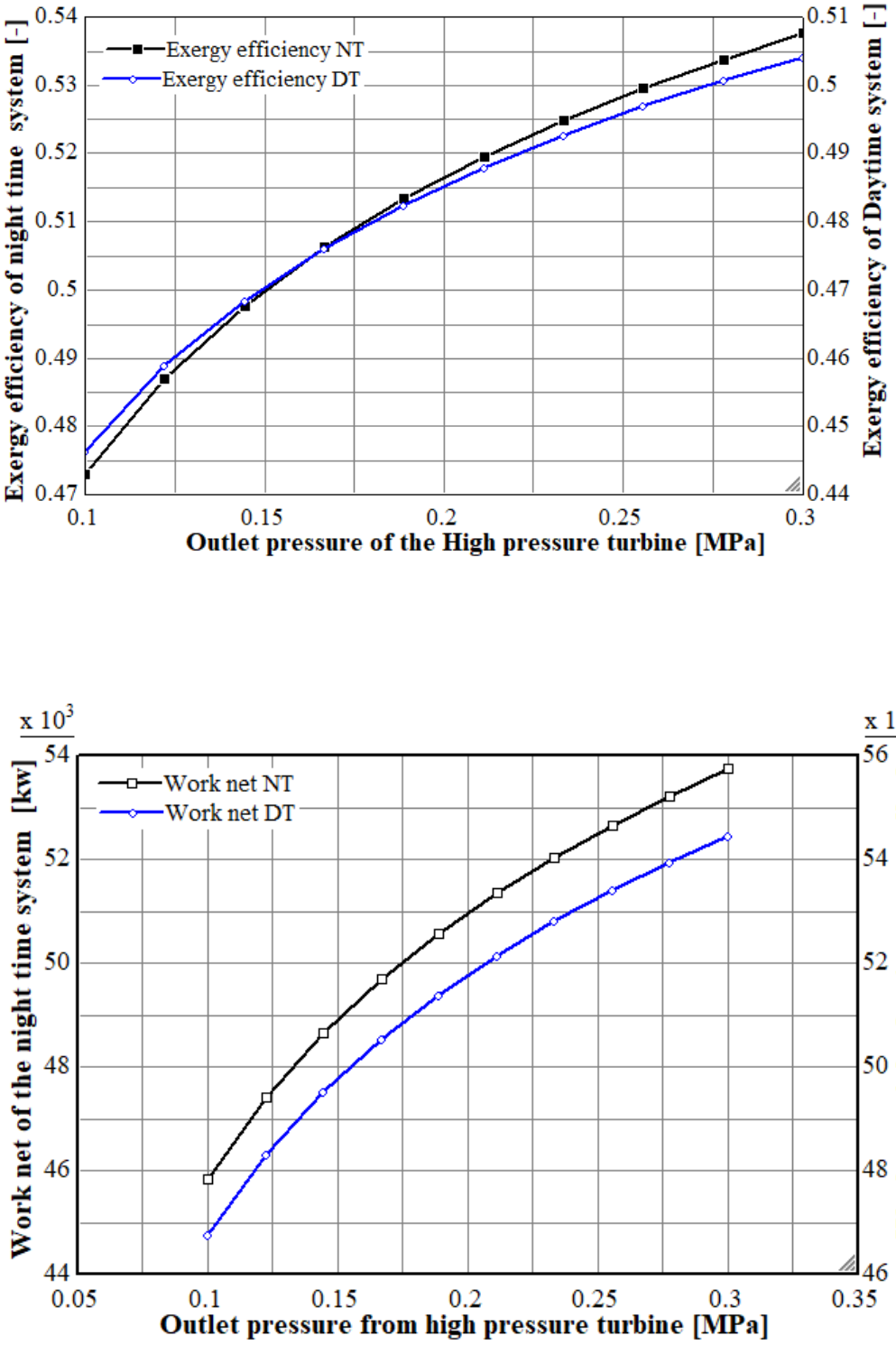

Figure 7.19: The exergy efficiency and work net of the double flash geothermal and solar system due to the variation of first turbine outlet pressure.

In the above Figure 7.19, the exergy work net and exergy efficiency explain the capability of the integrated SPTCdouble-flash geothermal power plant conversion

of energy and utilization of waste heat fluctuates as the dominant parameters vary. The effect of the outlet pressure from the high-pressure turbine is minimal relative to other parameters, as observed from the graph the fluctuation effect is positive, the higher the outlet pressure of the first geothermal turbine results in a lower amount of exergy destruction rate and enhanced overall exergy work net that consequence the improvement of exergy efficiency.

7.8 Variation of the Production well pressure

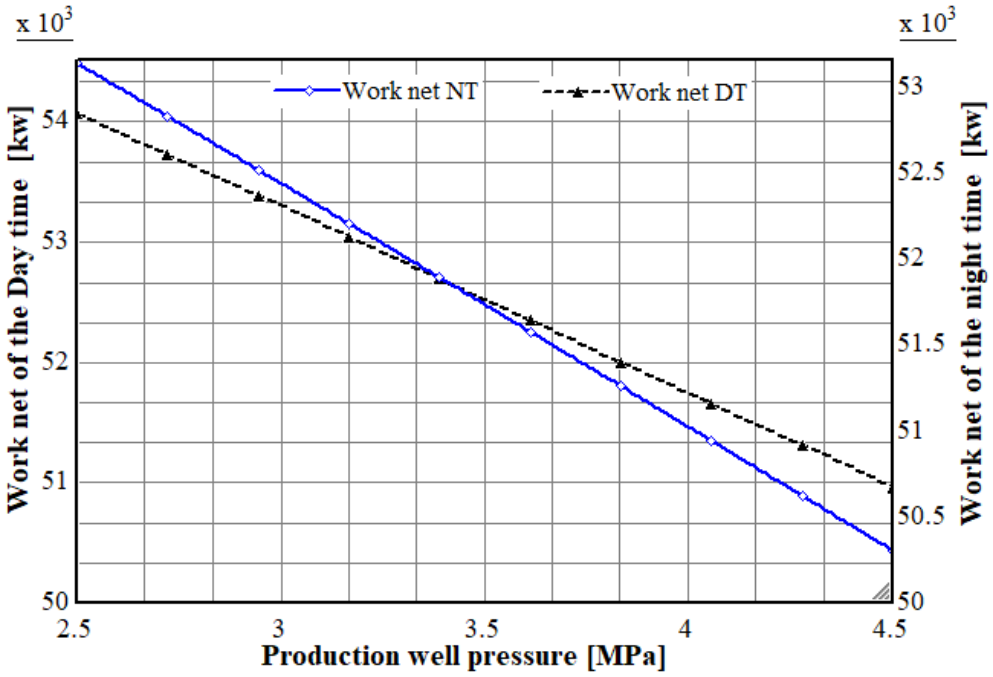

Figure 7.20: The work net of the double flash geothermal and solar system due to the variation of production well pressure.

In Figure 7.20, the work produced by the integrated system in two sessions, day and night time affected by the well condition operating pressure of the geothermal fluid. The work done reduces with increasing of the heat transfer fluid pressure at the well state. The power plant designed to operate at 3.5 MPa which means related to pressure the lower the better in performance.

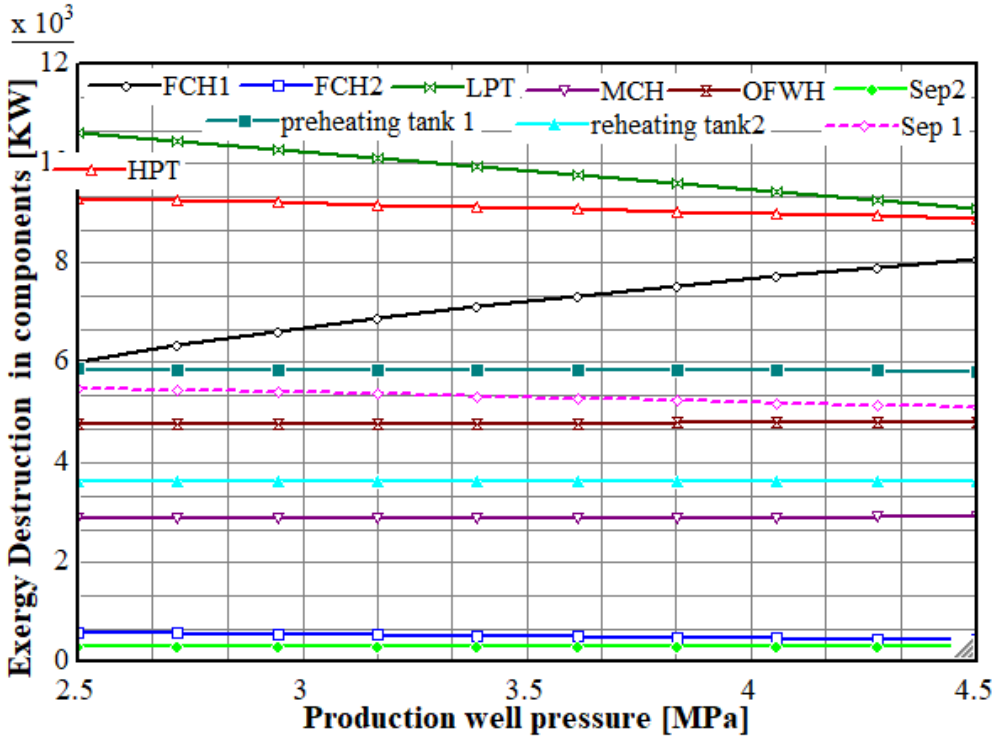

Figure 7.21: The exergy destruction rate of componenets of the combined double flash geothermal system due to the variation of production well pressure

As observed in Figure 7.21, the production well pressure of the eorking fluid affects few units, the rest components shows minimal or insignificant change as increasing and decreasing. The steam turbines exergy destruction rate has decreased while the first flash chamber is a component with high exergy destruction rate growth since it has used as a depressuriser.

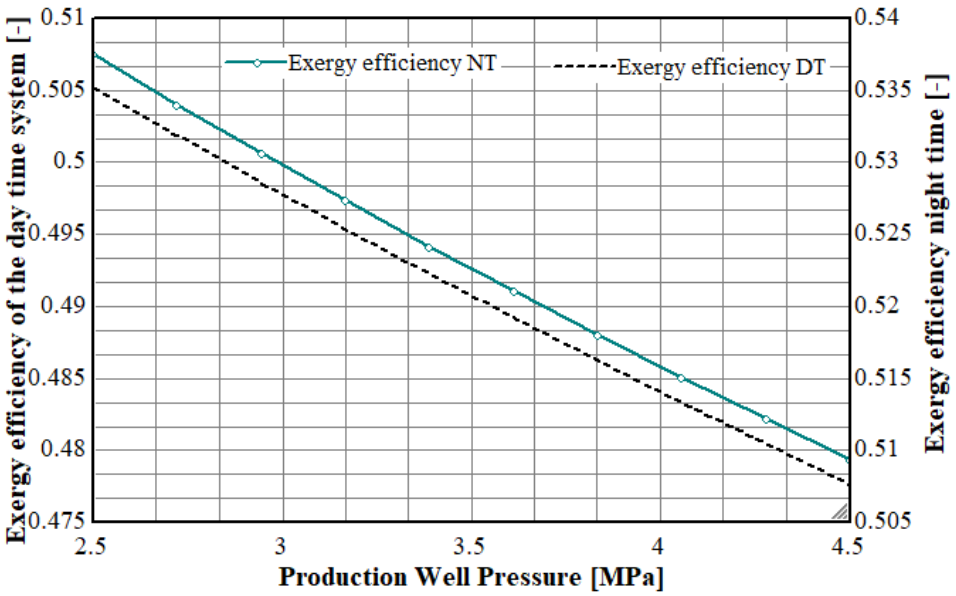

Figure 7.22: The exergy efficiency of the combined double flash geothermal and solar system due to the variation of production well pressure.

The work done by the system directly relates to the efficiency of the system, as the work net increase and reuction specific exergy (heat input) to the system occur results the capacity of the powerplant at an improved exergy efficiency. Even though the well condition pressure has reduced the work done by the system what minimize the functioning exergy efficiency as shown in Figure 7.22.

7.9 The effect of Inlet pressure to the first turbine

The useful energy which is named exergy efficiency and work net of the geothermal energy converting power plant connected to sterilization water treatment can be augmented on increasing of the inlet pressure directed from the first separator to the high-pressure steam turbine. The higher total work net produced by the high and low-pressure turbines results in enhanced exergy efficiency.

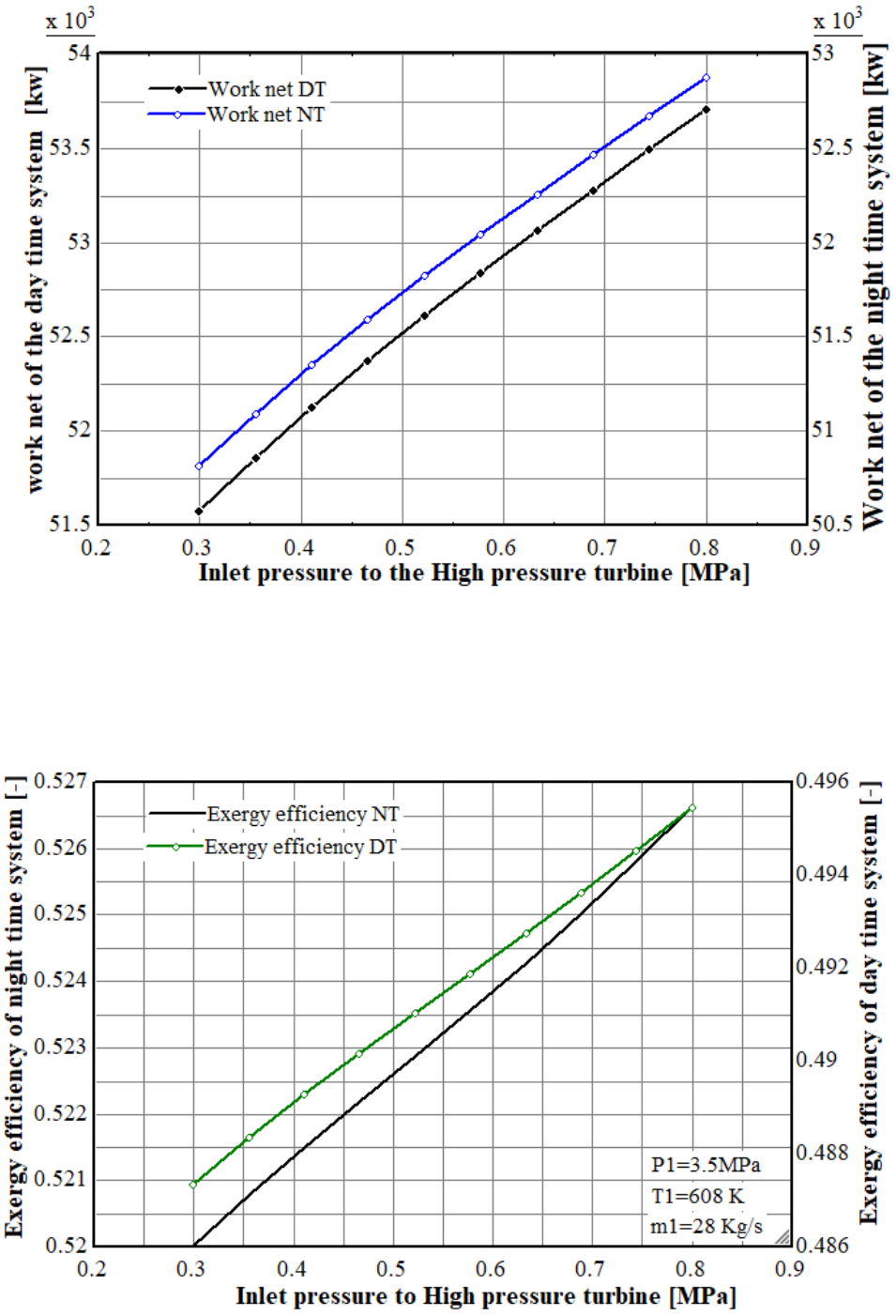

Figure 7.23: The exergy efficiency and work net of the double flash geothermal system due to the variation of first turbine inlet pressure.

The maximum work generated in the power plant leads to perform at a higher exergy efficiency as shown in Figure 7.23 the overall integrated SPTCdouble-flash geothermal with sterilization (boiling) in two different tanks as preheating and reheating mechanism to use the waste heat effectively and to minimize the waste heat operates

at a better exergy efficiency that increased when the high-pressure steam turbine inlet pressure increases.

Inlet pressure turbine is one of the parameters to characterize the capacity of the integrated power plant and output reveals that as it is positively dominant parameters exhibits in the energy conversion process.

As shown in Figure 7.23 the exergy work net has augmented as the inlet pressure of the geothermal system high-pressure increases. The exergy work net and exergy destruction in components are the key points to check out the real potential of the power plant since the increment of exergy work out and decrement of the results the higher exergy efficiency. The maximum work has been obtained and the overall performance is improved with an inlet pressure of the turbine variation to increment range.

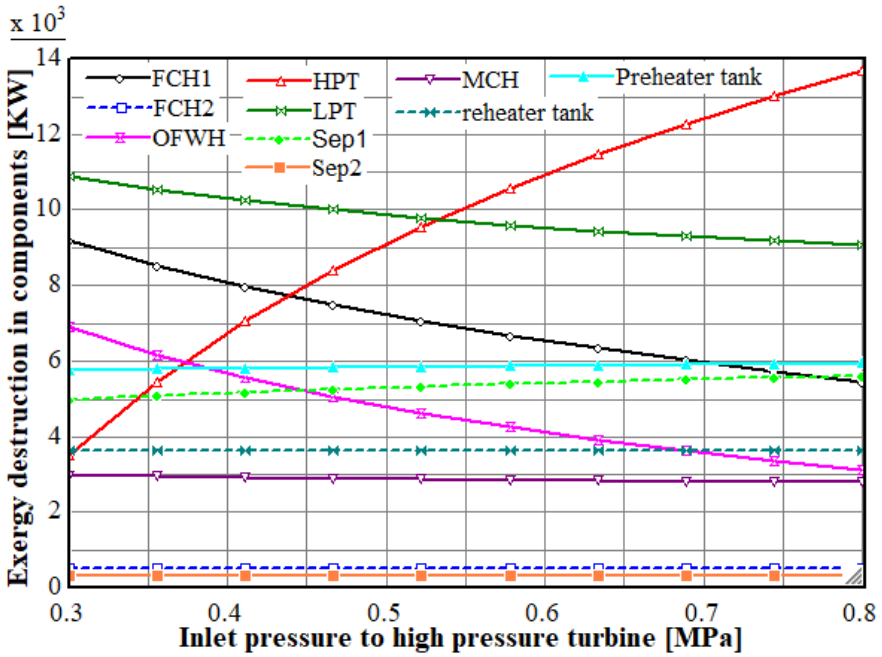

Figure 7.24: The exergy destruction rate of the double flash geothermal system due to the variation of first turbine inlet pressure.

Figure 7.24 represents how the exergy destruction formation of the components fluctuates with the geothermal high pressure steam turbine inlet pressure increasing. The result shows as the effect is different in all components which is some of the components are in a decreasing line while the other's destruction is in an increasing path. The high-pressure, first separator, second flash chamber, and the first preheating

tank the graph clarify that the exergetically destructed units in the system when the inlet pressure of first installed turbine in geothermal system increases.

The second Separator and first flashing chamber, second water reheating tank, open feedwater heater, low-pressure turbine, and mixing chamber irreversibility formation are decreasing.

7.10 The effect of second turbine outlet Pressure

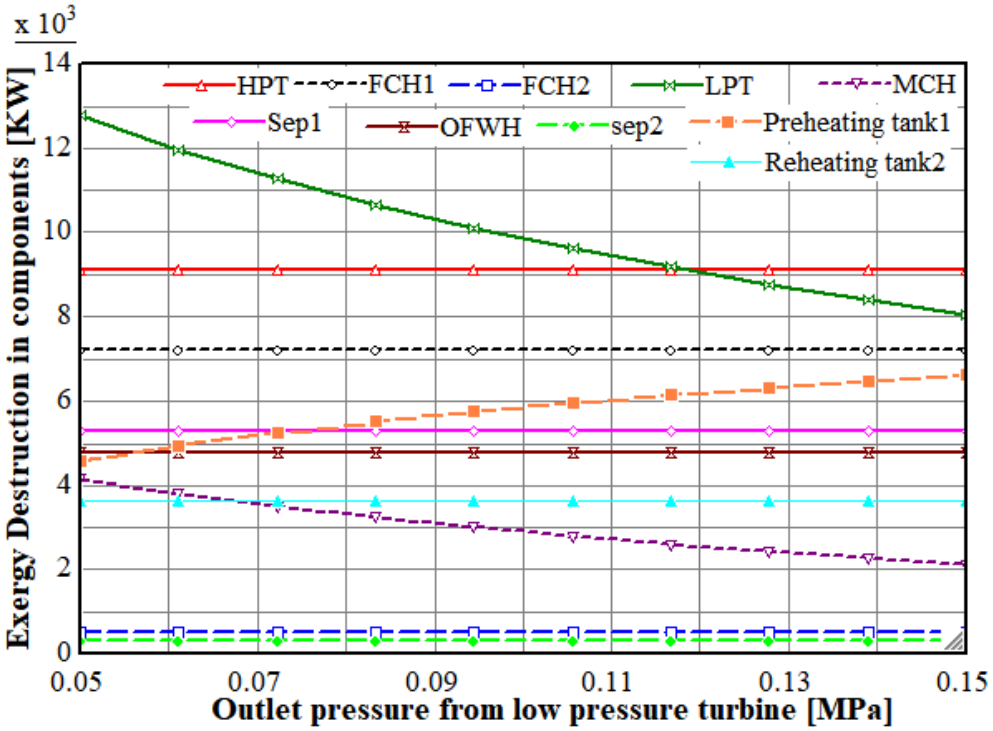

Figure 7.25: The exergy destruction rate of the combined double flash geothermal and solar system due to the variation ofsecond turbine outlet pressure.

The geothermal system is double flash type that has a two different turbines coupled with electric generator to the conversion of heat into mechanical then to electrical energy. As a dominant parameter the low pressure turbine outlet pressure variance has characterized. The graph represents in Figure 7.25 the exergy destruction rate of the mixing chamber and low pressure turbine reduces with increasing of the pressure of the exhaust steam of the low pressure turbine. The first tank that used to preheat water using the waste heat released from low pressure turbine is the component

that records higher exergy destruction with the pressure increament and the other units has not affected.

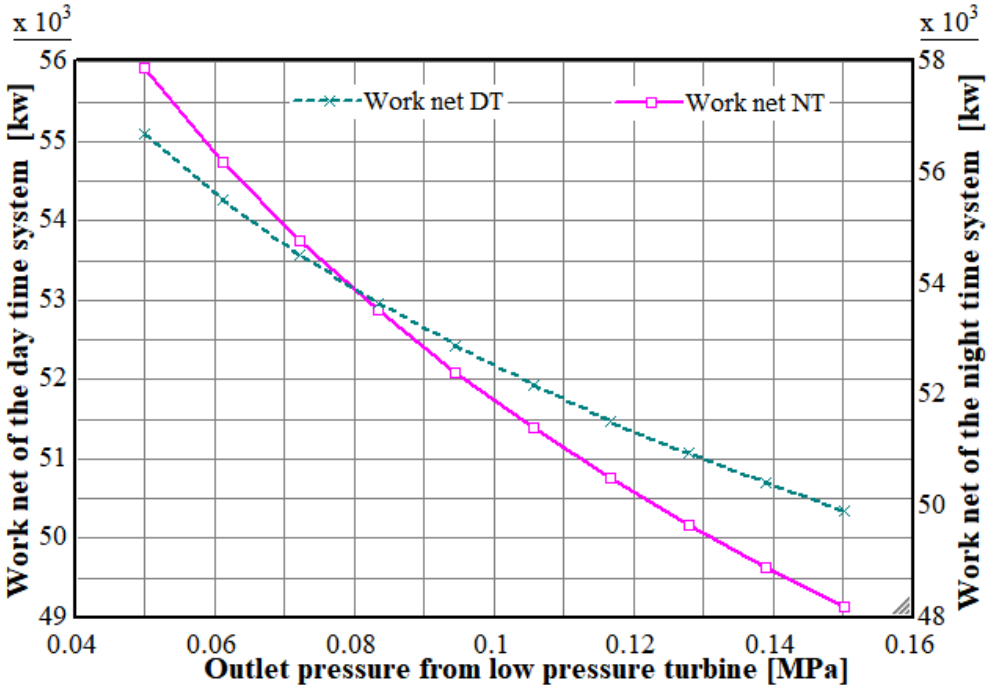

Figure 7.26: The work net of the combined double flash geothermal and solar system due to the variation of second turbine outlet pressure.

The outlet pressure of the low pressre turbine increament affects the overall potential of the power and water purification plant. The graph in Figure 7.26 shows how the work done in the day time and night time fluctuates if the outlet pressure of the low pressure turbine has increased. As a conclustion the low pressure turbine waste heat releasing pressure is a reason for capacity decreament.

The water treatment work has been started by using the low pressure turbine waste heat so that the exhaust steam pressure affects the thermal disinfection process.

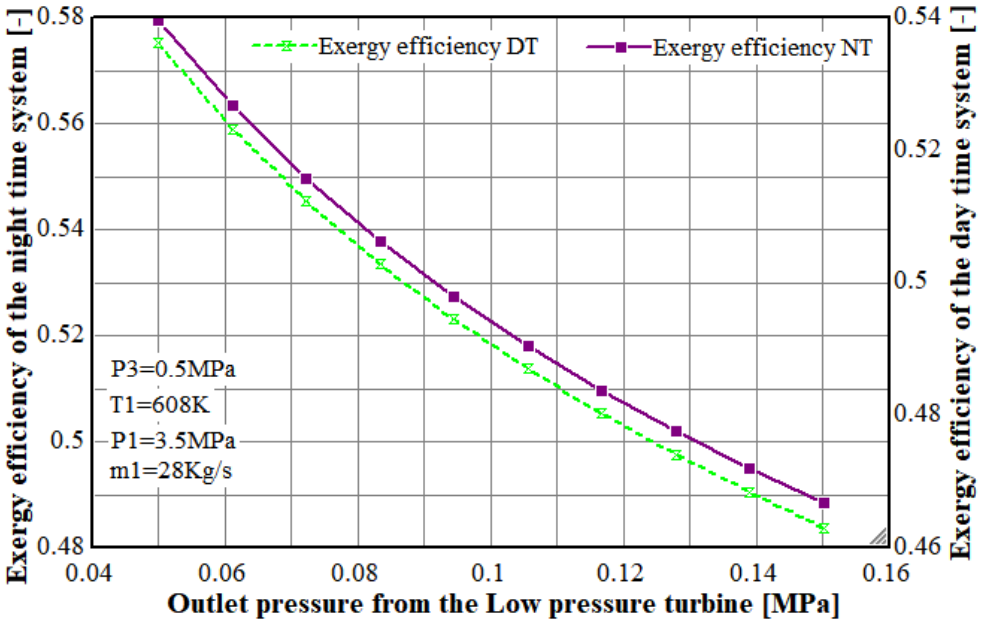

Figure 7.27: The work net of the combined double flash geothermal and solar system due to the variation of second turbine outlet pressure.

The increament of pressure has a significant effect on the entropy rather than enthalpy. According to the equation used to determine the specific exergy rate decreases and operates inefficiently due to pressure increasing. Figure 7.27 represents the exergy efficiency of the system decreases with increasing of the outlet pressure from low pressure turbine.

7.11 Water treatment results

The input data collected from different literature that measured to check the water quality for aquatic life. Lake Ziway is a source of municipal water for the community as well as used for fishing. Ethiopian Lake waters are available in different quality and Ziway lake water has lower salinity which is not brackish generally considered as a freshwater type.

Table 7.2: Input parameters (Ziway lake characterization)

Input parameter types	**Parameter values**
Dissolved oxygen	7.41 mg/l
Dissolved nitrogen gas	18 g/m3 assumption
Nitrate ($NO_3 - N$)	0.0039 g/m3
Sulfate sulfur $SO_4 - S$	$19.2112 g/m^3$
Soluble calcium (Ca)	$12.0234 g/m^3$
Soluble magnesium (Mg)	$8.5067 g/m^3$
Soluble potassium (K)	$27.36881 g/m^3$
Chloride (Cl)	$13.47214 g/m^3$
Sodium (Na)	$55.18 g/m^3$S
Entire cations	$4.02 meq/l$
Entire anions	$4.31 meq/l$
Conductivity	$370 - 410 \mu S/cm$
Alkalinity (caco3)	360.1
Nitric-nitrogen ($NO_2 - N$)	Default
Ammonia (NH4)	$0.193 g/m^3$
Ortho-phosphate (HPO4)	$0.016 g/m^3$
Chlorine [HOCL+OCL]	0
Soluble silica (Sio_2)	$46 mg/l$
PH	8.9
salinity	$0.40 g/l$
Biomass	$91 \mu g/l$

Ziway lake is available in the case study area so that it has considered as a water source for the water purification process in the integrated designed power plant. The main goal is to provide highly treated and pure water for the community using the thermal disinfection method even though, the water should be treated using different mechanisms considering the property and size of the contaminant particles and organisms. The removal of large size and finer size particles can be removed by clarifiers and equalization tanks but the accuracy is not met the recommended standard by WHO, RO treating mechanism is the advanced one.

Table 7.3: Exepermental results of the tap water quality in Ziway city

Measured qualities	**Tap Water**	**Reverse osmosis**
Conductivity	$472.15\mu s/cm$	$52\mu s/cm$
PO_4	$114.05\mu s/cm$	$> 5mg/l$
PH	7.49	6.9

7.11.1 Turbidity

The lake Ziway water is exposed to wastewaters from households, dust and dead part of the plant that comes down, this will increase the level of the water turbidity and makes it a danger to the humans' life to consume raw water.

The level of water turbidity can be differentiated by a simple look at the water in a glass or a tank. The acceptable range of turbidity of potable water should be between 5 NTU and 0.1 NTU, more of less than 0.1 NTU is perfect to be consumed.

The water color changed to cloudy shows its turbidity which is caused by dust, living organism pollutants, wastes, chemical disposals, and other pieces of specks of dirt. Through the reverse osmosis treatment the turbidity level of the water reduced to 0.05 NTU which is considered as a perfect level for consumption

7.11.2 PO_4

Phosphate-rich lake water improves the growth of plants and is assigned as a non-toxic element for humans as well as animals. If the amount is beyond the recommended range consequences the reduction in the amount of the dissolved oxygen in the water.

The highly polluted water phosphate range is always greater than 2 ppm while the clean potable water phosphate level is less than 0.1 ppm, for the protection of ecological health, the phosphate level should be less than 0.05 to prevent its effect on the dissolved oxygen of the water.The RO system filters the phosphate from the influent water to 0.035mg/l(ppm).

7.11.3 PH

PH is the major point that to be measured and corrected if the water is needed to be potable, the PH level of Ziway lake is 8.9 so correction is required to be consumed to keep the range approximately to the neutral instead of basic and acidic ranges.The reverse osmosis purifier is a well known in order to correct the PH level to the required range 6.9.

The reverse osmosis water treatment technology that has been operated at higher booster pressure to remove the contaminants reduced the PH level of the pretreated water to 6.9. The Ro system receives the pretreated heater through different methods including thermal

Mostly PH level of the Surface-water 6.5-8.5 and Groundwater 6-8.5 ranges which is not recommended for humans consumption.

7.11.4 TDS

The saline water has a high TDS amount per liter which consists of different types of salts that increases the salinity of the water, metals, total cations, and anions.

After the critical reading of the standards, TDS level has to be less than 300 mg/L and should not be less than 100 mg/l. TDS is not danger as the hardness has to be between the range of 0-60 mg/l of the water. The TSS content in the water should not exceed 30ppm.

The disadvantage of using reverse osmosis system for water treatment application, the water softer than the recommended rage by the WHO and removes useful minerals that leads to the mineral correction phse before distribution for the customer even though for the patients of the kidney failure the reverse osmosis output is highly needed.

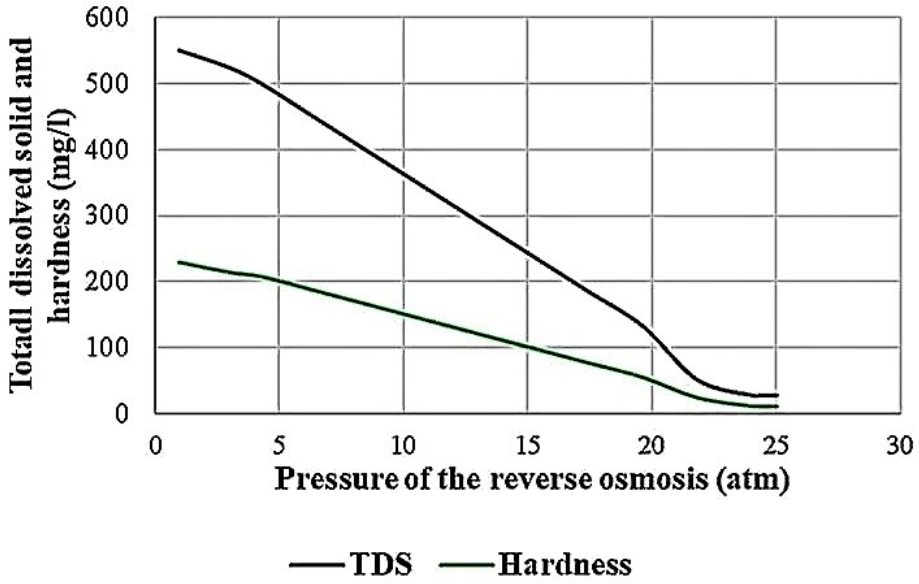

Figure 7.28: TDS level of the water during the purification process.

The water treatment process that passex through different stages gives the potable water that have a haednes of below 60 mg/l and the total dissolved solid under the recommeneded range of 300ppm.

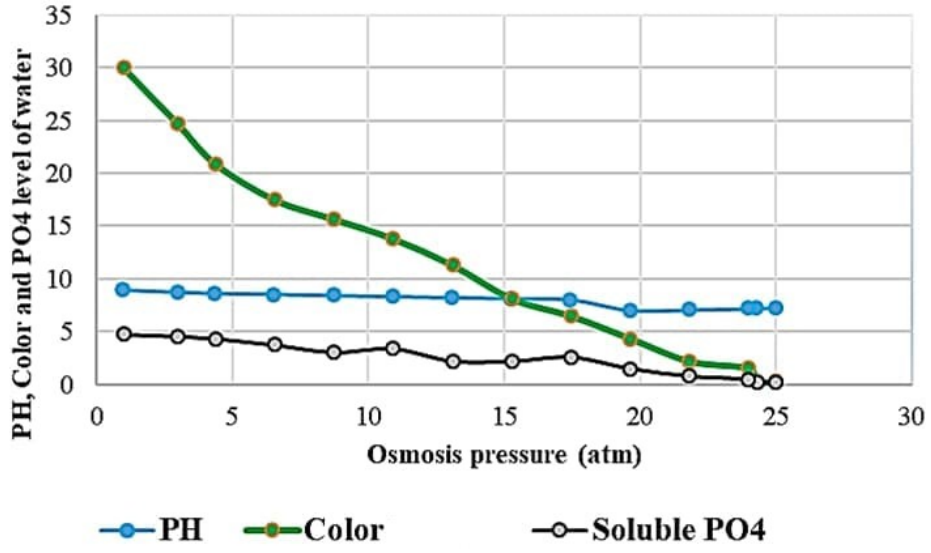

Figure 7.29: PH, Color, PO_4 variation with osmosis pressure

As observed from the graphs in Figure 7.28 and 7.29 the level of TDS, hardness of the water, PH value, color, and amount of soluble PO4 in the treated water is at

a safe level. The drawback of using the RO water treatment system makes the water too soft. Healthy humans should consume water that has a mineral (mineral rich water) due to this the water passes through in the final stage correction process related to the mineral correction. For instance the result of the TDS approaches to zero and TSS value is zero, which is beyond the recommended by WHO.

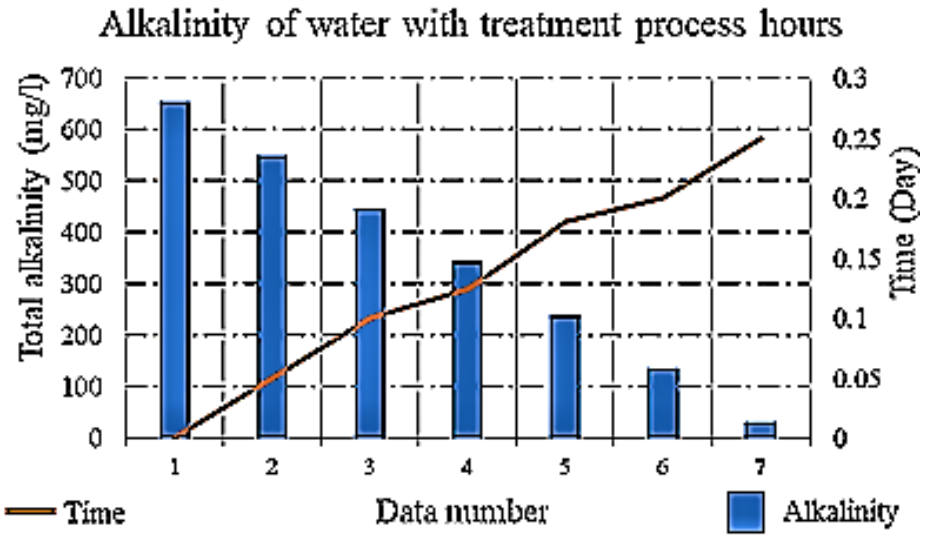

Figure 7.30: The variation total alkalinity of the water with time

Each purification unit takes a time specifically in equalization tank the water needs to be settled, then after the the particles gather to the bottom of the tank. The retention and purposeful time of the water treating method indicates the the quality of water variance as observed in Figure 7.30, the alkalinity was higher at the influent entering time to the first unit, with increasing of the treatment time the alkalinity of the water reduces to the recommended range between 20-200 mg/l.

7.11.5 Water treatment Operating Cost Summary

Table 7.4: Water treatment Operating Cost Summary

	Pumping Cost	Miscellaneous Cost	Chemical Dosage Cost	Sludge Disposal Cost	Total Cost
Ziway Lake Water (inf)	55.57	0	0	0	55.57
Thickener (infth)	3.67	1927.01	0	0	1930.67
Equalization tank (MLSS)	0	0	0	0	0
Clarifier (MLSSc)	37.76	875.91	0	0	913.68
Reverse Osmosis(TW)	2939.8	0	0	0	2939.8
Disposal (fertilizer)	0	0	0	304.58	304.58
Layout Total	3036.8	2802.92	0	304.58	6149.11

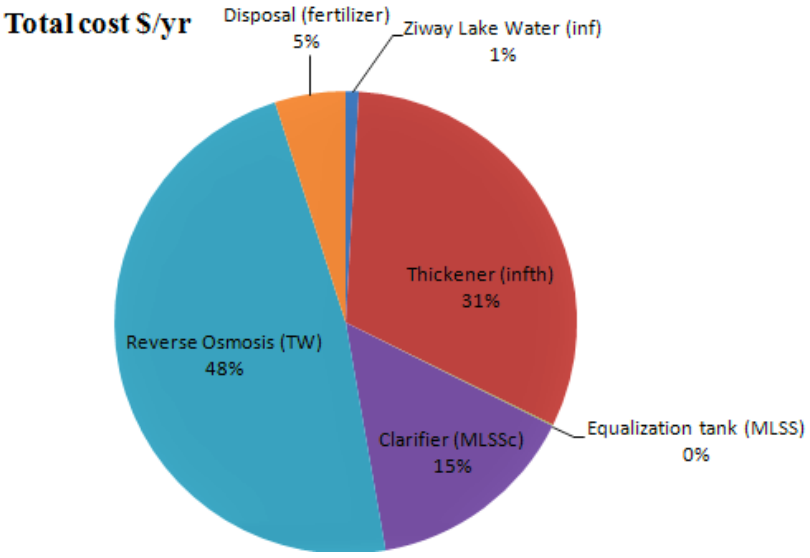

Figure 7.31: Total operating cost of the water treatment process

The total yearly running cost of the water purification process is estimated at 6149.11 USD, riverse osmosis system and thicker are the expensive one relatively from

other units and the disposal transportation cost can be eliminated by supplying it to the nearby farmers as a fertilizer.A clarifier is a principal component to remove particles with larger sizes, the need for maintenance, and the work of pump is high due to that it is the next expensive unit. The current work result shows the possibility of highly pure potable water generation using cost effective method. The existing water treatment system in the case study area used different chemicals imported with foreign currency and can not purify the water to the required level. The treated water can prevent the shortage for consumption and cleaning purposes by supplementing it to the municipal water.

Table 7.5: Water treatment system energy consumption Summary

	Pumping Power(KW)	**Mixing Power(KW)**	**Heating Power(KW)**	**Other Power (KW)**	**Total Power (KW)**
Ziway Lake Water (inf)	0.06	0	0	0	0.06
Thickener (infth)	0	0	0	2.2	2.2
Equalization tank (MLSS)	0	0	0	0	0
Clarifier (MLSSc)	0.04	0	0	1	1.04
Reverse Osmosis(TW)	3.35	0	0	0	3.35
Layout Total	3.45	0	0	3.2	6.67

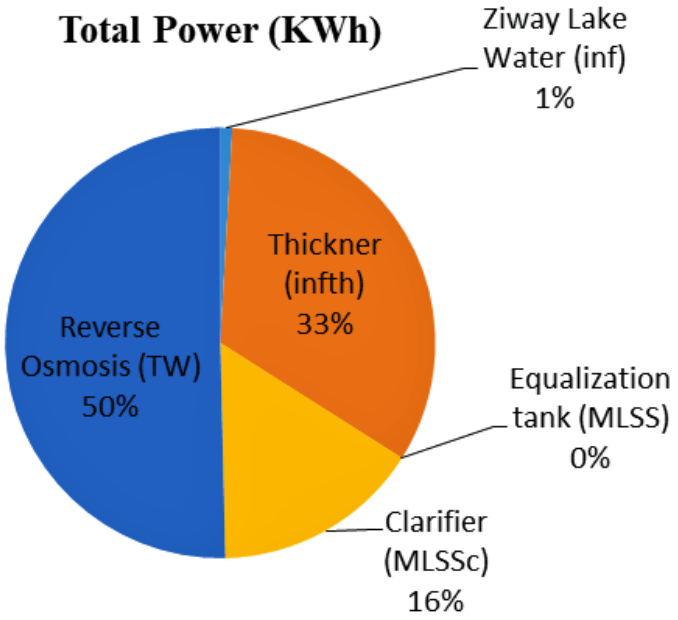

Figure 7.32: power consumption rate of the water purification units

The operating cost has increased as the rate of power consumption of the units increases, the RO treats water based on the pressure supplied by the pump. The power consumption of RO is higher than the others components due to the booster pump power consumption, additionally thickening the sludge needs more power. The thickening process has to reduced from the process to make cost-effective the water treatment mechanism, as observed from the pie chart of a Figure 7.32.

Table 7.6: Occurrence of water born pathogens in ziway tap water, [37].

Name	**Percentage**	**Killing temperature**(^0C)
Coliform	90.5	65-70
Fecal coliform	57.1	66
E.coli	35.3	>70
Entercoli	45	65-70
Clostridium perfiringens	80.9	65-70

Salmonella, shigella, vibro, hepatitis A, germs,cholera and other different bacterias and viruses are available in the treated tap water in Ethiopia, bacteria can be remove to a temperature exposure in between $65 - 70^0C$. viruse can not be killed at low temperature ranges like germ and bacteria, for instans hepatitis A can not resesit at a temperature above 85^0C so the sterilization mechanism instead of pasteurization improves the quality of water. The water treatment system can generate a pure water ranges 100-150 m3 day, the temperature of the water exceeds 135^0C which means all microorganisms can be removed. The energy consumption by the water boiling units is around 13.36% while the rest 86.64% of the supplied heat energy is used for power generation.

7.12 Validation of receiver outlet HTF temperature

Solar parabolic trough energy conversion capability is characterized based on the thermal analysis results, one of the major targets of the analysis is to find out the heat transfer fluid temperature at the outlet of the receiver. As shown in the table in the previous work the SPTC outlet temperature is 673K while the current work is 688 K.

Table 7.7: validation of the temperature of the HTF at the recievier outlet

Author, year	**Title**	**Direct beam radiation($\frac{w}{m^2}$)**	**Mass flow rate $\frac{kg}{s}$**	**Exit HTF temperature from SPTC (K)**
Harwinder singh and R.S. Mishra, 2018	Performance analysis of solar parabolic trough collector driven combined supercritical CO2 and organic Rankine cycle	800	0.055	673
Current work	Exergy analysis of solar-geothermal integrated power plant with sterilization and RO water purifier.	800	0.055	688

As shown in the table the current work achieves higher heat transfer fluid temperature under the same conditions of beam radiation and mass flow rate. The higher exit fluid temperature from the outlet receiver means the better performance has achieved related to exergy efficiency and useful heat gain.

Chapter 8

Conclusion and Recommendations

8.1 Conclusion

The two promising sustainable energies are integrated to convert solar energy and ground heat temperature into electrical energy using selective components, additionally based on the waste heat from the power plant sterilization water disinfection has simulated. The combined renewable energy sources namely, geothermal and solar thermal energy technologies are double flashing type and parabolic trough collector has used. The designed hybrid power plant connected to RO and sterilization water treatment plant perfect to address identified problems.

The thermal analysis of SPTC computes up to what kelvins the heat transfer fluid temperature increases, different terms of heat loss in the collector during the heat transfer, and other useful parameters. The sterilization heats the pre-treated water at 100_0C, to the level of its potential to kill diverse kinds of living organism pollutants and risky to human's health. The pre-treatment carried out using multiple stages of treating ways which are equalization tank, primary clarifier, and advanced RO mechanisms. In this way, the designed and potentially investigated system can provide high-quality potable water and power to the direct beneficiaries in the study area.

8.2 Recommendations

The performance of the SPTC-geothermal integrated power plant with sterilization and reverse osmosis water purification has investigated well, as listed under the objective eight specific objectives that can investigate the potential in deep. Due to the time shortage, the following points are recommended for further analysis.

- Economic analysis of the designed integrated SPTC double-flash geothermal power plant with a water purifier.
- Energy analysis of the overall thermodynamic performance of the designed system
- Experimental investigation of the thermal disinfection as a sample
- Additional waste heat recovery opportunity finding, for instance, drying application using low temperature.

Reference

1. Meseret Teklemariam and Kibret Beyene, “Geochemical monitoring of the aluto-langano geothermal field, Ethiopia” Twenty-Sixth Workshop on Geothermal Reservoir Engineering Stanford University, Stanford, California

2. United nation development program,2020. "2030 sustainable development goals/ Goal 7 ”affordable and clean energy", reviewed on sep-20-2020. https://www.et.undp.org /content/ethiopia/en/home/SDG/over view/goal-7.html/

3. https://www.iea.org/reports/global-energy-review-2020/renewables/ flagship report - April 2020, "Global energy review 2020", reviewed on sep-20-2020

4. Kalogriou, soteris 2015, "Solar energy engineering - processes and systems”

5. Dincer, I. and Rosen, M. A. (2000) Exergy.

6. Gyamfi, S. et al. (2018) Sustainable Hydropower in West Africa Chapter Outline 1. Introduction 75 2. Geographic and Climatic Conditions of West Africa 76 3. Renewable Energy, a Necessity for Sustainable Development 78 4. Renewable Energy and Sustainable Development 80 4.1 Connect, Sustainable Hydropower in West Africa. Elsevier Inc. DOI: 10.1016/B978-0-12-813016-2.00006-X.

7. https://www.iea.org/reports/geothermal/ Geothermal power generation in the Sustainable Development Scenario, 2000-2030/tracking clean energy progress/IEA,2020]

8. Geothermal gradient 2014“Geothermal gradients range from very low, near zero, in fore-arc regions, the zones between subduction zones and their associated volcanic belts where heat is convected downward by the subducting lithosphere” accessed on 02/07/2020
https://www.sciencedirect.com/topics/earth-and-planetary-sciences/ geothermal-gradient

9. Renewable Energy Options, 2015., *"WRSC Renewable Energy Solutions for utility scale applications",www.slideplayer.com/slide/4474849/,*
accessed on 06/27/2020

10. Renewable Energy World, 2021, “geothermal electricity production”, https://www.renewableenergyworld.com/types-of-renewable-energy/tech-3/geoelectricity/# gref

11.flagship report - April 2020, "Global energy review 2020", https://www .iea.org/repo -rts/global-energy-review-2020/renewables, reviewed on sep-20-2020

12. https://www.esi-africa.com/industry-sectors/generation/ethiopia-breaking-ground-in-geothermal-vision/ ESI Africa, 3/2020, Africa’s power journal, accessed on 4/07/2020

13. CCTNE Thursday December 3, 2020, ‘Climate change Geothermal energy ’ https://climatechange-theneweconomy.com/12291-2/ accessed on 15/08/2020 **14.** Taylan, O., & Berberoglu, H. (2013). "Fuel Production Using Concentrated Solar Energy".

Application of Solar Energy. DOI:10.5772/54057

15. Jhon Dodaro (2015), Molten salt storage, Stanford university department of energy, Viewed on 20 May 2020, <http://large.stanford.edu/cour- ses/2015/ph240/dodaro2/>

16. Michael A. boles and Yunus A. cengel, 2017.,"Thermodynamics an engineering approach"

17. Enhancement of, and effect of design parameters on, rankine cycles https://web.mit.edu/16.unified/www/FALL/thermodynamics/notes /node66.html

18. Rebecca Shore (2017), Water in crisis - Ethiopia, the water project organization, viewed on 29 April 2020 <https://thewaterproject.org/water-crisis/water-in-crisis-ethiopia>

19. Md Alam H. M., Elizabeth B., Claudia R., Dawit M., Mark R., (2018) 'Ethiopian energy status and demand scenarios: prospects to improve energy efficiency and mitigate GHG emissions', Energy. Elsevier Ltd, 149, pp. 161-172. <https://doi.org/10.1016/j.energy.2018.02.067>

20. Rahul Kitchlu, March 8-2018, 'Ethiopia's Transformational Approach to Universal Electrification/, the world bank https://www.world bank.org/en/news/feature, accessed date 6/23/2020/

21. Ulderico Bagallni, Bruno cova, Andrea Prudenzi, Leonhard Braun, Daniele Paladini, Tesfaye Batu, Daniel Mulatu, Bizuayehu Tesfaye, Mulat Azene, Melaku yigzaw,Estifanos Gebru, Mirko Armiento, Gluseppe Montesano, and Enel foundation,2019., Integration of variable renewable energy in the national electric system of ethiopia.

22. The world bank (2019), Electric power transmission and distribution losses (% of output) Ethiopia,<https://data.worldbank.org/indicator /EG.ELC.RNWX.KH?locatio -ns=ET> Viewed on 29 April 2020

23. water.org (2020), Ethiopia's water and sanitation crisis, viewed on 29 April 2020, < https://water.org/our-impact/ethiopia/>

24. Kerme, E. D. and Orfi, J. (2015) 'Exergy-based thermodynamic analysis of solar-driven organic Rankine cycle', Journal of Thermal Engineering, 1(5), pp. 192–202. DOI: 10.18186/jte.25809.

25. Layek, A. (2018) 'Exergetic analysis of basin type solar still', Engineering Science and Technology, an International Journal. Karabuk University, 21(1), pp. 99–106. DOI: 10.1016/j.jestch.2018.02.001.

26. Zhou, C. (2014) 'Hybridisation of solar and geothermal energy in both subcritical and supercritical Organic Rankine Cycles', Energy Conversion and Management. Elsevier Ltd, 81, pp. 72–82. DOI: 10.1016/j.enconman.2014.02.007.

27. Serrano-Sanchez, C., Olmeda-Delgado, M. and Petrakopoulou, F. (2019) 'Exergy and economic evaluation of a hybrid power plant coupling coal with solar energy', Applied Sciences (Switzerland), 9(5). DOI: 10.3390/app9050850.

28. Ezzat, M. F. and Dincer, I. (2016) 'Energy and exergy analyses of a new geothermal-solar energy-based system', Solar Energy. Elsevier Ltd, 134, pp. 95–106. DOI: 10.1016/j.solener.2016.04.029.

29. Al-Nimr, M. A., Bukhari, M. and Mansour, M. (2017) 'A combined CPV/T and ORC solar power generation system integrated with geothermal cooling and electrolyzer/fuel cell storage unit', Energy. Elsevier B.V., 133, pp. 513–524. DOI: 10.1016/j.energy.2017.05.142.

30. Islam, S. and Dincer, I. (2017) 'Development, analysis and performance assessment of a combined solar and geothermal energy-based integrated system for multigeneration', Solar Energy. Elsevier Ltd, 147, pp. 328–343. DOI: 10.1016/j.solener.2017.02.048.

31. Kazemi, H. and Ehyaei, M. A. (2018) 'Energy, exergy, and economic analysis of a geothermal power plant', ADVANCES IN GEO-ENERGY RESEARCH, 2(2), pp. 190–209. DOI: 10.26804/ager.2018.02.07.

32. Agrawal, A. and Rana, R. S. (2018) 'Energy and exergy analysis of single slope single basin solar still in Indian condition: An experimental analysis', Materials Today: Proceedings. Elsevier Ltd, 5(9), pp. 19656–19666. DOI: 10.1016/j.matpr.2018.06.328.

33. Dubey, K. K., and Mishra, R. S. (2019) 'Energy-exergy analysis of combined reheating-regenerative Rankine cycle using entropy generation principle', International Journal of Recent Technology and Engineering, 8(3), pp. 3340–3344. DOI: 10.35940/ijrte.C5008.098319.

34. Javadi F.S.,Metselaar H.S.C., Ganesan P., 2020., "Performance improvement of solar thermal systems integrated with phase change materials (PCM)" Solar energy, Vol. 206 pp. 330-352. https://doi.org/10.1016/ j.solener.2020.05.106

35. S.J. Self, B.V. Reddy and M.A. Rosen, 2015., "energy and exergy analysis of geothermal power plants with and without reinjection", Environmental science, ISSN 1819-3412.

36. K.M. Smiech, T.Kovacs, R.F. Wildschut, A.J. cradomonleon, B. devries-onclin, J.G. Bowen, L.L.F. Agostinho,2020., "Thermal disinfection of hospital wastewater in a pilot-scale continuous-flow system.

37. Mekuria Mekonen, Fassil Asefa, Brook Lemma, Chrstina Von Hareen, Peter Casper, 2014.,"Assessing the occurrence of waterborne pathogens in Lake Ziway and drinking water system of Batu (Ziway) Town, Ethiopia"

Appendix A

A.1 The EES code of SPTCdouble-flash geothermal integrated power plant with sterilization and RO water purifier

```
"Daytime geothermal system Exergy Analysis"
"Exergy input - Exergy output - Exergy consumption = Exergy
accumulation"
"Exi - Exe=Exheat - Exwork + Exmass,i - Exmass,e= Exdes=Irre"
"Thermal exergy transfer (EXQr)"
"EXQr = Qr(1-Tr/To)"
"EXw=w"
"I=To*Sgen"                "rate of irreversibility"
"state 1 production well"
T1=608.15
P1=3.5
H1=ENTHALPY(Steam,T=T1,P=P1)
S1=ENTROPY(Steam,T=T1,P=P1)
v1=Volume(steam,T=T1,P=P1)
cp1=Cp(steam,T=T1,P=P1)
rho1=Density(steam,T=T1,P=P1)
{"first separator inlet and outlet of  the first flash
chamber"}
H2=H1
P2=0.5
Q=0
Work=0
T2=T1
effSep=0.999
S2=ENTROPY(Steam,H=H2,P=P3)
{X2=quality(Steam,H=H2,P=P3)}
{"High pressure turbine inlet condition"}
P3=P2
S3=ENTROPY(Steam,x=1,P=P3)
H3=ENTHALPY(Steam,x=1,P=P3)
T3=temperature(Steam,x=1,P=P3)
```

```
{"first separator outlet and inlet to the second flash
 chamber"}
T4=T1
P4=P3
S4=ENTROPY(Steam,X=0,T=T4)
H4=ENTHALPY(Steam,X=0,T=T4)
{"High pressure Steam Turbine outlet"}
EffiseST=0.85
S6s=S3
P6=(0.5/0.2)^0.5
S6=((S6S-S3)/EffiseST)+S3
H6=ENTHALPY(Steam,S=S6,P=P6)
{"H6=((H6S-H3)/EffiseST)+H3"}
T6=Temperature(Steam,P=P6,S=S6)
{x6=quality(Steam,P=P6,S=S6)}
i=(S6-S11)
l2=(S7-S11)
x8=i-l2
{"the second flash chamber outlet and Second separator
 inlet"}
H5=H4
S5=ENTROPY(Steam,H=H5,P=P6)
X5=quality(Steam,H=H5,P=P6)
{"Low pressure turbine inlet"}
m1=28
x2=((H2-H4)/(H3-H4))*0.1
m4=(x2*m1)
m3=(1-x2)*m1
m5=m4
x5=(H5-H11)/(H8-H11)
m7=X5*m5
m11=(1-x5)*m5
m9=X8*m8
m6=12.2
"S8=ENTROPY(Steam,H=H8,P=P6)"
"open feed water heater"
```

```
{H7=ENTHALPY(Steam,X=1,T=T6)}
{H7*m7=((H6*m6)+(H5*m5))/(m7)}
H7=ENTHALPY(Steam,X=1,T=T6)
S7=ENTROPY(Steam,X=1,T=T6)
{second separator outlet}
T11=523
P11=0.1
X11=0
H11=ENTHALPY(Steam,X=0,P=0.1)
S11=ENTROPY(Steam,x=0,P=0.1)
"mass balance and energy balance in the open feed water
heater"
m8=m6+m7
"H8m8=H6m6+H7m7"
"H8=(H6*m6+H7*m7)/m8"
X6=(H7-H12)/((H8-H12))
S8=S11+(X8*(S7-S11))
"low pressure steam turbine outlet"
S9s=S8
P9=0.2
S9=((S8-S9s)/EffiseST)+S8
{T9=Temperature(Steam,P=P9,S=S9)}
{H9=(H8*m8)/m9}
H9=enthalpy(Steam,S=S9s,P=P9)
m12=(S9-S12)/(S9-S11)
{low pressure Turbine outlet}
X10=1
T10=473
P10=0.2
S10=entropy(Steam,P=P10,T=T10)
H10=enthalpy(Steam,P=P10,T=T10)
H12=enthalpy(steam, X=0,P=P10)
S12=entropy(steam,X=0,P=P10)
{H12=(H10-H9)+(H9-H11)
S12=(S10-S9)+(S9-S11)}
{Exergy balance of the double flash geothermal system}
```

```
{Exergy@i=(Hi-Ho)-To*(Si-So)}
To=25+273.15
Po=0.101325
Ho=enthalpy(Steam,P=Po,T=To)
So=entropy(Steam,P=Po,T=To)
{state 1, the first flash chamber}
ExergyFch=(H1-Ho)-To*(S1-So)
Ex1=ExergyFch
{state 2 primary separator inlet}
Exergysep1=(H2-Ho)-To*(S2-So)
Ex2=Exergysep1
{state 3 first HP turbine inlet}
ExergySThp=(H3-Ho)-To*(S3-So)
Ex3=ExergySThp
{state 4 first separator outlet & the second  flash chamber
inlet}
Exergysep1out=(H4-Ho)-To*(S4-So)
Ex4=Exergysep1out
{state 5, second separator inlet}
Exergysep2=(H5-Ho)-To*(S5-So)
Ex5=Exergysep2
{state 6, High pressure turbine outlet}
ExergySThpout=(H6-Ho)-To*(S6-So)
Ex6=ExergySThpout
{state 7, separator 2 outlet & open feed water inlet}
Exergysep2out=(H7-Ho)-To*(S7-So)
Ex7=Exergysep2out
{state 8, Low pressure turbine inlet}
ExergyLPst=(H8-Ho)-To*(S8-So)
Ex8=ExergyLPst
{state 9, Low pressure turbine outlet water treatment
boiling}
ExergyLPstout=(H9-Ho)-To*(S9-So)
Ex9=ExergyLPstout
{state 10, water treatment}
Exergyboiling=(H10-Ho)-To*(S10-So)
```

```
Ex10=Exergyboiling
{state 11, reinjection}
Exergyrein=(H11-Ho)-To*(S11-So)
Ex11=Exergyrein
{state 12, reinjection WT}
ExergyreinWT=(H12-Ho)-To*(S12-So)
Ex12=ExergyreinWT
{Exergy Destruction Or Irriversibility in each component
1. irriversibilty formation in flash chamber}
m2=m3-m4
{m1*Ex1=m2*Ex2+ExdesFch}
ExdesFch=m1*(Ex1-Ex2)
{2. irriversibilty formation in the first separator}
EXdesSep1=(m4*Ex4)+(m3*Ex3)-(m2*Ex2)
{3. irreversibility formation in the HPT}
Whpt=(m6*H6)-H3
Exdeshpt=m3*Ex3-m6*Ex6+Whpt
{4. irreversibility formation in the second Flash chamber}
ExdesFCH2=(m4*Ex4-m5*Ex5)-(m12*Ex12)
{5.irriversibilty formation in the separator 2}
Exdessep2=(m5*Ex5)-(m7*Ex7)
{6.irriversibilty formation in the LPT}
WLpt=m8*(H8-H9)
ExdesLpt=(m8*(Ex8-Ex9))+WLpt
{7. irreversibility formation in the open feedwater heater}
ExdesOFWH=(m8*Ex8)-((m6*Ex6)+(m7*Ex7))
{8. irriversibilty formation in the boiling process}
ExdesWT=(m9*Ex9)-(m12*Ex12)
{exergy efficiency of each component}
Exdesrein=m5*((H5)-(H11))+(m12*H12)
Wnet=(Wlpt+Whpt)
EXEFF2=(Wnet/Ex1)
Exqingeo=abs(Ex2-Ex1)
Exqinreheatergeo=abs(Ex8-Ex7)
ExqinWTgeo=abs(m1*(Ex11-Ex9))
Exqintotalgeo=(Exqingeo+Exqinreheatergeo-(m4*(Ex4-Ex11)))
```

```
Exworkgeo=abs(Ex8-Ex9)*m1
Exworkgeo2=abs(Ex3-Ex6)*m1
ExWnetgeo=Exworkgeo+Exworkgeo2+ExqinWTgeo
```

A.2 EES code of the SPTC

```
W=5.77 "m"          "Width of the PTC"
L=12"m"             "Length of the PTC"
LA=148.5 "m"
FL=1.71 "m"         "Focal distance of the PTC"
C=22.74             " Concentration ratio of the PTC"
Dri=0.066  "m"      "Receiver inner diameter"
Dro=0.07   "m"      "Receiver outer diameter"
Dci=0.109   "m"     "Cover inner diameter"
Dco=0.115   "m"     " Cover outer diameter"
Ari1=pi*dri*L "m^2" "Receiver inner surface"
Aro=pi*dro*L "m^2" "Receiver outer surface"
Aa=(W-Dro)*L
Aci=pi*dci*L "m^2" "Cover inner surface"
Aco=pi*dco*L "m^2" "Cover outer surface"
er=0.92             " Receiver emittance"
ec=0.9           "Cover emittance"
eg=0.96
cr=0.83          "Concentrator reflectance"
gamma=0.99       " Intercept factor"
thetaat0degree=1 " Incident angle modifier (zero
incident angle)"
theta=0 "degree" "Incident angle"
effoptmax=0.75   "Maximum optical efficiency (zero
 incident angle)"
Ta=298 "K"       "Ambient temperature acceptable range 280-
320 K"
Gb=625 "W/m^2" "Solar direct beam irradiation 500-1000 W/m2"
hfi=50    "W/m^2K"  "Heat transfer coefficient between cover
and ambient acceptable range 5-20 W/m2K"
V=5 "m/s"    "Volumetric flow rate acceptable range 0.001-
```

```
0.004 m3/s"
Tfi=285"K"   "Inlet temperature acceptable range 300-650K "
Re=(rho*V*Dco)/mu
cp=(1.50378800*10^(3))+((1.07500814*10^(-13))*Tfi)
-((1.64689463*10^(-16))*Tfi^2)
Nu#=0.3*((Re)^0.6)   " for 1000<Re<50,000"
hcca=(Nu#*Kx)/Dco
sigma=0.0000000567
mr=0.055 "kg/s"
K=15
Tr=400
Tmean=(Ta+Tc)/2
{rho=Density('C12H10,biphenyl',T=Tmean,P=0.1013)}
{mu=viscosity('C12H10,biphenyl',T=Tmean,P=0.1013)}
{Kx=conductivity('C12H10,biphenyl',T=Tmean,P=0.1013)}
rho=1064
mu=0.00429
Kx=0.1363
Hrca=eg*sigma*(Tc+Ta)*(Tc^2+Ta^2)
Hrrc=sigma*(Tr^2+Tc^2)*(Tr+Tc)/1.20247
Ul= 1/((dro/((hcca+hrca)*dco))+(1/hrrc))
Tc=((Aro*Hrrc*Tr)+(Aco*(Hrca+hcca)*Ta))/((Aro
*Hrrc)+(Aco*(Hrca+hcca)))
F=1/UL/(1/UL+Dco/(hfi*Dci)+(Dco/(2*K))*ln(Dco/Dci))
Fr=(mr*cp/(Aro*UL)*(1-exp(-UL*F*Aro/(mr*cp))))
Qu=Fr*((Gb*Aa)-(Aro*UL*(Tfi-Ta)))
Qu=(mr*cp*(Te-Tfi))
{Te=Tfi+(Qu/(mr*cp))}
effcol=Qu/(Gb*W*L)
Ts=4332.75 "K"
"exergy analysis of parabolic trough collector"
effo=er*eg
"Exergy balance"
"Ein- Eout -Eloss-Es -Edes = 0"
"Es=0"            "steady condition"
"inlet exergy rate, inlet exergy carried by fluid flow
```

```
and the radiation exergy rate from the sun"
exEin=mr*Cp*(528-Ta-Ta*ln(528/Ta))
effp=(1-((4*Ta)/(3*Ts)) + (1/3*((Ta/Ts)^4)))
exEinp=Gb*Aa*effp
"outlet exergy carried by fluid flow"
exEout=mr*Cp*(688-Ta-Ta*ln(688/Ta))
"useful exergy rate"
exEgain=(exEout-exEin)
"ExEinp=effo*Gb*Aa(1-(4/3)*(Ta/Ts)+(1/3)*(Ta/Ts))^4"
"exEgain=mr*Cp*(Te-Ta-Ta*ln(Te/Ta))-mr*Cp*
(Tfi-Ta-Ta*ln(Tfi/Ta))"
"exeff=exEgain/(Gb*Aco*(1-(Ta/Ts)))"
exeff=((exEin+exEout)/exEinp)
"exergy loss caused by different 4 terms"
"1. exergy loss rate due to heat leakage from reciever
tube to the ambient"
exloss1=UL*Aro*((Tr-Ta)*(1-(Ta/Tr)))
"2. exergy loss rate due to the temperture difference
between the absorber tube and the sun"
Exdes1=effo*Gb*Aro*Ta*((1/Tr)-(1/Ts))
"3. exergy loss rate caused by solar radiation losses
from the collector
surface to the absorber tube"
Exdes2=Gb*(Aco-(effo*Aro))*(1-(Ta/Ts))
"4. exergy loss rate due to temperature difference
between the absorber
tube and fluid"
Exdes3=abs(mr*cp*Ta*(ln(Te/Tfi)-((Te-Tfi)/Tr)))
exlosstotal=exloss1+Exdes1+Exdes2+Exdes3
"Edesabs= Qu*Ta*((1/Tr) - (1/Ts))"
exdesabs=effo*Gb*Aa*Ta*((1/Tr)-(1/Ts))
Edescond=abs(mr*Cp*Ta*(ln(Te/Tfi)-(Te-Tfi)/Tr))
"exeff=1-(( exEloss - exEchange - exdesabs)/ exEin)"
"exeff=1-(Elopt-Elth-exdesabs-Edescond )"
"exeff=1-((1-effo)+UL*Aro*((Tr-Ta)*2)/Tr)+Qu*Ta*((1/Tr)-
(1/Ts))
```

```
+m*Cp*Ta*((ln(Te/Tfi)-((Te-Tfi)/Tr)))"
"exeff=(mr*cp)/(effo*Gb*Aa*(Te-Tfi-Ta*ln(Te/Tfi)))"
A$='biphenyl-diphenyl oxide'
To#=298
{Ho=Enthalpy(A$,T=T16,P=P16)}
Ho#=20.1
{So=Entropy(A$,T=T16,P=P16)}
So#=1.5605
mPCM=0.05
TPCMi=120+273
TPCMe=415+273
TPCMmelting=220+273
Tec=688
CpPCM=1.256
Tsun=5777
Aa#=68.8
ExPCM=mPCM*CpPCM*(TPCMi-TPCMe)*(1-(Tec/TPCMmelting))
EffPCMcharging=Aa#*(1-(4/3)*(Tec/Tsun)+(1/3)*(Tec/Tsun))
"State 16 outlet of  the PCM and inlet to the Evaporator"
T16=688 "K"
P16=0.2
{H16=Enthalpy(A$,T=T16,P=P16)}
{S16=Entropy(A$,T=T16,P=P16)}
H16=854
S16=2.7015
ExE=(H16-Ho#)-To#*(S16-So#)
"State 17 outlet of  the evaporator and inlet to the
high pressure
turbine"
T17=T16
P17=P16
{H17=Enthalpy(A$,T=T17,P=P17)}
{S17=Entropy(A$,T=T17,P=P17)}
H17=1033
S17=2.155
ExHPT=(H17-Ho#)-To#*(S17-So#)
```

```
"state18 outlet of the high pressure turbine"
P18=P17
S18=S17
T18=663
effST=0.85
{H18=Enthalpy(A$,T=T18,P=P18)}
H18=774.4
ExHPTe=(H18-Ho#)-To#*(S18-So#)
"State 19 inlet to the low pressure turbine"
T19=T18
P19=0.05
X19=1
{H19=Enthalpy(A$,T=T19,P=P19)}
H19=987.7
{S19=Entropy(A$,P=P19,H=H19)}
S19=2.26
ExLPT=(H19-Ho#)-To#*(S19-So#)
"State 20  inlet to the condenser"
T20=453
S20=S19
P20=0.2
{H20=Enthalpy(A$,T=T[13],P=P[13])}
H20=810.67
Excond=(H20-Ho#)-To#*(S20-So#)
"State 21 inlet to the pump outlet of the  condenser"
T21=T20
{H21=Enthalpy(A$,T=T21,P=P21)}
Effpump=0.9
{H21=H20-(Effpump*(H19-H20))}
H21=791
{S21=Entropy(A$,T=T21,P=P21)}
S21=2.08
ExP=(H21-Ho#)-To#*(S21-So#)
"State 22 outlet from the pump"
S22=S21
T22=453
```

```
{H22Enthalpy(A$,T=T22=S22)}
H22=58.8
ExPe=abs((H22-Ho#)-To#*(S22-So#))
"Exergy rate Equations of the organic reheat rankine
cycle of SPTC"
ExqinEv=abs(ExHPT-ExE)*4
Exqinreheater=abs(ExLPT-ExHPTe)*4
ExqinT=ExqinEv+Exqinreheater
ExqoutCond=abs(ExP-Excond)*5.2
ExWoutHPT=abs(ExHPTe-ExHPT)*25
ExWoutLPT=abs(Excond-ExLPT)*25
ExWout=ExWoutHPT+ExWoutLPT
ExWinP=abs(ExPe-ExP)*8
ExWnet=ExWout-ExWinP
"EXERGY Efficiency of the ORRC of SPTC"
{ExeffSPTC=ExWnet/Ex}
"overall system exergy efficiency"
Exwnetsystem=ExWnet+ExWnetgeo
Exqintotalsystem=Exqintotalgeo+ExqinT
exergyefficiency=Exwnetsystem/Exqintotalsystem
```

Appendix B

Thermo-physical property of the heat transfer fluids B.2 Steam property

t (°C)	P	ρ_l	ρ_g	h_l	h_g	r	s_l	s_g	ϕ	ν_l ($\times 10^3$)	ν_g ($\times 10^3$)
310	98.605	690.95	54.52	1401.23	2727.0	1325.8	3.34911	5.6226	2.2735	1.44728	18.340
	99.958	688.70	55.45	1407.10	2724.6	1317.5	3.35882	5.6142	2.2554	1.45202	18.035
	101.326	686.42	56.39	1412.99	2722.1	1309.1	3.36856	5.6057	2.2372	1.45583	17.734
	102.707	684.12	57.35	1418.91	2719.5	1300.6	3.37832	5.5972	2.2189	1.46173	17.437
	104.104	681.80	58.33	1424.86	2716.9	1292.0	3.38812	5.5886	2.2005	1.46570	17.145
315	105.51	679.46	59.32	1430.84	2714.2	1283.3	3.39795i	5.5799	2.1820	1.47176	16.856
	106.94	677.09	60.34	1436.86	2711.4	1274.6	3.40781	5.5712	2.1634	1.47591	16.572
	108.38	674.70	61.38	1442.90	2708.6	1265.7	3.41770	5.5624	2.1447	1.48215	16.293
	109.84	672.28	62.44	1448.99	2705.7	1256.7	3.42763	5.5535	2.1259	1.48748	16.017
	111.31	669.83	63.51	1455.10	2702.8	1247.6	3.43760	5.5446	2.1070	1.49291	15.745
320	112.79	667.36	64.62	1461.25	2699.7	1238.5	3.44760	5.5356	2.0880	1.49843	15.476
	114.29	664.87	65.74	1467.44	2696.6	1229.2	3.45765	5.5265	2.0688	1.50406	15.212
	115.81	662.34	66.89	1473.67	2693.5	1219.8	3.46773	5.5173	2.0496	1.50980	14.951
	117.34	659.78	68.06	1479.93	2690.2	1210.3	3.47786	5.5081	2.0302	1.51565	14.693
	118.89	657.20	69.26	1486.24	2686.9	1200.7	3.48803	5.4987	2.0107	1.52161	14.439
325	120.46	654.58	70.48	1492.58	2683.5	1190.9	3.49825	5.4893	1.9911	1.52769	14.189
	122.04	651.93	71.73	1498.97	2680.1	1181.1	3.50852	5.4798	1.9713	1.53390	13.942
	123.64	649.25	73.00	1505.40	2676.5	1171.1	3.51884	5.4702	1.9513	1.54024	13.698
	125.25	646.53	74.31	1511.88	2672.9	1161.0	3.52921	5.4605	1.9313	1.54671	13.457
	126.88	643.78	75.65	1518.41	2669.1	1150.7	3.53963	5.4506	1.9110	1.55332	13.219
330	128.52	641.0	77.01	1525.0	2665.3	1140.3	3.5501	5.4407	1.8906	1.5601	12.985
	130.19	638.2	78.41	1531.6	2661.4	1129.8	3.5607	5.4307	1.8700	1.5670	12.753
	131.87	635.3	79.84	1538.3	2657.4	1119.1	3.5713	5.4205	1.8493	1.5740	12.524
	133.57	632.4	81.31	1545.0	2653.3	1108.3	3.5819	5.4103	1.8283	1.5813	12.298
	135.28	629.5	82.82	1551.8	2649.0	1097.2	3.5927	5.3999	1.8072	1.5887	12.075
335	137.01	626.5	84.36	1558.6	2644.7	1086.1	3.6035	5.3894	1.7859	1.5963	11.854
	138.76	623.4	85.94	1565.5	2640.3	1074.7	3.6144	5.3787	1.7643	1.6040	11.636
	140.53	620.3	87.56	1572.5	2635.7	1063.2	3.6253	5.3679	1.7426	1.6120	11.421
	142.32	617.2	89.22	1579.5	2631.1	1051.5	3.6364	5.3569	1.7205	1.6202	11.208
	144.12	614.0	90.93	1586.7	2626.3	1039.6	3.6475	5.3458	1.6983	1.6286	10.997

B.2 Biphenyl-diphenyl Oxide (Therminol Vp-1) property

Temperature		Vapor density	Vapor heat capacity	Vapor enthalpy	Vapor thermal conducti	Vapor viscosity	
°C	°F	kg/m³	kJ/(kg·K)	kJ/kg	W/(m·K)	mPa·s	cSt
12	54	—	0.976	419	0.0081	#	—
20	68	—	1	427	0.0085	#	—
30	86	0.00023	1.04	437.2	0.009	#	—
40	104	0.00055	1.07	447.7	0.0095	#	—
50	122	0.0012	1.1	458.6	0.01	#	—
60	140	0.00245	1.14	469.8	0.0105	#	2720
70	158	0.00473	1.17	481.3	0.011	#	1450
80	176	0.00866	1.2	493.2	0.0116	#	817
90	194	0.0152	1.23	505.3	0.0121	#	479
100	212	0.0256	1.27	517.8	0.0126	#	293
110	230	0.0415	1.3	530.7	0.0132	#	185
120	248	0.0651	1.33	543.8	0.0137	#	121
130	266	0.0994	1.36	557.2	0.0143	#	81.5
140	284	0.148	1.39	571	0.0148	#	56.3
150	302	0.214	1.42	585	0.0154	#	39.8
160	320	0.303	1.45	599.4	0.016	#	28.8
170	338	0.422	1.48	614	0.0166	#	21.2
180	356	0.575	1.51	628.9	0.0171	#	15.9
190	374	0.771	1.54	644	0.0177	#	12.1
200	392	1.02	1.57	659.4	0.0183	#	9.38
210	410	1.33	1.6	675.1	0.0189	#	7.36
220	428	1.71	1.63	691	0.0195	0.01	5.85
230	446	2.17	1.66	707.1	0.0201	#	4.7
240	464	2.72	1.68	723.5	0.0207	#	3.82
250	482	3.38	1.71	740.1	0.0213	#	3.13
260	500	4.17	1.74	756.9	0.0219	#	2.59
270	518	5.09	1.77	773.8	0.0226	0.011	2.16
280	536	6.17	1.79	791	0.0232	# #	1.82
290	554	7.42	1.82	808.3	0.0238	#	1.54
300	572	8.86	1.84	825.8	0.0245	#	1.31
310	590	10.5	1.87	843.4	0.0251	#	1.13
320	608	12.4	1.9	861.1	0.0258	0.012	0.97
330	626	14.6	1.92	879	0.0264	#	0.841
340	644	17	1.95	896.9	0.0271	#	0.731
350	662	19.8	1.97	915	0.0277	#	0.639
360	680	22.9	2	933.1	0.0284	#	0.56
370	698	26.5	2.03	951.3	0.0291	#	0.493
380	716	30.5	2.05	969.5	0.0298	#	0.435
390	734	35	2.08	987.7	0.0304	#	0.384
400	752	40.1	2.11	1005.8	0.0311	#	0.341
410	770	45.8	2.14	1024	0.0318	#	0.302
420	788	52.4	2.17	1042	0.0325	0.014	0.268

Appendix C

C.1 Phyton code for the solar angles and radiation estimation in the case study area (Ziway)

```
from math import *
from numpy import *
from scipy import *
from matplotlib.pyplot import *
from scipy.interpolate import make_interp_spline, BSpline
Isc=1367; # solar constant (w/m2)
L=7.9277; # Laltitude
LOD=38.7211; # Longitude
Gext=[];
D=[];
B=[];
N=[17, 47, 75, 105, 135, 162, 198, 228, 258, 288, 318, 344 ];
#% sunshine hours
n_bar=[10.1,9.46,9.903,9.17,8.58,7.5,5.2,5.65,7.1,8.71,9.4,
10.1];
SS=[]
S=[]
sol=[]
Ib=[]
D=[]
Eot=[]
IBT=[]
TETA=[]
TETA_M=[]
K_TETA=[]
KLUZ3=[]
GEXT_I=[]
OMEGA=[]
HB_BAR=[]
BETA=[]
TETAS=[]
```

```
TF=[]
for j in range (len(N)):
    #print('N=',j)
    Gext_i=Isc*(1+(0.0333*cos((pi/180)*((360/365)*N[j]))))
    print('Gext[',N[j],']=',round(Gext_i, 2))
    GEXT_I.append(Gext_i)
print()
for j in range (len(N)):
    TZ_GMT=3;
    D_i=23.45*sin((pi/180)*(360/365)*(N[j]-81));
    # angle of declination
    B_i=(360/364)*(N[j]-81);
    print('B_i=',B_i)
    EoT=(9.87*sin(2*(pi/180)*B_i))-(7.53*cos((pi/180)*(B_i)))
    -(1.5*sin((pi/180)*(B_i)));
    print('D_i[',N[j],']=',round(D_i, 2),'EoT[',N[j],']=',
    round(EoT,2))
    Lzt=15*TZ_GMT;
    longcorr=4*(Lzt-LOD);
    solarcorr=(longcorr+EoT)/60;
    # solar time correction
    print('solarcorr=',solarcorr)
    omega_s=-tan((pi/180)*(D_i))*tan((pi/180)*(L));
    #Sunrise / Sunset hour angle
    print('omega_s=',omega_s)
    omega_rs=(180/pi)*acos((omega_s)); # Sunrise / Sunset
  hour angl e
    print('omega_rs=',omega_rs)
    Ns_bar=(2/15)*omega_rs;
    print('Ns_bar=',Ns_bar)
      #From solar noon , sunrise 12-omega_rs/15 and sunset
      =12+omega_rs
    Ssr=12-omega_rs/15; # Sun rise solar time
    print('Ssr=',Ssr)
    Sss=12+omega_rs/15; # Sunset s o l a r time
    print('Sss=',Sss)
```

```
        #solar time = local time + solarcorrection
    Lsr=(Ssr-solarcorr);#%Sunr is elocal time
    print('Lsr=',Lsr)
    Lss=(Sss-solarcorr); #%Sunset local time
    print('Lss=',Lss)
    S.append(Lsr)
    SS.append(Lss)
    #print('S=',len(S))
    #print('SS=',len(SS))
    print()
    sol.append(solarcorr)
    #print('sol=',sol)
    Eot.append(EoT)
t=linspace (S[len(S)-1],SS[len(SS)-1],len(N));
print('t=',t)
print()
for j in range (12):
    Ts_i=t[j]+sol[j];
    print('t=',t[j],'sol=',sol[j])
    print('Ts_i=',Ts_i)
    omega=15*(Ts_i-12);
    print('omega=',omega)
    sin_alpha=sin((pi/180)*L)*sin
    ((pi/180)*(D_i))+cos((pi/180)*(L))
    *cos((pi/180)*(D_i))*cos((pi/180)*(omega)); # altitude
    angle
    alpha=(180/pi)*asin((sin_alpha)); # altitude angle
    #print('alpha=',alpha)
    teta_z=90-alpha; # Zenit angle
    #print('teta_z=',teta_z)
    sin_alpha_s=cos(
    (pi/180)*(D_i))*sin((pi/180)*(omega))/
    cos((pi/180)*(alpha));
    alpha_s=(180/pi)*asin(sin_alpha_s);
    #print('alpha_s=',alpha_s)
    #hs=arcsin((cos(pi/180)*(L))*(cos(pi/180)*(D_i))*(cos(pi/180)*
```

```
(omega))+((sin(pi/180)*(L))*(sin(pi/180)*(D_i))));
#AF=(arcsin(cos(pi/180)*(D_i)*(sin(pi/180)*(omega)))/
(cos(pi/180)*(hs);
# angle of incident the tracking system rotate E-W
direction
coszenith=(cos((pi/180)*teta_z))**2;
#print('cod=',cod)
cosdec=(cos((pi/180)*(D_i)))**2
#print('coD=',coD)
sinomega=(sin((pi/180)*omega))**2;
#print('sid=',sid)
cos_teta=sqrt(coszenith+cosdec*sinomega);
#costeta=sqrt(1-(cosdec*sinomega));
#tanbeta=tan(teta_z)*(abscos(pi/180)*alpha_s);
#beta1=atan(tanbeta);
#print('tilt angle=',tanbeta)
#print('cos_teta=',cos_teta)
teta=(180/pi)*acos(cos_teta);
teta=1-(180/pi)*acos(cos_teta);
#print('teta=',teta)
 # incident angle modifier
tetas=teta**2;
teta_m=mean(teta);
print('tetas=',tetas)
#print('teta_m=',teta_m)
K_teta=1-5.25097*(10**(-4))*(teta/cos((pi/180)*teta))-2.85
9621* (10**(-5))*(tetas/cos((pi/180)*teta));
#print('K_teta=',K_teta)
KLuz3=cos((pi/180)*teta)-0.0003512*teta-0.00003137*tetas;
#print('KLuz3=',KLuz3)
K_tetam=mean(K_teta ) ;
#print('K_tetam=',K_tetam)
K_luzm=mean(KLuz3);
#print('K_luzm=',K_luzm)
tan_rho=-sin((pi/180)*alpha_s)/tan((pi/180)*alpha);
rho=(180/pi)*atan(tan_rho);
```

```
#print('rho=',rho)
D_i=23.45*sin((pi/180)*(360/365)*(N[j]-81));# angle
of declination
Gex_1=cos((pi/180)*L)*cos((pi/180)*D_i)*sin((pi/180)
*omega_rs);
print('Gex_1=',Gex_1)
omega_s=-tan((pi/180)*(D_i))*tan((pi/180)*(L)); #Sunrise
/ Sunset
hour angle
omega_rs=(180/pi)*acos((omega_s)); # Sunrise / Sunset
hour angl e
Gex_2=((pi/180)*omega_rs)*sin((pi/180)*11.08)*sin((pi/180)
*D_i);
#print('Gex_2=',Gex_2)
Gex=Gex_1+Gex_2 ;
#print(' Gex=', Gex)
e6=1000000;
Gext_i=Isc*(1+(0.0333*cos((pi/180)*((360/365)*N[j]))))
Ho_bar=((24*3600/pi)/e6)*Gext_i*Gex; #Extrateresterial
solarradiation in horizontal surface (MJ/(m2day) )
#print('Ho_bar=',Ho_bar)
TF=cos((pi/180)*teta)/cos((pi/180)*teta_z); #tilt factor
for aperture plane
#pint('TF=',TF)
#Pr ediction of Monthly Average Daily Global Radiation
on a Horizontal Surface
Ns_bar=(2/15)*omega_rs;
r=n_bar[j]*(1/Ns_bar)
print('r=',r)
a_1=-0.11+0.235*cos((pi/180)*L)+0.323*r;
a_2=1.449-0.533*cos((pi/180)*L)-0.694*r;
r_h=a_1+a_2*r;
H_bar=Ho_bar*r_h;
#   Prediction of Monthly Average Daily Diffuse and
Beam Radiation on a Horizontal Surface
h_d=0.931-0.814*r;
```

```
 Hd_bar=H_bar*h_d;
 Hb_bar=H_bar-Hd_bar;
 print('Hb_bar=',Hb_bar)
# ESTIMATION OF Monthly Average Hourly Global Radiation
on a Horizontal Surface
 b_1=0.409+0.5016*sin(omega_rs-60);
 b_2=0.6609-0.4767*sin(omega_rs-60);
 rt_1=(pi/24)*(b_1+b_2*cos((pi/180)*omega));
 rt_22=(cos((pi/180)*omega)-cos((pi/180)*omega_rs));
 rt_3=sin((pi/180)*omega_rs)-(pi*omega_rs/180)*cos((pi/180)
 *omega_rs);
 rt_2=rt_22/rt_3;
 rt=rt_1*rt_2;
 I_bar=rt*H_bar;
# Prediction o f Monthly Average Hourly Diffuse
and Beam Radiation on a Horizonal Surface
 rd_1=cos((pi/180)*omega)-cos((pi/180)*omega_rs);
 rd_2=sin((pi/180)*omega_rs)-(pi*omega_rs/180)*cos((pi/180)
 *omega_rs);
 rd=(pi/24)*rd_1/rd_2 ;
 Id_bar=Hd_bar*rd;
 print('Id_bar=',Id_bar)
 Ib_bar=(I_bar-Id_bar)*(1000/3.6);
 print('Ib_bar=',Ib_bar)
 Ibt=Ib_bar*TF*K_teta;
 Rs=12.49/(5.77*TF);
 #% monthly average hourly beam radiation kwh/m^2
 Ib_a=Ib_bar*TF;
 print('Ib_a=',Ib_a)
 lossend=1-tan((pi/180)*teta)/148.5;
 slope=atan((cos((pi/180)*D_i)*sin((pi/180)*omega))/((sin
 ((pi/180) *L)*sin((pi/180)*D_i))+(cos((pi/180)*L)
 *cos((pi/180)*D_i)*cos((pi/180)*omega))));
 print('Beta=',slope)
 print()
 print('tilt angle=',TF)
```

```
    print()
    Ib.append(Ib_a)
    D.append(D_i)
    IBT.append(Ibt)
    TETA.append(teta)
    TETA_M.append(teta_m)
    K_TETA.append(K_teta)
    KLUZ3.append(KLuz3)
    OMEGA.append(omega)
    HB_BAR.append(Hb_bar)
    BETA.append(slope)
    TETAS.append(tetas)
    TF.append(TF)
print('D=',D)
print('Ib_a=',Ib)
print('EoT=',Eot)
print('Ibt=',IBT)
print('teta=',TETA)
print('teta_m=',TETA_M)
print('k_teta=',K_TETA)
print('kluz3=',KLUZ3)
print('Gext_i=',GEXT_I)
print('omega=',OMEGA)
print('Hb_bar=',HB_BAR)
print('Beta=',BETA)
print('Tetas=',TETAS)
#print('Tilt angle=',TF)
```

C.2 Online Solar radiation estimation using open source

Sun

Time	Azimuth	Elevation	I Direct	I Diffuse
00:37	113.68	-0.00	0.00	0.00
00:52	114.24	3.39	6.20	27.40
01:07	114.89	6.77	33.94	61.72
01:22	115.64	10.13	77.27	86.22
01:37	116.50	13.47	128.67	103.44
01:52	117.47	16.78	184.07	116.12
02:07	118.57	20.06	241.21	125.86
02:22	119.80	23.30	298.68	133.62
02:37	121.20	26.50	355.52	139.96
02:52	122.76	29.65	411.02	145.25
03:07	124.52	32.75	464.60	149.73
03:22	126.51	35.77	515.80	153.56
03:37	128.75	38.71	564.22	156.86
03:52	131.28	41.56	609.53	159.71
04:07	134.14	44.29	651.41	162.18
04:22	137.37	46.88	689.62	164.30
04:37	141.02	49.31	723.90	166.11
04:52	145.13	51.54	754.07	167.64
05:07	149.73	53.54	779.95	168.91
05:22	154.85	55.27	801.40	169.93
05:37	160.46	56.69	818.28	170.72
05:52	166.51	57.75	830.52	171.28
06:07	172.89	58.41	838.05	171.63
06:22	179.47	58.66	840.82	171.75
06:37	186.06	58.48	838.82	171.66
06:52	192.49	57.88	832.05	171.35
07:07	198.60	56.88	820.57	170.83
07:22	204.28	55.52	804.42	170.07
07:37	209.48	53.84	783.70	169.09
07:52	214.16	51.88	758.53	167.86
08:07	218.35	49.68	729.04	166.37
08:22	222.07	47.28	695.40	164.61
08:37	225.37	44.72	657.81	162.54
08:52	228.29	42.01	616.50	160.13
09:07	230.87	39.18	571.73	157.35
09:22	233.15	36.25	523.78	154.13
09:37	235.18	33.24	473.00	150.39
09:52	236.97	30.15	419.78	146.02
10:07	238.57	27.01	364.55	140.87
10:22	239.99	23.82	307.89	134.72
10:37	241.25	20.58	250.46	127.22
10:52	242.36	17.31	193.19	117.85
11:07	243.35	14.00	137.38	105.74
11:22	244.23	10.67	85.13	89.39
11:37	245.00	7.31	40.10	66.29
11:52	245.66	3.94	9.19	33.46
12:07	246.24	0.55	0.06	1.58
12:22	246.73	-2.86	0.00	0.00

Appendix D

D.1 calculated solar data's of the case study area Reverse Osmosis-ionic strength

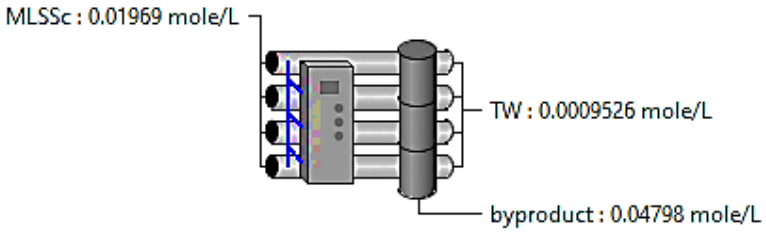

COD

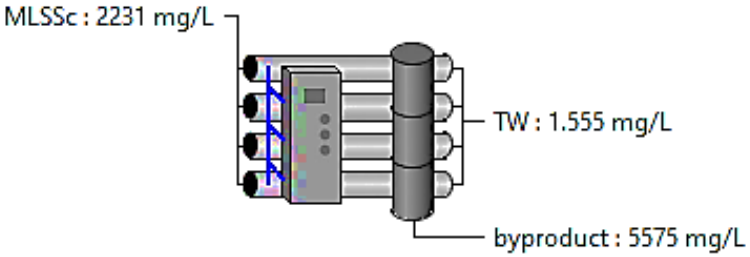

Conductivity

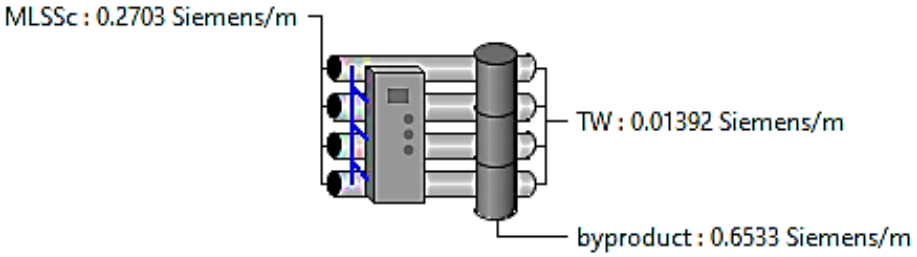

D.2 Simulation Results

		Feed	Filtrate	Brine
Flow	m3/d	143	111.19	31.81
TDS	mg/L	551.0	27.55	1336
Ionic Strength	mole/L	0.01969	0.0009526	0.04798
Conductivity	microS/cm	2703	139.2	6533
pH	-	8.9	6.9	12.35
Soluble PO4-P	mgP/L	5.0	0.25	12.12
Langelier Stability Index	-	4.108	0.364	5.22
Ryznar Stability Index	-	3.753	9.966	1.912
p Alkalinity	mgCaCO3/L	628.6	30.37	1523
M Alkalinity	mgCaCO3/L	630.6	31.72	1525
Total Alkalinity	mgCaCO3/L	654.3	32.72	1587
Total Hardness	mgCaCO3/L	230.8	11.54	559.6
Turbidity	NTU	1214	0.05	3035
Color	mg/L(Pt-Co)	30.0	1.5	72.75

D.3 Operational Variables

		TW
Recovery	%	60.0
Membrane Area	m2	840.0
Flux	L/m2/h	2.848
Standardized Flux	L/m2/h	4.035
Net Driving Pressure (Arithmetic Mean)	kPa	1637
Tempertaure Correction Factor	-	1.159
Flux Change	%	-89.91